Mixed Solid-State Fermentation

Numerical modeling and Experimental validation

Promotoren

Prof. Dr. Ir. R.M. Boom
Hoogleraar in de Levensmiddelenproceskunde aan de Wageningen Universiteit

Prof. Dr. W.J. Briels
Hoogleraar in de Computational Dispersion Rheology aan de Universiteit Twente

Co-promotor

Dr. Ir. A. Rinzema
Universitair docent bij de sectie Proceskunde aan de Wageningen Universiteit

Promotiecommissie
Prof. Dr. D.J. Tildesly
Unilever R&D, Port Sunlight

Dr. Ir. M.L.F. Giuseppin
Avebe

Prof. Dr. Ir. G.P.A. Bot
Wageningen Universiteit

Prof. Dr. Ir. J. Tramper
Wageningen Universiteit

Mixed Solid-State Fermentation

Numerical modeling and Experimental validation

Proefschrift

ter verkrijging van de graad van Doctor op gezag van de rector magnificus

van Wageningen Universiteit, prof. dr. ir. L. Speelman

in het openbaar te verdedigen op woensdag 25 juni 2003

des namiddags te half twee in de Aula.

door Maarten A.I. Schutyser

# Contents

Chapter 1

Introduction

Solid-State Fermentation

Fungi play an essential role in nature's continuous rebirth, because they recycle dead organic matter into useful ingredients. Fungi digest food outside their bodies by releasing enzymes into the surrounding environment. Since many generations, people have made use of the hydrolytic power of fungi for the preparation of foods. For example, for the production of soy sauce, proteases from fungi are used to convert proteins into small peptides and amino acids. During this enzymatic conversion a typical spectrum of products is formed, which finally results in the characteristic taste and smell of soy sauce. Other, more western food products in which fungi have been traditionally used are Roquefort, Camembert and Chorizo.

From the 1940's, western industries started to focus on the production of fungal enzymes and specific secondary metabolites by cultivation of fungi in liquid media, also called submerged fermentation (SmF) (Pandey et al., 2003). An alternative method for cultivation of fungi is solid-state fermentation (SSF), in which fungi are grown on a moist solid substrate in the absence of free flowing water. For specific applications SSF offers improved yields and product spectra compared to SmF. Currently, the main reason for the limited industrial application of SSF is the lack of engineering data and knowledge about the design and scale-up of solid-state fermenters. This is in contrast with SmF, for which engineering data is now readily available.

The work that is presented in this thesis is part of a larger research project that aims at exploring the possibilities for industrial exploitation of fungal SSF. Focus is directed towards developing more knowledge about the physiological and molecular genetic aspects, *i.e.* to study the response of fungi under SSF conditions (Biesebeke et al., 2002), and towards developing non-empirical engineering methods for development of SSF processes. The project consists of several subprojects, which cover the whole range of scales from gene to large-scale fermenter (Fig. 1).

The subproject that resulted in this thesis was aimed at the development of non-empirical models for mixed solid-state fermenters. The advantage of non-empirical models is that 'trial and error'-based design and scale-up of fermenters can be avoided. To make a direct link between the particle and the fermenter level, a modeling approach was chosen that predicts
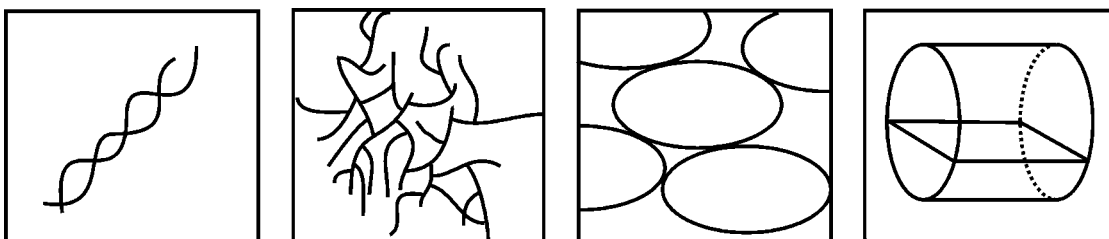
Figure 1. From the gene, to the fungus, to the particle and to the fermenter level.

macroscopic phenomena from individual contributions of particles: the discrete particle approach. The models were experimentally validated using whole-wheat grains as substrate particles and the fungus *Aspergillus oryzae* as a model organism.

Mixing in Solid-State Fermenters

Traditional solid-state fermenters, such as tray or packed bed fermenters, do not contain mixing equipment. During cultivation, metabolic heat is removed through the wall via conduction, or by evaporative cooling, *i.e.* removal of heat by evaporation of water and subsequent removal of moist air. Spatial gradients in temperature and moisture contents develop rapidly in these systems, especially when fast growing fungi are cultivated (Weber et al., 2002). Sometimes these problems are circumvented by unconventional approaches, for example in the Zymotis fermenter (Roussos et al., 1993) or in the Plafractor (Suryanarayan et al., 2001, US patent nr. US 6,197,573 B1). In both fermenters heat removal efficiency is increased by extra internal heat exchange surface area, i.e. steel heat exchangers provided with fluid cooling.

In this study we focused on the application of mixed solid-state fermenters. Control of temperature and moisture gradients was demonstrated in previous research during continuously mixed SSF of *A. oryzae* on whole wheat grains in a paddle mixer (35 L) (Nagel, 2002). During the fermentation, metabolic heat was partially removed via evaporative cooling and subsequent water loss was compensated by addition of water to the bed via spray nozzles. Mixing allowed the addition and distribution of water in the system and also enhanced efficient conductive heat transfer via the wall. Spatial gradients in temperature and moisture contents could thus be minimized by the use of continuous mixing.

However, mixing during SSF sets some additional requirements for the solid substrate and the fungus. Mechanical action leads to a change in the development of the morphology of the fungus or even to breakage of hyphae. During continuously mixed SSF of *A. oryzae* on wheat grains it was observed that the fungus grew primarily inside the kernel, probably forced to do so by the shear (Nagel et al., 2001). It is not exactly known what effect the change in morphology of the fungus has on the production of enzymes or secondary metabolites. Recently, it was found that the aerial hyphae of *A. oryzae*, cultivated on wheat dough, contribute considerably to the total oxygen consumption of the culture (Rahardjo et al., 2002). This suggests that allowing aerial hyphae to grow in a mixed SSF could lead to significantly larger yields.

To limit the detrimental effect of mixing, discontinuously mixed SSF is an interesting alternative way of process operation. Mixing action is only applied when:

- spatial temperature or moisture content gradients become too large.

- water addition is needed to avoid desiccation of the substrate.

- a strong network of aerial hyphae develops that aggregates the substrate bed.

During static periods the growth of fungi is not hampered by mechanical action, but intermittent mixing is required to reduce aggregate sizes, and to provide process control and thus to prevent failure of the fermentation.

The rotating drum was chosen as the model fermenter design. Additionally, the helical blade mixer, which is a promising fermenter design (Oostra et al., in prep.), has also been subject of study. The rotating drum has a long history; its first reported use involved the production of amylase with *A. oryzae* on wheat bran (Takamine, 1914). An important advantage of the rotating drum is that the dominant mixing behavior, i.e. the radial mixing, can be described in two dimensions. An experimental set-up of the rotating drum fermenter (28 L) was developed for validation purposes. Macroscopic phenomena, such as mixing, heat transfer, fungal growth, etc., in the rotating drum filled with moist wheat grains, were modeled by applying the discrete particle modeling approach.

Earlier modeling studies considered either continuously mixed or static SSF systems (Sargantanis et al., 1993, Weber et al., 2002). Recently, a modeling study focused on discontinuously mixed SSF, assuming that after a 'mixing event' the bed would be ideally mixed (von Meien and Mitchell, 2002). This assumption could not be avoided, because the model developed in this work could not predict the mixing behavior.

Discrete particle modeling

To resolve the flow behavior of a granular (discrete particle) system, different modeling approaches have been used in the past (Schutyser et al., 2001). The most widely used and most popular approach is the simulation method that is based on molecular dynamics simulations. In this approach the macroscopic flow behavior is captured via calculation of the trajectories of each of the individual particles. The particle trajectories are calculated by direct integration of Newton's equations of motion. The forces on the particles arise from interactions between particles and interactions between the particles and the system (Fig. 2).
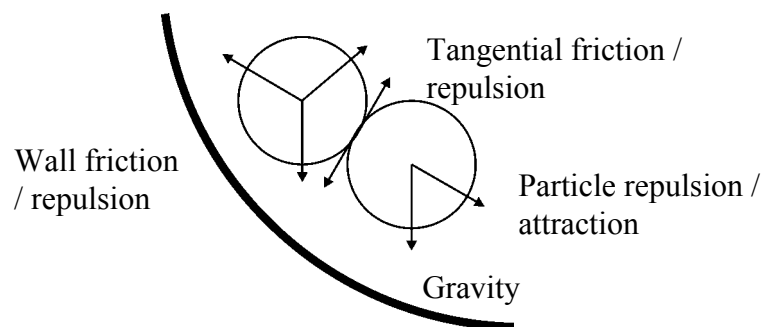
Figure 2. Force calculations during discrete particle simulation.

This modeling approach is called the distinct element method and was been originally proposed by Cundall and Strack (1979). This approach is sometimes also referred to as particle or granular dynamics simulations (McCarthy et al., 2000; Ristow, 1994). In this thesis the simulation method will be referred to in more general terms: discrete particle simulations or discrete particle modeling.

In recent years, mixing and flow behavior of several granular systems have been extensively studied with discrete particle modeling:

- Some of the first studies that applied discrete particle modeling focused on hopper flow, in which for example arching phenomena in the exit flow region were studied (Langston et al., 1995; Ristow, 1994).

- The mixing of powders in rotating and/or rocking drums has been studied extensively (Dury and Ristow, 1998; Wightman et al., 1998; Yamane et al., 1998). Most studies concentrated on the mixing of spherical particles (e.g. glass beads), only very few studies implemented ellipsoidal or irregularly shaped particles (Buchholtz et al., 1995). Several studies involved segregation of particles of different sizes in rotating drums (Cleary et al., 1998; Dury and Ristow, 1997; Moakher et al., 2000; Wightman and Muzzio, 1998).

- The discrete particle approach, coupled with a computational fluid dynamics model, has been used for accurate description of the dynamics of fluidized beds (Hoomans et al., 1996; Kawaguchi et al., 1998; Xu and Yu, 1997).

- Some studies developed models for vibrated beds, which are frequently used to fluidize granular materials, which cannot be easily fluidized by air (Yang and Hsiau, 2000; Shishodia et al., 2001)

- More recently, studies focused on the modeling of more complex mixer geometries, such as the helical ribbon mixer (Kaneko et al., 2000), the flat-bladed stirrer (Stewart et al., 2001) and tumbler mixers (Moakher et al., 2000).

The disadvantage of discrete particle modeling is that the computation time increases quickly with the size of the system. The use of discrete particle modeling to study systems with many particles is thus limited ($N < 1 \cdot 10^5$). In the discrete particle model that was developed in this study, the wheat grains were described as spherical particles in order to minimize computational effort. If ellipsoidal or irregularly shaped particles need to be implemented, computational effort may increase with a factor 10 (Ristow, 1994). The assumption of spherical particles in the model was found to be valid, since the model predictions generally matched the experimental results well.

The discrete particle approach cannot only predict mixing and flow behavior of granular systems, but is also suited for prediction of coupled phenomena such as heat and mass transfer and (de)agglomeration processes. In this thesis the discrete particle model is extended to describe conductive heat and water transfer, substrate aggregation due to aerial hyphae and heat and moisture exchange between the continuous air phase and the solid-substrate particles. The discrete particle approach facilitates fast implementation of models at the particle scale. Only recently, other studies have also reported discrete particle modeling of heat and mass transfer processes (Hunt, 1997; Kaneko et al., 1999; Li and Mason, 2000; Li and Mason, 2002). Cohesive forces between particles have been implemented to describe the fluidization dynamics of sticky powders (Mikami et al., 1999). A number of studies investigated the effect of impact of powder agglomerates on a target surface (Ning et al., 1997; Thornton et al., 1999). A first attempt has been made to model the granulation process, in which particles are agglomerated by addition of a binder liquid, in a rotating drum (Mishra et al., 2002) and in a fluidized bed (Goldschmidt, 2001).

It can be concluded that the discrete particle modeling approach has only recently become feasible as a method suitable for prediction of complicated processes that occur during handling of granular materials. One of the main reasons for this is that the ever-increasing computational power of the current computers allows us to perform calculations, which previously resulted in unrealistic computation times. Given the state of the art in this area, and the many phenomena that play a role during SSF (mechanical mixing, heat and mass transfer, biological growth, etc.) the discrete particle approach seems to be a very promising approach also for this process.

Outline of this thesis

The general aim of this research project was to acquire more fundamental knowledge about the effect of mixing on spatial gradients in temperature, moisture and fungal growth during SSF and vice versa. This knowledge should lead to overall recommendations for rational design and scale-up of mixed solid-state fermenters. The discrete particle approach was used to develop non-empirical models.

In chapter 2, the development of a discrete particle model is described, predicting radial mixing of substrate particles in a 2D rotating drum. To validate the model predictions, a rotating drum with colored wheat grains and image analysis techniques were used.

Subsequently, the discrete particle model was extended to three dimensions to study the axial mixing behavior in rotating drum fermenters (Chapter 3). Several baffle designs were investigated for their influence on the radial and axial mixing behavior.

Besides mixing in a rotating drum, also the mixing behavior in a helical blade mixer was studied (Chapter 4). Helical blade mixers are promising solid-state fermenters, since forced

aeration can be easily applied and mixing is claimed to be gentle. In this study the model predictions were compared to positron emission particle tracking (PEPT) measurements (Parker et al., 2002). The PEPT measurements facilitated non-invasive measurements of flow behavior inside the mixer by tracking the movements of one tracer particle.

Chapter 5 then describes the extension of the 2D discrete particle model of the rotating drum with heat and water transfer. Efficient removal of metabolic heat during SSF is important to reduce the occurrence of temperature gradients in the bed. There are two main heat removal mechanisms, conductive and evaporative cooling. The conductive cooling mechanism is modeled by interparticle and particle-wall heat transfer. The effect of desiccation due to the evaporative cooling on fungal growth can be considerable, since evaporative cooling is the main mechanism for heat removal in large-scale fermenters. To avoid growth limitations due to lowered water activities, water can be added via spray nozzles to the substrate bed. In an extension of the discrete particle model, the absorption of water into particles and the transfer of sprayed water between particles during the addition of water were included. The model predictions were validated with a fluorescent tracer in the spraying liquid.

In chapter 6 we performed several fermentations in a newly developed drum fermenter set-up to study the influence of aerial hyphae, holding particles together, on mixing behavior. To implement the influence of the aerial hyphae in the discrete particle model, it was needed to quantify the tensile strength of hyphal bonds in SSF. A novel experimental set-up to measure the tensile strength was developed: *A. oryzae* was cultivated between two wheat dough disks and the tensile strength of the aerial mycelium was measured with a texture analyzer.

In the final chapter the discrete particle model was extended with a continuum-based model for the air phase in the rotating drum, which is important for the description of evaporative cooling. Since evaporative cooling is the main mechanism for heat removal during SSF, evaluation of design and scale-up parameters of mixed solid-state fermenters is difficult without taking into account evaporative cooling.

References

Biesebeke te R, Ruijter G, Rahardjo YSP, Hoogschagen MJ, Heerikshuisen M, Leven A, Driel van KGA, Schutyser MAI, Dijksterhuis J, Yang Z, Weber FJ, Vos de WM, Hondel KAMJJ , Rinzema A, Punt PJ. 2002. *Aspergillus oryzae* in solid-state and submerged fermentation. FEMS Yeast Research 2:245-248.

Buchholtz V, Pöschel T, Tillemans H. 1995. Simulation of rotating drum experiments using non-spherical particles. Physica A 216:199-212.

Cleary PW, Metcalfe G, Liffman K. 1998. How well do discrete element granular flow models capture the essentials of mixing processes? App Math Model 22:995-1008.

Cundall PA, Strack ODL. 1979. A discrete numerical model for granular assemblies. Géotechnique 29:47-65.

Dury CM, Ristow GH. 1997. Radial segregation in a two-dimensional rotating drum. J Phys I 7:737-745.

Dury CM, Ristow,GH. 1998. Flow dynamics of binary mixtures in rotating drums, ICMF, Lyon, France.

Goldschmidt, MJV. 2001. Hydrodynamic modelling of fluidised bed spray granulation. Ph.D. Thesis, University of Twente.

Hoomans BPB, Kuipers JAM, Briels WJ, Swaaij van WPM. 1996. Discrete particle simulation of bubble and slug formation in a two-dimensional gas fluidised bed: a hard sphere approach. Chem Eng Sci 51:99-118.

Hunt ML. 1997. Discrete element simulations for granular material flows: Effective thermal conductivity and self-diffusivity. Int J Heat and Mass Transfer 40:3059-3068.

Kaneko Y, Shiojima T, Horio M. 1999. DEM simulation of fluidized beds for gas-phase olefin polymerization. Chem Eng Sci 54:5809-5921.

Kaneko Y, Shiojima T, Horio M. 2000. Numerical analysis of particle mixing characteristics in a single helical ribbon agitator using DEM simulation. Powder Technol 108:55-64.

Kawaguchi T, Tanaka T, Tsuji Y. 1998. Numerical simulations of two-dimensional fluidized beds using the discrete element method (comparison between the two- and three-dimensional models). Powder Technol 96:129-138.

Langston PA, Tüzün U, Heyes DM. 1995. Discrete element simulation of granular flow in 2D and 3D hoppers: Dependence of discharge rate and wall stress on particle interactions. Chem Eng Sci 50:967-987.

Li J, Mason DJ. 2000. A computational investigation of transient heat transfer in pneumatic transport of granular particles. Powder Technol 112:273-282.

Li J, Mason DJ. 2002. Application of the discrete element modelling in air drying of particulate solids. Dry Technol 20:255-282.

Meien von OF, Mitchell, DA. 2002. A two-phase model for water and heat transfer within an intermittently-mixed solid-state fermentation bioreactor with forced aeration Biotechnol Bioeng 79:416-428

McCarthy JJ, Khakhar DV, Ottino JM. 2000. Computational studies of granular mixing. Powder Technol 109:72-82.

Mikami T, Kamiya H, Horio M. 1999. Numerical simulation of cohesive powder behavior in a fluidized bed. Chem Eng Sci 53:1927-1940.

Mishra BK, Thornton C, Bhimji D. 2002. A preliminary numerical investigation of agglomeration in a rotary drum. Min Eng 15:27-33.

Moakher M, Shinbrot T, Muzzio FJ. 2000. Experimentally validated computations of flow, mixing and segregation of non-cohesive grains in 3D tumbling blenders. Powder Technol 109:58-71.

Nagel FJI. 2002. Process control of Solid-State Fermentation. Ph.D. Thesis, WUR.

Nagel FJI, Tramper J, Bakker MSN, Rinzema A. 2001. Temperature control in a continuously mixed bioreactor for solid-state fermentation. Biotechnol Bioeng 72:219-230.

Ning Z, Boerefijn R, Ghadiri M, Thornton C. 1997. Distinct element simulation of impact breakage of lactose agglomerates. Adv Powder Technol 8 :15-37.

Pandey A. 2003 Solid-state fermentation. Biochem Eng J 13:81-84.

Parker DJ, Forster RN, Fowles P, Takhar PS. 2002. Positron emission particle tracking using the new Birmingham positron camera. Nuclear Instruments And Methods In Physics Research Section A Accelerators Spectrometers Detectors And Associated Equipment 477:540-545.

Rahardjo YSP, Weber FJ, Comte le EP, Tramper J, Rinzema A. 2002. Contribution of aerial hyphae of *Aspergillus oryzae* to respiration in a model solid-state fermentation system. Biotechnol Bioeng 78:539-544.

Ristow GH. 1994. Granular Dynamics: A Review about recent Molecular Dynamics simulations of granular materials. In: Staufferd D, editors. Annual Reviews of Computational Physics.World Scientific. p 275-308.

Roussos S, Raimbault M, Prebois J-P, Lonsane BK. 1993. Zymotis, a large scale solid state fermenter. Appl Biochem Biotechnol 42:37-52.

Sargantanis J, Karim MN, Murphy VG, Ryoo D. 1993. Effect of operating conditions on solid substrate fermentation Biotechnol Bioeng 42:149-158

Schutyser MAI, Padding JT, Weber FJ, Briels WJ, Rinzema A, Boom R. 2001. Discrete particle simulations predicting mixing behavior of solid substrate particles in a rotating drum. Biotechnol Bioeng 75:666-675.

Shishodia N, Wassgren CR. 2001 Particle segregation in vibrofluidized beds due to buoyant forces. Phys Rev Lett 87:084302,1-4

Stewart RL, Bridgwater J, Zhou YC, Yu AB. 2001. Simulated and measured flow of granules in a bladed mixer - a detailed comparison. Chem Eng Sci 56:5457-5471.

Takamine J. 1914. Enzymes of Aspergillus oryzae and the application of its amyloclastic enzyme to the fermentation industry. J Ind Eng Chem 6:824-829.

Thornton C, Ciomocos MT, Adams MJ. 1999. Numerical simulations of agglomerate impact breakage. Powder Technol 105:74-82.

Weber FJ, Oostra J, Tramper J, Rinzema A. 2002. Validation of a model for process development and scale-up of packed-bed solid-state reactors. Biotechnol Bioeng 77:381-393.

Wightman C, Moakher M, Muzzio FJ, Walton OR. 1998. Simulation of flow and mixing of particles in a rotating and rocking cylinder. AIChE J 44:1266-1276.

Wightman C, Muzzio FJ. 1998. Mixing of granular material in a drum mixer undergoing rotational and rocking motion II. Segregating particles. Powder Technol 98:125-134.

Xu BH, Yu AB. 1997. Numerical simulation of the gas-solid flow in a fluidized bed by combining discrete particle method with computational fluid dynamics. Chem Eng Sci 52:2785-2809.

Yamane K, Nakagawa M, Altobelli SA, Tanaka T, Tsuji Y. 1998. Steady particulate flows in a horizontal rotating cylinder. Phys Fluids 10:1419-1427.

Yang SC, Hsiau SS. 2000. Simulation study of the convection cells in a vibrated granular bed. Chem Eng Sci 55:3627-3637.

Chapter 2

Discrete particle simulations predicting mixing behavior of solid substrate particles in a rotating drum fermenter

Abstract

A soft-sphere discrete particle model was used to simulate mixing behavior of solid substrate particles in a slow rotating drum for solid-state fermentation. In this approach, forces acting on and subsequent motion of individual particles can be predicted. The (2D) simulations are qualitatively and quantitatively validated by mixing experiments using video and image analysis techniques. It was found that the simulations successfully predicted the mixing progress as a function of the degree of filling and size of the drum. It is shown that only relatively large straight baffles perpendicular to the drum wall (67% of the drum radius) increase the mixing performance of the rotating drum. Considering the different aspects of mixing dealt with in this work, it is concluded that the soft-sphere discrete particle model can serve as a valuable tool for investigating mixing of solid substrate particles. Finally, it is expected that this model may evolve into a potential tool for design and scale-up of mixed solid-state fermenters.

Introduction

Solid-State Fermentation (SSF) involves the cultivation of microorganisms on moist solid substrates in the absence of free-flowing water. SSF is an emerging fermentation technology, although its roots date back many ages (Vollbrecht, 1997). Typical fermented foods produced by SSF are, for instance, Tempe and soy sauce. In the last decade, SSF has gained renewed interest due to its potential for, e.g. the production of fungal spores as biological control agents (Weber et al., 1999), bioconversion of solid wastes (Stuart et al., 1998), and the production of secondary metabolites (Barrios-Gonzáles and Mejía, 1996). However, large-scale SSFs are still scarcely used in industry, as design and operation rules for large-scale solid-state fermenters are still absent.

A critical issue is heat accumulation. Heat removal is of great importance because high local temperatures inhibit microbial growth. The main cooling mechanisms employed in SSF systems are conductive cooling in tray fermenters and evaporative cooling in aerated packed beds (Weber et al., 1999). However, for fast growing fungi like *Aspergillus oryzae,* conduction imposes severe constraints on the tray dimensions. A disadvantageous side effect of evaporative cooling is that it results in shrinkage of the substrate, with subsequent channeling in the bed and critically low water activity (Weber et al., 1999). To circumvent these problems, mixed systems, which offer better control of temperature and moisture content, have been developed (Nagel et al., 2001). They show for a horizontal paddle mixer that a combined temperature and moisture content control strategy leads to a high growth rate of *Aspergillus oryzae*.

Unfortunately, disadvantages of mixed systems have also been reported. Some authors consider shear forces, even during gentle mixing, to be responsible for inhibiting or slowing down fungal growth (Han et al., 1999). Especially during the initial mixing period, germinating, hyphae may be damaged due to shear (Fung and Mitchell, 1995). However, in other research mixing did not seem to impede fungal growth at all and, in some cases, even stimulated production of secondary metabolites (Marsh et al., 1998).

We believe that acquiring detailed knowledge of the fundamentals of the mixing process in SSFs will help to understand these nontrivial effects of mixing. Therefore, we focused our research on the mixing behavior of solid-substrate particles in the absence of microorganisms. Experiments were conducted in a rotating drum (with and without baffles) with moistened and autoclaved wheat grains. The rotating drum was chosen because of its simplicity (with respect to modeling) and its potential for large-scale SSF. In the past, the application of slowly rotating drums for SSF, has not always been successful, which was partially due to the use of substrate particles with pronounced adhesive properties, such as steamed rice, wheat bran, or soybeans (Mitchell et al., 2000). Because of these adhesive particle properties the bed may undergo a slumping flow regime, in which the bed as a whole slides down the internal interface of the

drum. Recently, our group found (using a paddle stirrer) that if non-adhesive whole-wheat kernels are used as substrate particles, particles do not stick to each other during fermentation, which leads to optimal mixing behavior and control (Nagel et al., 2001).

Important operating parameters (e.g. degree of filling and rotation rate) of the rotating drum were evaluated. These parameters have direct effect on heat transfer, mass transfer, mixing and shear in the bed and as a consequence influence the local environment experienced by the microorganism (Marsh et al., 1998; Stuart et al., 1998). In order to evaluate the latter operating parameters, data was obtained on the mixing behavior by video and image analysis. These experimental data were compared with the predictions of soft-sphere discrete particle simulations (DPS). In the DPS, individual particle interactions, which are specific for the physical characteristics of the particles, and subsequent movements are calculated. This approach has shown to be successful in providing insight in the dynamics of mixing in particle systems (McCarthy et al., 1996). The ever-increasing power and efficiency of computers make this computationally intensive method feasible. In this article soft-sphere DPS are proposed as a tool for studying mixing of nonadhesive solid substrate particles (wheat grains) in a rotating drum. In addition, we report the influence of baffles and process scale of the drum on mixing performance.

Model development

Discrete particle simulations

The mixing process of a wheat bed in a rotating drum was modeled using a discrete particle model. Various discrete particle simulation methods have been shown to provide a convenient way to study granular flow. Among these are Monte Carlo simulations (Rosato, 1986), cellular automata models (Ktitarev and Wolf, 1998), and bottom-to-top restructuring (Baumann et al., 1994). However, the most widely used simulation method is based on molecular dynamics simulations in which interaction forces are modeled on individual grain particles. This method is called granular dynamics (Ristow, 1994). In these simulations particle motion is calculated directly without prior knowledge of experimental data about the particle flow. One of the limitations is that these calculations are computationally very extensive and therefore the number of particles involved is still limited ($<10^6$).

The modeling approaches adopted in granular dynamics simulations can be roughly divided into two groups, depending on the density and character of the granular flow modeled. A hard-sphere particle approach for low-density, fast flow; and a soft-sphere particle approach for high density, slow flow (the *quasi-static regime*). In the hard-sphere approach, instantaneous, impulsive collisions are assumed. Characteristic for this approach is that a sequence of collisions is processed, one collision at a time (i.e. event-driven). In the soft-sphere approach

particle movements are calculated by integrating Newton's equation of motion, where a contact dependent force law describes the forces on the particles. Cundall and Strack (1979) were among the first to develop a simulation method based on this approach.

During contact, particles are allowed to deform, or, in computational terms, to overlap, and the resulting force is a repulsive force combined with a damping term to provide inelasticity. The tangential or shear force is modeled using a combination of a viscous force and a dynamic friction.

In various recent studies, this soft-sphere simulation method was applied for studying the dynamics of particle flow, e.g. in rotating drums (Dury and Ristow, 1997), fluidized beds (Hoomans, 2000; Mikami, 1998), hopper flow (Ristow, 1994), pipe flow (Tsuji et al., 1992), silo filling (Cleary, 2000), and tumbling blenders (Moakher et al., 2000). Most of these studies are in the field of powder technology and focus on granular flow of fine powders or dry particulate mixtures. Similarities between mixing of powders and mixing of solid substrate particles during SSF lead us to believe that this simulation method is a promising tool for studying mixing in SSF.

Contact calculations in granular dynamics simulations

In this study, we focus on radial mixing, since this is the dominant mode of mixing in the fermenter geometries considered. It is assumed that the flow in the radial direction, as observed from the sides of the drum, is in fact only a two-dimensional flow. Mixing in the axial direction of the drum is considered to be much slower than radial mixing (Prigozhin and Kalman, 1998). For this reason simulations are conducted for two dimensions.

The contact forces (i.e. particle-particle and particle-wall contact) are modeled in a similar way. The particle-particle contact calculations are explained further. The wheat grain particles are modeled as spherical particles of similar size (monodispersed). The contact between two particles is detected by calculation of the distance between the centers of both particles ($\vec{r_{ij}} = \sqrt{r_{ijx}^2 + r_{ijy}^2}$). If two particles are in contact, their computational overlap (δ) is defined as $\delta = \sigma - \left|\vec{r_{ij}}\right|$, where σ is the diameter of the particles. When the two particles come into contact two forces arise, one directed along the axis through the center of the particles (normal forces) and one that is normal to this axis (tangential forces). Since we deal with inelastic collisions, the normal contact force model requires two terms: repulsion and some sort of dissipation. Therefore the normal contact force ($\vec{F_n}$) is calculated according to the following force model (also known as linear-dashpot or damped harmonic oscillator force):

$$\vec{F}_n = \left(-k_n \delta \; - \eta_n \left(\vec{v}_{rij} \cdot \vec{n}_{ij} \right) \right) \vec{n}_{ij} \qquad (1)$$

in which: k_n is the stiffness coefficient (N·m^{-1}); η_n is the normal damping coefficient (kg·s^{-1}) ; v_{rij} is the normal velocity difference (m·s^{-1}); n_{ij} is the normal unit vector (-).

The first term describes an elastic, repulsive contact force. The stiffness coefficient can be determined experimentally through compression-force experiments. The second term models a viscous damping force. The advantage of this contact model is that its analytical solution (with initial conditions $\delta_{(t=0)} = 0$ and $v_{rij(t=0)} = v_i$) allows the calculation of the restitution coefficient (e_v), which represents the relative velocity that remains after a collision has taken place (i.e., it is a measure of elasticity) (Hoomans, 2000; Schäfer et al., 1996):

$$e_v = \exp\left(\frac{-\eta_n}{m} t_n \right) \qquad (2)$$

where

$$t_n = \pi \left(\frac{2k_n}{m} - \left(\frac{\eta_n}{m} \right)^2 \right)^{-1/2} \qquad (2a)$$

in which: t_n is the duration of a collision (s) and m is the mass of the particle (kg).

If the restitution coefficient can be determined experimentally and the stiffness coefficient is known, one can derive the normal damping coefficient.

A priori, we expect that the tangential friction force ($\vec{F}_s$) is described by Coulomb's law of friction (Fig. 1) (Schäfer et al., 1996):

$$\vec{F}_s \leq \mu_s \vec{F}_n \text{ for static friction } (v_{sij} = 0)$$

$$\vec{F}_s = \mu_d \vec{F}_n \text{ for dynamic friction } (v_{sij} \neq 0) \qquad (3)$$

in which: μ_s is the static friction coefficient (-); μ_d is the dynamic friction coefficient (-); $\vec{v}_{sij} = \vec{v}_{rij} - (\vec{v}_{rij} \cdot \vec{n}_{ij}) \vec{n}_{ij}$ is the relative tangential velocity. The "$\leq$" symbol in the first line of Eq. 3 means that in case $v_{sij} = 0$ the tangential force F_s acts as a reaction force; when this reaction force exceeds $\mu_s F_n$ the second line of Eq. 3 applies.

Since this interaction model is difficult to incorporate in its complete form, we have followed Schäfer et al. (1996) in using an approximation (Eq. 4) in the form of a combination of a viscous friction and a dynamic friction (Fig. 1):

$$\vec{F}_s = -\min\left(\left| \gamma_s v_{sij} \right|, \left| \mu_d F_n \right| \right) \cdot \text{sign}(\vec{v}_{sij}) \qquad (4)$$

in which: γ_s is the viscous friction coefficient (kg·s^{-1}).
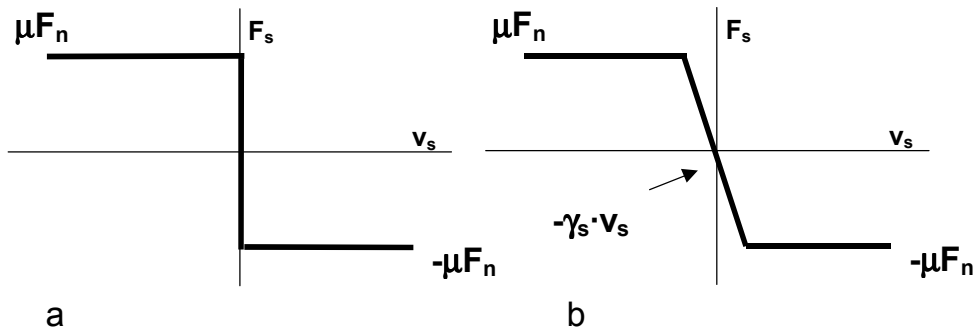
Figure 1. Tangential interaction at constant normal force a) Coulomb's interaction law b) combined viscous and dynamic friction model.

It should be emphasized that this model is a regularized model to simplify the numerical integration of Newton's equations of motion. The first term of Eq. 4 describes a simple viscous friction force, which is proportional to the relative tangential velocity. Using this force, the deceleration of a particle is a linear function of the initial velocity and therefore the particle velocity will be slowed down to zero. The second term describes a dynamic friction force, which results in a finite tangential velocity after collision. The transition between the two forces is governed by the values of μ_d and γ_s. In this study it appeared that this simple approach already gave an adequate description of the mixing behavior of our particulate system. A limitation of this tangential force model is the absence of static friction, which is present at $v_{sij} = 0$ in order to withstand gravitational force components in the tangential direction of the contacts.

Materials and Methods

Simulation method

The initial conditions for the simulations were obtained according to the following. The particles were placed in the drum and were allowed to fall freely under the influence of gravity. This resulted in a bed of particles at the bottom of the drum, which was used as the initial condition for simulation.

The trajectories of the particles were calculated according to the following procedure. Starting from the initial condition, for each individual particle all forces are calculated. The acceleration (a) can be calculated from the resulting force (F) acting on the particle using the simple Newton's second law $a = \dfrac{F}{m}$. Subsequently, the Newtonian equations of motion are integrated using a leap-frog algorithm to obtain the new velocity and position of each particle (Allen and Tildesly, 1987). Knowing the new positions of the particles, the calculation procedure is restarted by updating all the forces. To minimize the amount of time spent detecting contacts, a

neighbor list is constructed. This neighbor list contains the identification numbers of neighboring particles for each particle. Particles located within the 'cutoff' distance from a given particle are considered to be part of that particle's neighbor list. Whenever a particle moves a distance larger than the cutoff distance, the neighbor list is reconstructed.

The time step, which determines when to update forces and integrate the equations of motion, is an important model parameter. If too-large time steps are applied unrealistic overlaps may occur and as a consequence erroneous trajectories of particles may be predicted. Schäfer et al (1996) developed a criterion to prevent this: an accurate simulation (reproducing the analytic e_v with relative errors of the order 10^{-4}) requires a time step $\Delta t = t_n/100$ (Schäfer et al., 1996). According to this criterion we applied a time step of $2 \cdot 10^{-5}$ sec., which guaranteed computational stability.

The code for the granular dynamics simulations used in this study is an adapted molecular dynamics code (Fortran 90) (Allen and Tildesly, 1987). The simulations were conducted on a XP1000 ALPHA workstation.

Entropy of mixing calculations

To examine the evolution of the mixing process for both experimental and computational results, we defined the entropy of mixing as a degree of mixedness. In previous research the degree of mixedness was usually based on variance or standard deviation of samples (Muguruma et al., 1997; Hogg et al., 1966). The main reason for choosing the entropy of mixing as a degree for mixing is that this scale is more convenient for interpretation. We used
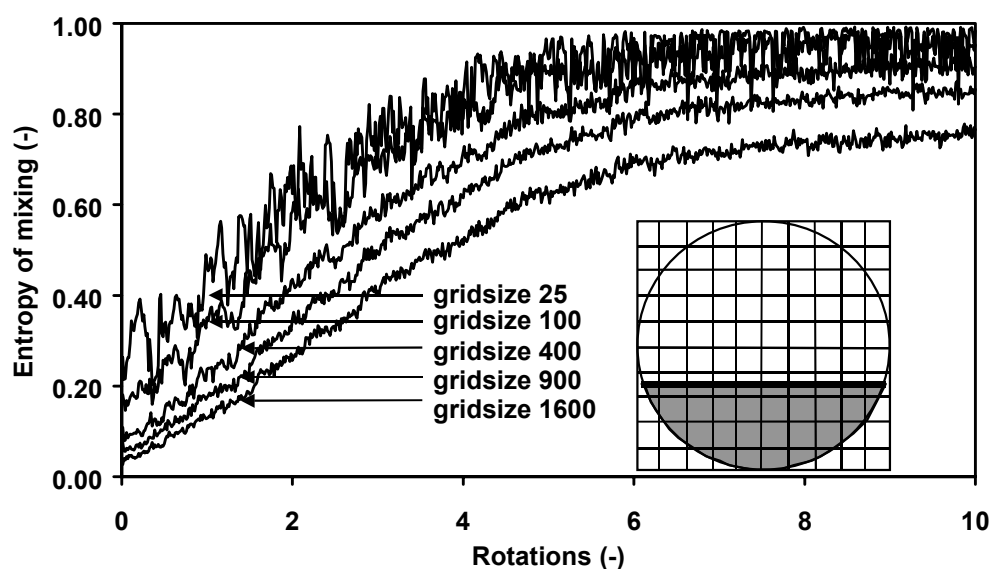
Figure 2. Effect of the grid on the calculated entropy of mixing.

two colored fractions, initially present as two horizontal layers. The entropy of mixing calculations started by defining a grid of size (I,J) across the drum (Fig. 2). Subsequently, for each grid cell local entropies of mixing ($S(i,j)$) were calculated according to:

$$S(i, j) = x_1(i, j)log(x_1(i, j)) + x_2(i, j)log(x_2(i, j)) \qquad (5)$$

in which: $x_1(i,j)$, $x_2(i,j)$ are the fractions of the colored particles in cell (i,j).

Subsequently the local entropies of mixing were summed to obtain the total entropy of mixing (S_{tot}) at a certain moment of rotation:

$$S_{tot} = \frac{1}{S_0} \sum_{i,j} S(i, j) \cdot \frac{N_{cel}(i, j)}{N} \qquad (6)$$

in which: S_o is the entropy of a randomly mixed system, which depends on the fraction of colored particles in the system; $N_{cel}(i,j)$ is the number of particles in cell (i,j); N is the total number of particles in the system. The ratio of the number of particles in one cell and the total number of particles is applied to correct for cells with a relatively small overall number of particles.

For the experimental results, the colored pixels are regarded instead of the particles as a whole. The reason for this is that the image analysis software cannot recognize the particles individually.

The entropy of mixing values are affected by measurement parameters such as the sample size (number of particles in one cell) and the number of cells containing particles, both for simulation and experiment (Fig. 2). The noise in the entropy of mixing data is larger when fewer samples are drawn. For most calculations we used a number of 100 grid cells and a constant sample size of about 40 particles. If the sample size is too small the entropy of mixing does not approach a value of unity (perfectly mixed condition). The initial entropies are not equal to zero, which is explained by the presence of grid squares overlapping the border of the two colored layers and the finite number of samples. Thus, to obtain accurate data it is important to study a system containing a large number of particles.

Experimental setup

The wheat grains used in all the experiments are from one single batch of commercial origin (Blok, Woerden, NL). The wheat grains were treated according to a method used to prepare substrate particles for SSF. The whole wheat grains were soaked for 2.5 h in excess tap water of 60 °C to give a final moisture content of 0.87 kg w / kg DM. Subsequently, the soaked grains were sieved and autoclaved for 1 h at 121 °C. Methylene blue (Merck, Germany) and Bengal rose B (Fluka, Switzerland) were used for coloring the two grain fractions. Two Perspex drums, rotating on a horizontal table, were used with an internal diameter of 0.148 m and 0.3 m (length:

0.21 m and 0.4 m), respectively. The latter drum was designed at a similar scale as the bioreactor used in previous research (Nagel et al., 2001). Most of the mixing experiments were conducted at a low rotation rate of 0.5 rpm.

For data acquisition a webcam (Philips USB PC Camera) was used with an image resolution of 640 x 480 pixels. Good lighting and the use of appropriate dyes for the wheat grains were found to be critical for the image processing of the acquired pictures (using Matlab 5.3 with image processing toolbox). The two colored fractions were separated by applying proper color threshold values, which were found through visual observation. The experimental setup and image processing methods provided reliable and reproducible data for the calculation of the mixing progress in terms of entropy of mixing.

## Results and Discussion

Model parameters

The relations (Eqs. 1, 4) that describe the interparticle and particle-wall interactions contain a number of parameters (Table I). In our approach we assume that the grains are spherical particles with a diameter (d_p) equal to the average equivalent diameter of moistened wheat grains ($d_e = \sqrt[3]{6m/\rho\,\pi}$ where ρ is the volumetric weight (= density) and m is the mass of the body). In experiments we observed that most of the particles in the top layer are sliding and not rotating. We approximated these conditions by using particles without rotation rather than particles with rotation (Dury and Ristow, 1997).

During collision of two bodies, two types of forces may occur: forces directed along the axis through the center of the particles (normal forces), and forces that are normal to this axis (tangential forces).

For simplicity, normal interparticle and particle-wall interactions were assumed to be of similar form and size during contact. The repulsion on contact could be measured in compression experiments with single wheat grains (Fig. 3). The force applied on the wheat grain (lying flat) was measured during contact as a function of the displacement of the flat plate. The initial reversible deformation of the wheat grain was interpreted as elastic deformation. During this initial contact the deformation or compression was estimated not to exceed more than 5 % of the diameter of the particle. The slope is a measure of the resistance of the wheat grain during elastic contact (Fig. 3). It was observed that the force is not linearly increasing, even for the initial contact. This was expected, since even for perfect spheres the force increases non-linearly due to the increasing contact area (Rajamani et al., 2000). However, to minimize computational effort a linear relationship was assumed. The stiffness coefficient (k_n) is

Table I. Simulation parameters.

Description	Value
Particle diameter, d_p (m)	$4.9 \cdot 10^{-3}$
Particle mass, m (kg)	$7.2 \cdot 10^{-5}$
Stiffness coefficient, k_n (N/m)	125
Damping coefficient, η_n (kg/s)	0.079
Restitution coefficient, e_v (-)	0.1
Dynamic interparticle friction, μ_{pp} (-)	0.5
Dynamic particle-wall friction, μ_{pw} (-)	1.5
Viscous interparticle friction, γ_{pp} (kg/s)	1.0
Viscous particle-wall friction, γ_{pw} (kg/s)	3.0
Time step, dt (s)	$2 \cdot 10^{-5}$
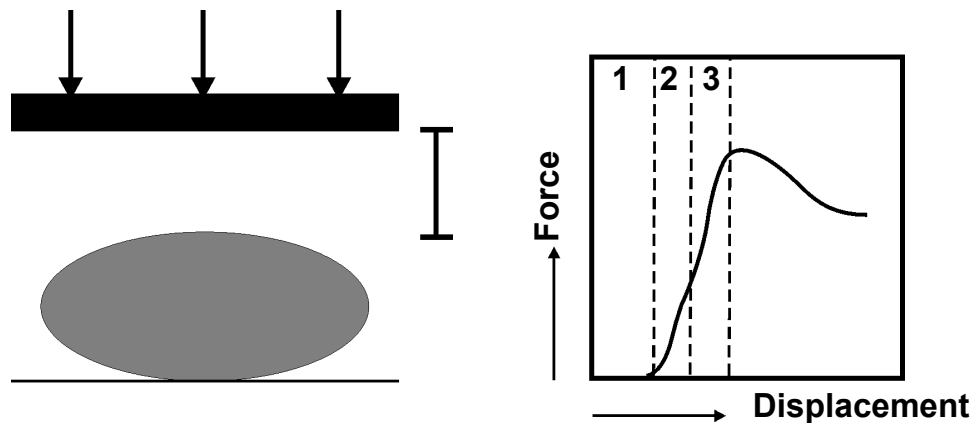
Figure 3. Schematic drawing of a single wheat grain compression experiment and a force-displacement plot in which: 1) contact 2) onset of plastic deformation 3) yield point.

estimated by averaging the results of several experiments, taking the average slope during initial compression.

At further compression plastic deformation takes place. At even further compression, at a certain point the repulsive force decreases or remains constant with increasing deformation. This point is referred to as the yield point and is an indication for initial cell rupture. It is a measure for the sensitivity to damage (Sitkei, 1986).

A rough estimate could be made of the restitution coefficient (e_v) by measurement of the maximum height that particles rebound when dropped onto a plane surface formed from the same material (Boateng and Barr, 1997). Besides the fact that these measurements are not trivial, the restitution coefficient for anistropic particles also depends on orientation. For these

reasons a restitution coefficient of 0.1 was estimated, based on the observation that the relative rebound height of a dropped moistened wheat grain was roughly 10%. The normal damping coefficient (η) during contact could be derived from the stiffness coefficient and the restitution coefficient by analytically solving the normal force equation (Eq. 2, 2a) (Hoomans, 2000; Schäfer et al., 1996).

The tangential friction force in our model is described by a combination of a steep viscous friction and a dynamic friction (Eq. 4) (Schäfer et al., 1996). The dynamic friction force is calculated with a realistic friction coefficient (μ_{pp}) of 0.5; the value of this friction coefficient is in the range of values (0.3 – 0.5) reported before (McCarthy and Ottino, 1998; Tsuji et al., 1992). The tangential particle-wall interaction is modeled using a higher friction coefficient (μ_{pw}) of 1.5. If a much lower friction coefficient is chosen, unrealistic slip of the particles over the surface of the drum occurs. The parameter describing the viscous friction force (γ_{pp} and γ_{pw}) is chosen to be twice as high as the corresponding friction coefficient (respectively, 1.0 and 3.0), based on qualitative observations of the simulated mixing progress. These values are in the range (1 - 20 kg/s) of the values used by Schäfer et al. (1996).

Visual observations of experiment and simulation

For dry wheat grains we observed that most particles in the top layer (surface) are sliding down continuously. Below the top layer (a few grains thick) the bed of wheat grains rotates as a solid body around the horizontal axis. More interesting for us is the flow of soaked, autoclaved wheat grains, since these are substrate particles for SSF. For these particles a similar flow pattern is observed, although the flow in the top layer changed slightly and showed more avalanche behavior (i.e., sudden movement of a collection of particles, some time after which no particles are moving). We found that a relatively simple granular dynamics model is able to predict the essentials of the flow dynamics of moistened wheat grains in a rotating drum. Especially the prediction of a solid body rotating around the horizontal axis and a top layer, which is only a few grains thick, shows that the model is capable of capturing the dynamics of this particulate system.

In the experiments, we observed avalanches at the surface, while our model predicts an almost continuous slow flow downhill. These avalanches occur probably due to the presence of moisture at the surface and the stickiness (starch residues) of the soaked and autoclaved wheat grains, while in the model no attractive forces are yet incorporated. Small deviations in the simulated flow (primarily in the middle of the bed) occur, probably due to the use of a viscous friction in our model instead of a static friction. The simulated angle of repose (the steepest angle of the surface at which the grains remain standing, rather than sliding or crumbling away) is found to be smaller than in the experiment, because of 1) again, the absence of static friction
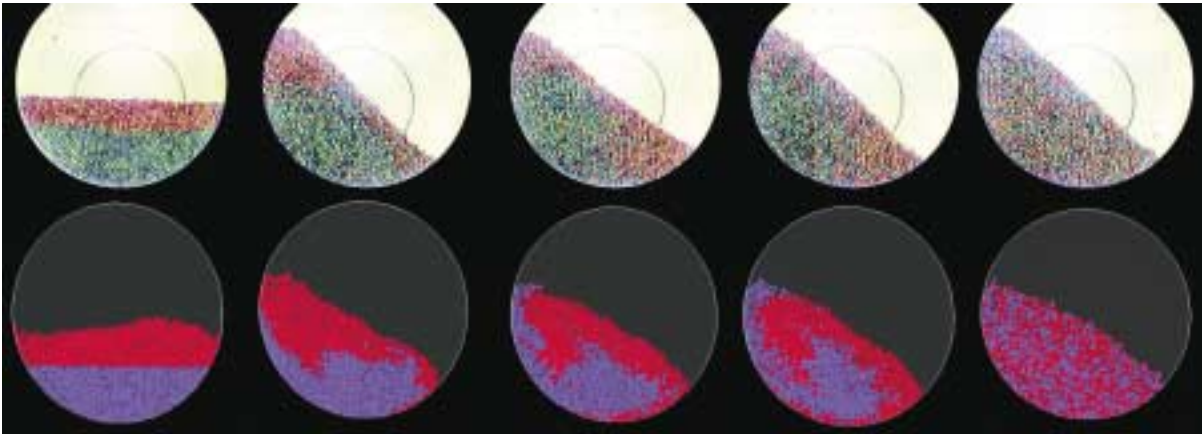
Figure 4. Comparison of simulation (below) and experimental results (above) at 0, 1, 2, 3 and 10 rotations for ε = 0.4 and rotation speed of 0.5 RPM.
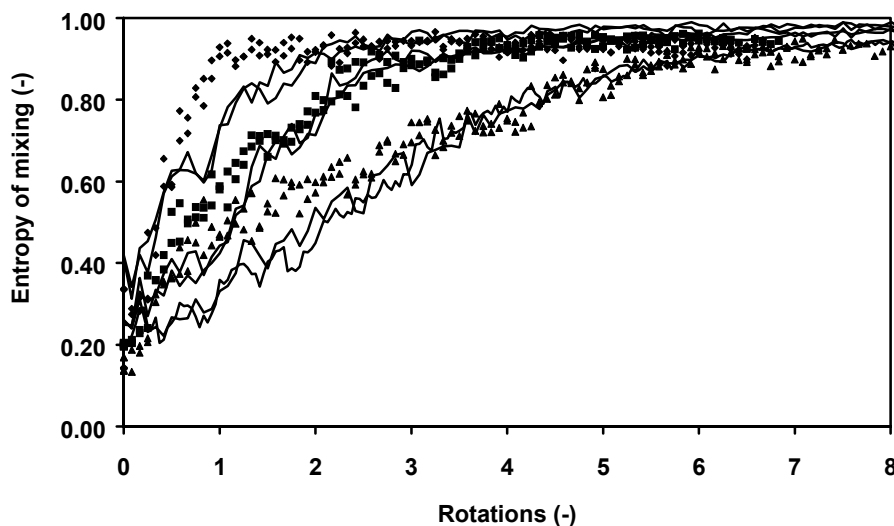
Figure 5. Comparison of simulation (lines) and experimental results (dots) for mixing progress (in terms of entropy) in a rotating drum for different fill levels (diameter 30 cm, 0.5 rpm). ▲ ε = 0.4, N=1364 ■ ε = 0.33, N = 1137 ◆ ε = 0.2, N=682.

and 2) the fact that in the experiment the particles are ellipsoidal and slightly cohesive, while the particles in the model are spherical and no attractive forces were included in the model.

We emphasize that it is important to keep the model as simple as possible. Therefore, although this model still may be improved, we will show that this relatively simple model can be used to evaluate many aspects in mixing of wheat grains in a rotating drum.

Evaluation of the mixing performance in a rotating drum

Our model calculations give accurate predictions of particulate mixing of wheat grains in a rotating drum at slow rotation. We conducted simulations and validation experiments for three

Table II. Mixing time as a function of scale and fill level.

Diameter of the drum (m)	Fill level, ε (-)	Top area / volume ratio of the bed (m^{-1})	Mixing time[1] (rotations)
0.3	0.2	18.5	1.5
0.3	0.33	12.3	3
0.3	0.4	10.5	6
0.15	0.33	24.8	1.5
0.3	0.33	12.3	3
1	0.33	3.7	10

The top area / volume ratio values are calculated according to formula A4 in the Appendix.
[1] The mixing time is estimated at an entropy of mixing value of 0.9.

different fill levels (ε = 0.2, 0.33, and 0.4), defined as the volume fraction of the total reactor that is occupied by the load (see Appendix).

Qualitative validation of our simulations is shown in Figure 4 for fill level 0.4 with pictures of simulation and experiment after several rotations. The predictions of the model show good agreement with the experimental results. In Figure 5 the entropy of mixing (Eqs. 5, 6) is given as a function of the number of rotations for both experiments and simulations. From this figure we can conclude that the model predictions are also quantitatively confirmed by the experimental data. The small differences between the duplicate model predictions are explained by the chaotic behavior of the mixing process (different initial particle positions are used). From experimental observation and simulations we find that mixing mainly occurs at the surface of the bed (in the top layer). Both experimental data and calculations predict faster mixing at lower fill level, which was to be expected since the top area / volume ratio of the bed increases with decreasing fill level (see Table II and Appendix). For the fill levels 0.2, 0.33, 0.4 more or less complete mixing is achieved after 1.5, 3, and 6 rotations, respectively. Here, complete mixing is found to be achieved when the entropy of mixing reaches a value of 0.9 (based on visual observations). For fill level 0.2, model predictions deviate from experimental data, due to 1) a relatively small number of samples, and 2) the limited number of particles, which resulted in unrealistic flow patterns. It should be emphasized, however, that no attempt was made to optimize the values of the parameters to obtain a better agreement with experiments. The model can thus be regarded as predictive.

The simulated mixing progress is influenced by the collision parameters used in the contact models. During simulation more than 95% of the tangential forces calculated were found to be viscous forces. This means that the contribution of the dynamic friction to the motion of the particles is negligible. If we omit the dynamic friction, no significant change in the mixing progress is observed (Fig. 6). The reason for this is the fact that the particles have a very low restitution coefficient and hence kinetic energy is rapidly dissipated. As a consequence,

tangential velocities are low. The tangential forces are thus determined by static friction; in our approach, modeled as a high tangential viscous force. The model we used for the description of the tangential friction forces gave an adequate description of the behavior observed.

The rotation rate of the drum is an important process variable, especially because of shear sensitivity during fungal growth (Silman, 1980; Stuart et al., 1998). We conducted several simulations and showed, in agreement with our expectations, that the mixing progress depends little on the rotation speed (in the range of rotation rates considered here), but mainly on the number of rotations made (Fig. 7). Of course, mixing time itself is directly influenced by the rotation rate of the drum. For SSF, mixing time is very important, e.g. regarding heat removal, aeration, etc.

Effect of baffles on the mixing performance.

Baffles are often used in rotating drums for SSF to improve mixing performance and heat and mass transfer. Several authors reported that the presence of baffles during SSF leads to better overall performance (Fung and Mitchell, 1995; Lindenfelser and Ciegler, 1975; Marsh et al., 1998). However, the design of the baffles in these studies was based on experience rather than on fundamental knowledge of their influence on the mixing performance. Our model approach makes it possible to predict the effect of baffles on the mixing process. The baffles were modeled as straight-overlapping arrays of particles that have the rotational movement of the drum imposed on them. In this study we evaluated the effect of four straight baffles (5 cm and 10 cm length (i.e. 33 % and 67 % of the drum radius) and a thickness of 5 mm) on the flow behavior and the mixing performance at two fill levels (Figs. 8 and 9). The baffles were evenly spaced and fixed normal to the drum wall. The predictions of the simulations were verified in experiments. It may be expected that the presence of small baffles hardly influences the dynamics, and therefore also the mixing performance of the system. We observed that the small baffles followed the same path as the wheat grains and the wall and that only few wheat grains were lifted during passage of a baffle through the surface.
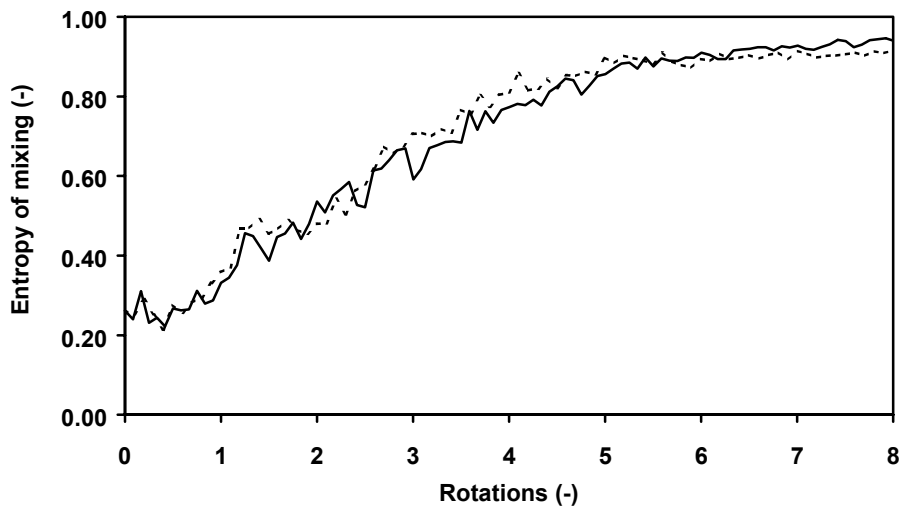
Figure 6. Effect of viscous friction and dynamic friction on the mixing process. In a rotating drum (diameter 30 cm, 0.5 rpm) for $\varepsilon = 0.4$. (—— 95 % viscous forces - - - 100 % viscous forces)
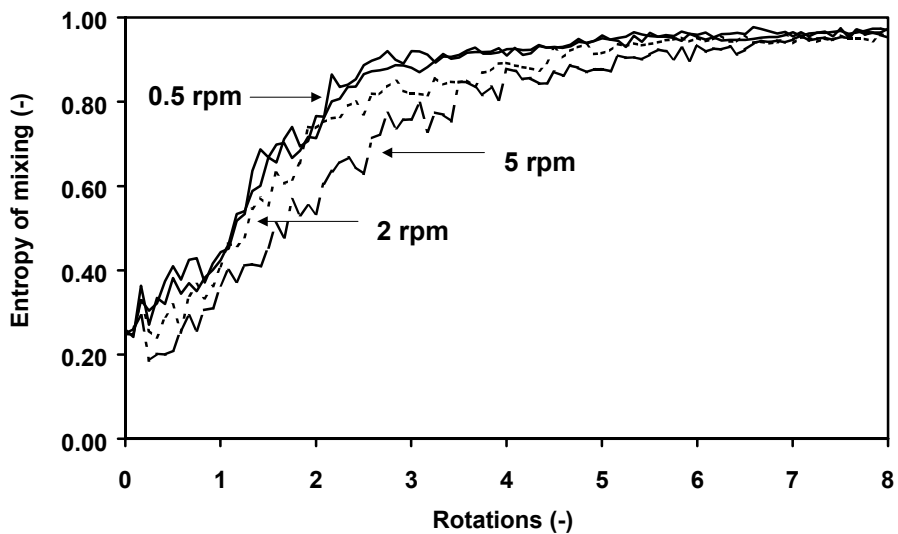
Figure 7. Simulation results for different rotation rates for $\varepsilon = 0.33$ (—— 0.5 rpm (duplicate) -··- 2 rpm - - - 5 rpm)
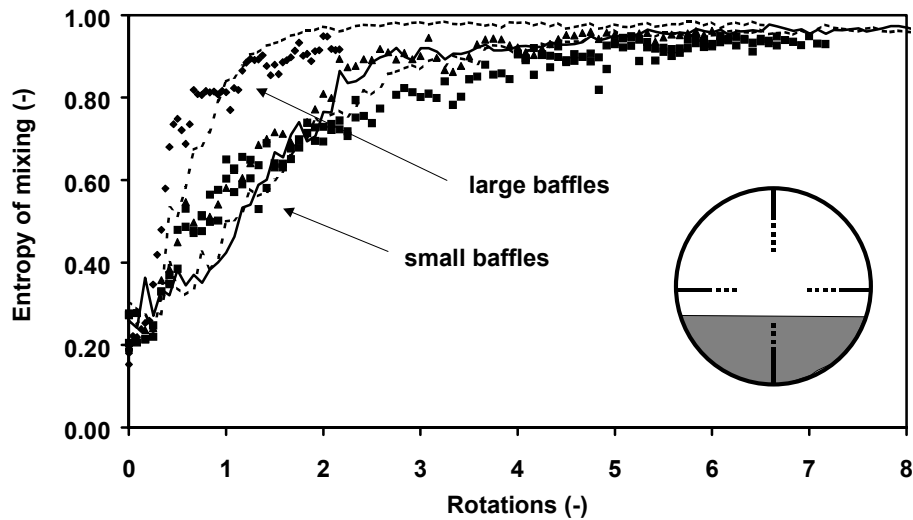
Figure 8. Simulations and measurements of mixing in a rotating drum with and without baffles for ε = 0.33 (diameter 30 cm, 0.5 rpm). ▲ experiment without baffles ■ experiment with small baffles ◆ experiment with large baffles ―― model without baffles - - - model with small and large baffles. The small baffles in the drum are depicted as solid lines, while the large baffles are extended, depicted as dashed lines.
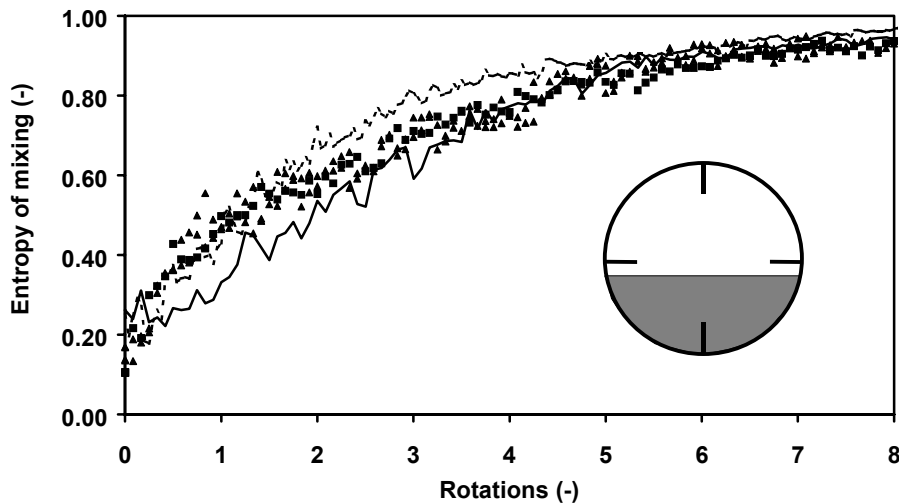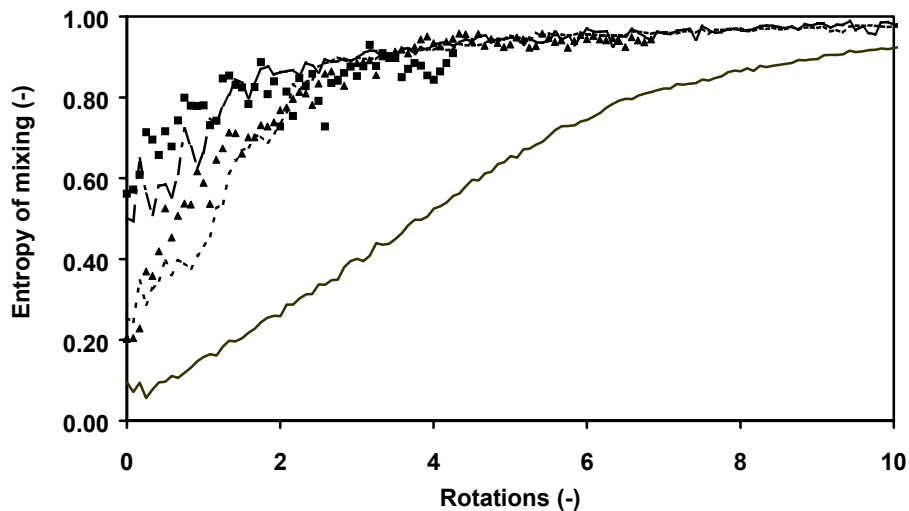

Figure 9. Simulations and measurements of mixing in a rotating drum with and without baffles for ε = 0.4 (diameter 30 cm, 0.5 rpm). ▲ experiment without baffles ■ experiment without baffles ―― model without baffles - - - model with baffles.

Figures 8 and 9 confirm that the small baffles hardly affect the mixing rate in both experiment and simulation. In simulations and experiments with large baffles we did find a significant change in the mixing time (a reduction from 3 to 1.5 rotations) (Fig. 8). This increase was due to the larger size of the baffles, lifting many more wheat grains and disturbing the solid body rotation. From these results we could conclude that only large baffles, that protrude deeply into the bed, have a significant effect on the flow dynamics of the bed and thus improve mixing performance. We should emphasize, however, that under different process conditions in SSF, e.g., when slumping flow occurs, the presence of small baffles may also be beneficial (Marsh et al., 1998). The optimal baffle size in a rotating drum system will be strongly dependent on the particle characteristics, the fill level, and the rotation rate of the drum. In contrast with many fast rotating drums in other applications, which often have small baffles (<33 % of the drum radius), slowly rotating drums for SSF need to have large baffles (e.g., as presented above), that can disturb the solid body rotation and turn the bed for optimal mixing performance. Using the simulation method presented here, other designs than straight baffles (e.g., angled baffles or baskets) can be evaluated for increasing mixing performance.

Effect of scale-up on the mixing performance

The lack of knowledge about designing and scaling-up solid-state fermenters is one of the main reasons for the limited application of SSF in industry (Hardin et al., 2000; Pandey, 1991). As scaling-up effects have a serious impact on mixed SSF, it is of utmost importance to develop modeling tools to predict these effects beforehand. Therefore, we studied the effect of scaling-up a rotating drum on mixing performance (Fig. 10). Three different sizes were evaluated (diameters: 0.15, 0.3 and 1 m), using a fill level of 0.33. Validation experiments were only conducted for the two small drums. Due to the varying size of the systems, the entropy gridsize was varied proportionally to the number of particles, in order to keep the sample size constant. The initial entropies of mixing of the various reactor sizes vary as the number of cells overlapping both colored particle layers varied. This illustrates the reason why mixing experiments should be performed with a relatively large number of particles.

Figure 10 shows that the mixing rate decreases sharply with increasing size of the drum. We find that for constant fill level, the top area/volume ratio of the bed is inversely proportional to the drum radius and therefore it decreases with increasing scale (see Appendix). When we compare the time needed for mixing and the drum radius we find that they are proportional to each other (Table II). These results show that our model is capable to predict the effect of scale-up on the mixing performance in a rotating drum. We can also conclude that the top area/volume ratio of the bed gives a good indication of the dependence of the mixing time on both the fill level and the drum radius.

Figure 10. Simulations (lines) and measurements (symbols) of mixing in a rotating drum at different scales $\varepsilon = 0.33$ (0.5 rpm). ■, ····· drum diameter 0.148 m, N = 277 ▲ , - - - drum diameter 0.3 m, N = 1137 —— drum diameter 1 m, N = 12634.

Conclusions

The mixing behavior of the solid substrate particles, moistened wheat grains, was successfully predicted by soft-sphere granular dynamics simulations. This was demonstrated by the fact that the model predictions of the mixing progress were in good qualitative agreement with the validation experiments. Moreover, the model predictions were quantitatively validated by comparing the simulated and experimental mixing progress in terms of entropy of mixing. The model predicted a decrease in mixing rate with increasing fill level, in agreement with the experiments. The rotation rate was not found to have a significant effect on mixing in the range of rpm values used. The mixing performance was improved when large straight baffles (67 % of the drum radius) were implemented; this in contrast to smaller baffles, which did not result in any improvement of mixing performance. Furthermore, it was shown that the simulations predict a linear increase in mixing time with increasing drum radius. This illustrates that the granular dynamics simulations can serve as a valuable tool for evaluating the mixing behavior of solid substrate particles in a rotating drum. Only nonadhesive particles were regarded in this paper. However, even when particles show adhesive properties the simulation method offers perspectives for SSF, as the forces can be easily modeled by implementing attractive forces between particles. Such an extended model could be used to predict making and breaking of aggregates and might be a valuable tool to study the reported negative effects of agglomeration during SSF in rotating drums. The results presented here lead us to believe that this simulation

method may be further developed into a tool for scaling-up and designing mixed SSF bioreactors.

Appendix: Top surface and volume ratio

The ratio of the top surface and the volume of the bed depends on the drum radius and the fill level of the drum. For the following calculations it is assumed that the fill level is below 0.5. First, we define the fill level of the drum (ε) as the ratio of the volume of the bed and the total volume of the drum:

$$\varepsilon = \frac{\frac{1}{2} \cdot L \cdot r^2 \cdot (\theta - \sin(\theta))}{L \cdot \pi \cdot r^2} = \frac{\theta - \sin(\theta)}{2 \cdot \pi} \qquad (A1)$$

in which: r is the radius of the drum; θ is the central angle in radians (Fig. A1).
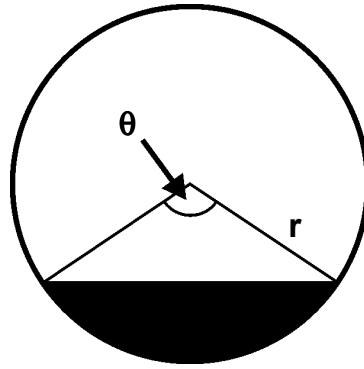
Figure A1. Schematic drawing of a filled drum with θ the central angle and r the radius of the drum.

Subsequently, the top surface of the bed (A_{top}) is calculated:

$$A_{top} = 2 \cdot r \cdot \sin(\frac{\theta(\varepsilon)}{2}) \cdot L \qquad (A2)$$

in which: L is the length of the drum.

Also, the volume of the bed (V_b) is calculated:

$$V_{bed} = \varepsilon \cdot \pi \cdot r^2 \cdot L = \frac{\theta(\varepsilon) - \sin(\theta(\varepsilon))}{2 \cdot \pi} \cdot \pi \cdot r^2 \cdot L \qquad (A3)$$

The ratio of the top surface and the bed volume (R_b) follows from Eq. A2 and A3:

$$R_b = \frac{A_{top}}{V_b} = \frac{4}{r} \cdot \frac{\sin(\frac{\theta(\varepsilon)}{2})}{\theta(\varepsilon) - \sin(\theta(\varepsilon))} \qquad (A4)$$

References

Allen MP, Tildesly DJ. 1987. Computer simulation of liquids. Oxford: Oxford University Press.

Barrios-Gonzáles J, Mejía A. 1996. Production of secondary metabolites by solid-state fermentation. Biotechnol. Ann Rev. 2:85-121.

Baumann G, Janosi IM, Wolf DE. 1994. Particle trajectories and segregation in a two dimensional rotating drum. Europhys Lett 27:203.

Boateng AA, Barr PV. 1997. Granular flow behaviour in the transverse plane of a partially rotating cylinder. J Fluid Mech 330:233-249.

Cleary PW. 2000. DEM simulation of industrial particle flows: case studies of dragline excavators, mixing in tumblers and centrifugal mills. Powder Technol 109:83-104.

Cundall PA, Strack ODL. 1979. A discrete numerical model for granular assemblies. Géotechnique 29:47-65.

Dury CM, Ristow GH. 1997. Radial segregation in a two-dimensional rotating drum. J Phys I 7:737-745.

Fung CJ, Mitchell DA. 1995. Baffles increase performance of solid-state fermentation in rotating drum bioreactors. Biotechnol Tech 9:295-298.

Han B, Kiers JL, Nout RMJ. 1999. Solid-substrate fermentation of soybeans with *Rhizopus* spp.: Comparison of discontinuous rotation with stationary bed fermentation. J Biosc Bioeng 88:205-209.

Hardin MT, Mitchell DA, Howes T. 2000. Approach to designing rotating drum bioreactors for solid-state fermentation on the basis of dimensionless design factors. Biotechnol Bioeng 67:264-282.

Hogg R, Cahn DS, Healy TW, Fuerstenau DW. 1966. Diffusional mixing in an ideal system. Chem Eng Sci 21:1025-1038.

Hoomans, BPB. 2000. Granular Dynamics of Gas-Solid Two-Phase Flows. Ph.D. Thesis, University of Twente.

Ktitarev DV, Wolf DE. 1998. Stratification of granular matter in a rotating drum: a cellular automaton modeling. Granular Matter 1:141-144.

Lindenfelser LA, Ciegler A. 1975. Solid-Substrate Fermenter for Ochratoxin production. Appl Microbiol 29:323-327.

Marsh AJ, Mitchell DA, Stuart DM, Howes T. 1998. O2 uptake during a solid-state fermentation in a rotating drum bioreactor. Biotechnol Letters 20:607-611.

McCarthy JJ, Ottino JM. 1998. Particle dynamics simulation: a hybrid technique applied to granular mixing. Powder Technol 97:91-99.

McCarthy JJ, Shinbrot T, Metcalfe G, Wolf JE, Ottino JM. 1996. Mixing of granular materials in slowly rotated containers. AIChE J 42:3351-3363.

Mikami T, Kamiya, H, Horio M. 1998. Numerical simulation of cohesive powder behavior in a fluidized bed. Chem Eng Sci 53:1927-1940.

Mitchell DA, Krieger N, Stuart DM, Pandey A. 2000. New developments in solid-state fermentation II Rational approaches to the design, operation and scale-up of bioreactors. Proc Biochem 35:1211-1225.

Moakher M, Shinbrot T, Muzzio FJ. 2000. Experimentally validated computations of flow, mixing and segregation of non-cohesive grains in 3D tumbling blenders. Powder Technol 109:58-71.

Muguruma Y, Tanaka T, Kawatake S, Tsuji Y. 1997. Discrete particle simulation of a rotary vessel mixer with baffles. Powder Technol 93:261-266.

Nagel FJI, Tramper, J, Bakker, MSN, Rinzema, A. 2001 Temperature control in a continuously mixed bioreactor for solid-state fermentation. Biotechnol Bioeng. 72:219-230.

Pandey A. 1991. Aspects of fermenter design for solid-state fermentations. Proc Biochem 26:355-361.

Prigozhin L, Kalman H. 1998. Radial mixing and segregation of a binary mixture in a rotating drum: Model and experiment. Phys Rev E 57:2073-2080.

Rajamani RK, Mishra BK., Venugopal R., Datta A. 2000. Discrete element analysis of tumbling mills. Powder Technol 109:105-112.

Ristow GH. 1994. Granular Dynamics: a review about recent molecular dynamics simulations of granular materials. In: Staufferd D, editor. Annual reviews of computational physics. Marburg Germany. World Scientific. p 275-308.

Rosato A. 1986. Monte Carlo Simulations of particulate matter segregation. Powder Technol 49:59-69

Schäfer J, Dippel S, Wolf DE. 1996. Force schemes in simulations of granular materials. J Phys I 6:5-15.

Silman RW. 1980. Enzyme formation during solid-substrate fermentation in rotating vessels. Biotechnol Bioeng 22:411-420.

Sitkei G. 1986. Mechanics of agricultural materials. Amsterdam: Elsevier.

Stuart DM, Mitchell DA, Johns MR, Litster JD. 1998. Solid-state fermentation in rotating drum bioreactors: operating variables affect performance through their effects on transport phenomena. Biotechnol Bioeng 63:383-391.

Tsuji Y, Tanaka T, Ishida T. 1992. Lagrangian numerical simulation of plug flow of cohesionless particles in a horizontal pipe. Powder Technol 71:239-350.

Vollbrecht D. 1997. Feststoff-fermentation - Ein historischer überblick. Chemie Ingenieur Technik 69:1403-1408.

Weber FJ, Tramper J, Rinzema A. 1999. A simplified material and energy balance approach for process development and scale-up of Coniothyrium minitans conidia production by solid-state cultivation in a packed-bed reactor. Biotechnol Bioeng 65:447-458.

Chapter 3

Three-dimensional simulation of grain mixing in three different rotating drum designs for solid-state fermentation

Abstract

A previously published two-dimensional discrete particle simulation model for radial mixing behavior of various slowly rotating drums for solid-state fermentation (SSF) has been extended to a three-dimensional model that also predicts axial mixing. Radial and axial mixing characteristics were predicted for three different drum designs: (1) without baffles; (2) with straight baffles; (3) with curved baffles. The axial mixing behavior was studied experimentally with video and image-analysis techniques. In the drum without baffles and with curved baffles the predicted mixing behavior matched the observed behavior adequately. The predicted axial mixing behavior in the drum with straight baffles was predicted less accurately, and it appeared to be strongly dependent on particle rotation, which was in contrast to the other drum designs. In the drum with curved baffles complete mixing in the radial and axial direction was achieved much faster than in the other designs; that is, it was already achieved after three to four rotations. This drum design may therefore be very well suited to SSF. It is concluded that discrete particle simulations provide valuable detailed knowledge about particle transport processes, and this may help to understand and optimize related heat and mass transfer processes in SSF.

Introduction

Mixing of granular materials is one of the most frequently used process operations in industry. Despite this, little fundamental knowledge is available on the mixing and flow behavior of granular media (Metcalfe et al., 1995). Discrete particle models are currently regarded as a promising tool for obtaining more insight into the details of these mixing processes (McCarthy et al., 1996). In this investigation we focus on a biotechnological process, solid-state fermentation (SSF), in which transfer phenomena are coupled with biomass production and therefore determine final product quality. More fundamental knowledge on substrate particle mixing behavior should provide a useful basis for unraveling the complex local transport phenomena and increasing the productivity of this process. We believe that this knowledge can be acquired by using advanced numerical simulations, such as discrete particle simulations (Schutyser et al., 2001).

In this study, the mixing behavior of substrate particles for SSF (i.e., moist wheat grain) is studied. Wheat grains have been used successfully in the past as a solid matrix for the cultivation of fungi (Nagel et al., 2001). This method of cultivation is an alternative for submerged cultivation of fungi. For centuries, SSF has been used in the production of foods such as soy sauce, Tempe and mushrooms. Recently, the Western food industry has shown renewed interest in SSF because of its advantages in the production of certain foods, food ingredients and other bioactive compounds of interest (Pandey et al., 2000). As a result of this renewed interest, more research has been initiated on process control and scale-up of SSF. One of the main issues, hindering application of SSF on an industrial scale, has been the coupled control of temperature and moisture content during fermentation. Spatial gradients in temperature and moisture content are inherent to traditional static fermentation systems (e.g., packed beds or tray fermenters), especially when fast-growing fungi are used (Weber et al., 1999). Mixed systems (e.g., rotating drums or stirred beds) have been found to offer much better control in this respect, but little is known about the mechanisms of mixing and the coupled transport phenomena. A disadvantage of mixed fermentation systems is the occurrence of shear forces, which may damage fungal hyphae (Han et al., 1999). To elucidate the details of particle mixing behavior and to offer better possibilities for rational design of large mixed SSF fermenters the development of predictive modeling tools is essential (Schutyser et al., 2001).

This study presents three-dimensional (3D) discrete particle simulations of mixing behavior in a rotating drum system, which is an attractive mixing device for SSF, because of its scale-up potential, the low capital investment needed for the equipment involved, and its simplicity with respect to modeling (Han et al., 1999). In previous research, 2D discrete particle simulations of radial mixing behavior have already shown to offer improved insight (Schutyser et al., 2001). In

this work, an extension of this model has been made to include axial mixing in a 3D rotating drum. Based on simulations and validation experiments, mixing behavior is evaluated for three different drum designs: (1) without baffles; (2) with straight baffles; and (3) with curved baffles.

Discrete particle model development

Discrete particle simulations, also called granular dynamics simulations, are based on the same principles as molecular dynamics simulations. The movements of an array of particles are predicted from forces acting on all individual particles. These forces include gravitation and interactions between particles. The simulations require no knowledge of the flow behavior of the media a priori. A limitation of this simulation method is that large systems require considerable computational effort. Given the speed of today's single-processor computers the number of particles in the model system is limited to approximately 10^6.

During the simulation, contact between particles is detected at very brief time intervals ($2 \cdot 10^{-5}$ sec.). When particles are in contact, interaction forces are calculated. A repulsive force combined with a dissipative force determines the force in the normal direction. A tangential or shear force is calculated, using a combination of viscous and dynamic friction, which is explained in more detail in what follows. Schäfer et al. (1996) have provided an extensive review of the different contact force models. From the resulting force on each particle, new particle velocities and positions are calculated by integrating the Newtonian equation of motion using a leap-frog integration routine. Subsequently, particles are moved to their new position and forces are evaluated again. The wheat grains are modeled as perfect spheres (diameter 4.9 mm) in order to minimize computational effort. Deformation of these spheres is modeled as a computational overlap between spheres. In previous research we have shown that accurate predictions could be made of radial mixing behavior in a rotating drum, despite these simplifications (Schutyser et al., 2001).

The repulsion force, that is, the normal component of the contact force ($\vec{F}_n$), between two particles is calculated using the linear-dashpot model:

$$\vec{F}_n = \left(-k_n \delta - \eta_n \left(\vec{v}_{rij} \cdot \vec{n}_{ij} \right) \right) \vec{n}_{ij} \tag{1}$$

where k_n is the stiffness coefficient (N·m^{-1}), δ is the computational overlap (m), η_n is the normal damping coefficient (kg·s^{-1}), $\vec{v}_{rij}$ is the normal velocity difference (m·s^{-1}), $\vec{n}_{ij}$ is the normal unit vector (-).

The first term is a repulsive interaction force, whereas the second term is a dissipative force. The values of the collision parameters, k_n and η_n are chosen as 125 and 0.079, respectively (Schutyser et al., 2001). The stiffness coefficient is based on compression-force experiments, whereas the damping coefficient is based on a restitution coefficient of 0.1 (i.e., the relative velocity that remains after a collision). The friction force, that is, the tangential force ($\vec{F}_s$), between two particles, is described by:

$$\vec{F}_s = -\min\left(\left|\gamma_s\, v_{sij}\right|, \left|\mu_d F_n\right|\right) \cdot \operatorname{sign}(\vec{v}_{sij}) \tag{2}$$

where γ_s is the viscous friction coefficient (kg·s^{-1}), μ_d is the dynamic friction coefficient (-), $\vec{v}_{sij}$ is the tangential velocity difference (m·s^{-1}). The values of the friction parameters (γ_s, μ_d) were also taken from Schutyser et al. (2001); that is, respectively 1.0 and 0.5 for particle-particle interaction and 3.0 and 1.5 for particle-wall interaction.

So far, all the force interactions are identical for three- (3D) and two-dimensional (2D) simulations. In a 3D-simulation, interactions of particles with the walls at the axial ends of the drum also need to be included. For this purpose, we need to define the axes, which are depicted in Fig. 1. The origin is located in the center of the drum. The repulsion force for particles in contact with the wall at an end of the drum (y-direction) is modeled using the following computational overlap:

$$\delta = r_p - \left(\frac{L_d}{2} - \left|r_y\right|\right) \tag{3}$$

where r_p is the radius of a particle (m), L_d is the length of the drum (m), r_y is the y coordinate of the center of the particle (m). The tangential interaction with the sidewall is modeled only for the x and z direction. The tangential velocity difference (v_s) between particle i and the wall is given by:
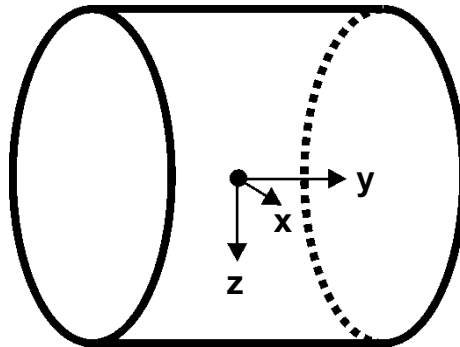
Figure 1. Definition of the axis in a rotating drum, starting from the point of origin, located in the center of the drum.

$$v_s = \omega r_{ixz} - (n_{ix}v_{iz} - n_{iz}v_{ix}) \tag{4}$$

where ω is the angular velocity of the drum (rad·s^{-1}), r_{ixz} is the distance of the particle in the x-z direction to the horizontal axis (m), nix, niz are the normal unit vectors of particle i in the x-z direction to the horizontal axis (-). The tangential velocity difference is used to calculate the tangential force component with Eq. (2). The interaction of the lateral side of the drum with a particle is modeled similarly as for the 2D case, thus taking into account only radial interaction. If a particle moves in the axial direction its velocity component in this direction remains unchanged after collision.

For all drum designs except one, particle rotation was neglected in our model. Only for the drum with straight baffles, the effect of particle rotation on axial mixing was evaluated. In this case, the tangential velocity difference has to account for rotation velocities of both particles:

$$\vec{v}_{sij} = \vec{v}_{rij} - \left(\vec{v}_{rij} \cdot \vec{n}_{ij} \right) \vec{n}_{ij} + \left(\vec{\omega}_i + \vec{\omega}_j \right) \times r_p \, \vec{n}_{ij} \tag{5}$$

where ω_i is the rotation velocity of particle i (rad·s^{-1}).

Subsequently, a friction force [Eq. (2)] is calculated for each contact. In general, several particles are in contact with particle i at the same time. Therefore the total torque ($\vec{M}_i$) on particle i is given by the following summation:

$$\vec{M}_i = \sum_j \left(r_p \, \vec{n}_{ij} \times \vec{F}_{sij} \right) \tag{6}$$

From the resulting torque on particle i we can calculate the change in rotation velocity. This is described by the equation of rotational motion:

$$I \frac{d\vec{\omega}_i}{dt} = \vec{M}_i \tag{7}$$

where I is the moment of inertia, for a sphere with mass m and radius r_p it is equal to $\frac{2}{5}mr_p^2$ (kg·m^2).

Dispersion model

Particle movement in the axial direction occurs primarily in the top layer of the bed and is considered to be random, because motion of particles in the direction of the axis can only result from interparticle collisions. Consequently, axial mixing can be considered as analogous to diffusion in gases, liquids or solids (Hogg et al., 1966). Fick's second law has been used

frequently to describe diffusive particle mixing in the axial direction of a drum (Hogg et al., 1966):

$$\frac{\partial C(y,t)}{\partial t} = D^* \frac{\partial^2 C(y,t)}{\partial y^2} \qquad (8)$$

where D^* is the axial dispersion coefficient (m^2·s^{-1}), y is the position along the horizontal axis (m), t is the time (s), $C(y,t)$ is the relative concentration of one labeled fraction (kg·m^{-3}).

For mixing in a rotating drum it is more practical to describe the dispersion coefficient as a function of the number of rotations (N), D (m^2·rev^{-1}):

$$\frac{\partial^2 C(y,N)}{\partial y^2} = \frac{1}{D} \frac{\partial C(y,N)}{\partial N} \qquad (9)$$

As the dispersion coefficient is defined as a function of the number of rotations, we neglect the fact that the dispersion coefficient is also a function of the angular drum velocity (Rao et al., 1991). However, in this study all simulations and experiments are carried out in a limited range of rotation rates (0.5 - 2 rpm), in which the bed shows very similar flow behavior. Therefore, the effect of angular velocity is not significant in this study.

If the dispersion of two colored fractions of particles is studied, initially placed according to the boundary conditions in Eq. (10a) and (10b), Eq. (9) can be solved. Using the proper boundary conditions, one can find the following solution for the concentration profile as a function of the axial position and the number of rotations (Hogg et al., 1966):

$$C(y,N) = \frac{1}{2} + \frac{2}{\pi} \sum_{n=1}^{\infty} \frac{1}{(2n-1)} \cdot \exp\left[\frac{-(2n-1)^2 \pi^2 DN}{L_d^2}\right] \cdot \sin\left[\frac{(2n-1)\pi y}{L_d}\right] \qquad (10)$$

for the boundary conditions

(10a) $C(y,0) = 0$ $(-L_d/2 \leq y < 0)$

          $= 1$ $(0 < y \leq L_d/2)$

(10b) $\left.\frac{\partial C(y,N)}{\partial y}\right|_{x=-L_d/2} = 0$

       $\left.\frac{\partial C(y,N)}{\partial y}\right|_{x=L_d/2} = 0$

Equation (10) is similar in form to the more general equation given by Lacey et al (1954), and for the specific boundary conditions [Eqs. (10a) and (10b)], the two equations are equivalent. From Eq. (10) it is possible to predict the relative concentrations of the two colored fractions at any point in the bed after any number of rotations.

We have used Eq. (10) to extrapolate simulation results for axial mixing, because the computation time required to simulate nearly complete axial mixing is too long. Axial mixing in rotating drums is much slower than radial mixing. Equation (10) was first used to estimate a dispersion coefficient from the axial concentration profiles, as predicted by the discrete particle model, and to find the number of rotations required to achieve complete mixing. Note that the diffusion model was only used for the drums without baffles and with straight baffles; the curved baffles caused strong convective transport, which prohibited the use of the diffusion model.

Entropy of mixing

Because it is difficult to derive the degree of mixedness of the system from an axial concentration profile, it is desirable to have only one parameter to characterize the degree of mixedness. In previous research we introduced the entropy of mixing (S) as a parameter to estimate the degree of radial mixedness of the bed after a certain number of rotations (Schutyser et al., 2001). When the entropy of mixing is 0.9 or higher, we consider the system to be completely mixed. The entropy of mixing is here used to estimate the degree of mixedness in the axial direction. The system is subdivided into equally sized cells. In each cell, the numbers of colored particles are counted as a function of mixing time. The entropy of mixing is calculated according to the following equation:

$$S = \frac{1}{S_0} \sum_i \left(x_1(i) log(x_1(i)) + x_2(i) log(x_2(i)) \right) \frac{N_{cel}(i)}{N_p} \qquad (11)$$

where S_o is the entropy of a completely mixed system, which depends on the fraction of colored particles in the system, $x_1(i)$, $x_2(i)$ are the fractions of the two colored particles in cell i, $N_{cel}(i)$ is the number of particles in cell i, N_p is the total number of particles in the system.

Materials and methods

Discrete particle contact detection

The most computationally extensive part of the simulations is the detection of contact between particles. Several sophisticated contact detection algorithms have been developed to reduce the computational effort. In earlier research a conventional neighbor list algorithm was used (Schutyser et al., 2001); however, if a system contains more than 5000 particles, the neighbor

list becomes inefficient to store easily. Therefore an alternative method, called linked cell method, was used (Allen and Tildesly, 1987; Iwai et al., 1999). In this algorithm the system is divided into M x M x M cells. First all the particles are sorted into their appropriate cell. This sorting is rapid and is performed at each time-step. Two arrays are created during this sorting process. The 'head-of-chain' array has one element for each cell and contains the identification number of one particle in the cell. This number is used to address the element of a linked-list array, which contains the number of the next particle in the cell, and so on. In a simulation, the forces are calculated by looping over all cells. For a given cell the algorithm sorts through the linked list and all pairs that can have interaction are selected. A particle may also interact with a particle located in a neighboring cell. To avoid counting interactions twice, only a limited number of neighboring cells are considered.

Several simulations were conducted to optimize the size of the grid cells for fast simulation and it was found that a cell size ($5 \cdot 10^{-3}$ m) of about one particle diameter ($4.9 \cdot 10^{-3}$ m) provided optimal performance. In this case the linked-list structure in the cell is in fact usually not used. The algorithm looks whether a cell is occupied and if so it calculates the interactions of the particle with the particles in the neighboring cell. After this optimization procedure we could simulate 1 second real-time (50.000 time steps) in 2.5 hours computational time of a particle system containing 36000 particles on an XP1000 ALPHA workstation. To simulate 7 rotations (10^7 time steps) of a drum rotating at a speed of 2 rpm, 15 days of calculation were needed.

Experimental validation of mixing behavior

For experimental studies of axial mixing behavior one should be able to 'freeze' the system and determine the degree of mixing in successive sections of the drum. Wightman et al. (1996) described a method to solidify a bed of powder particles (diameter 66 μm), that involved impregnating mixtures with a binder solution. Subsequently, the bed was sliced into different axial sections, which were scanned and analyzed for their particle composition. In this study, a similar approach is reported to study axial mixing of wheat grains in a rotating drum, using a gelatin solution as a binder solution. The solution was poured into the bed and by cooling-down overnight, the gelatin was allowed to harden. From the different sliced axial sections, data could be obtained about the composition of the mixture at almost any point in the system after a certain period of mixing. A disadvantage of this method is that it is elaborate, because for each number of rotations a new experiment has to be conducted.

Experimental conditions

The wheat grains were treated according to the procedure applied for substrate particles for SSF. The whole wheat grains were soaked for 2.5 h in excess tap water of 60 °C. Subsequently, the soaked grains were sieved and autoclaved for 1 h at 121 °C. A Perspex rotating drum with

an internal diameter of 0.3 m and a length of 0.2 m, rotating on a roller table, was used to study mixing. One of the main criteria for the size of this drum was that we could simulate the entire system with a discrete particle model within reasonable calculation time. Straight and curved baffles (Fig. 2) were constructed from, Perspex and foldable plastic sheet, respectively. The height of the straight and the curved baffles was equal to two thirds of the drum radius. This size was chosen because in a previous study it was found that this size of baffles guaranteed relatively fast radial mixing (about 3-4 rotations) (Schutyser et al., 2001). The drum with 4 curved baffles was placed under an angle of 20° to compensate for the transport of the grains by the baffles to the higher right side (Fig. 2). This set-up guaranteed a more or less even distribution of material along the horizontal axis of the drum.

Methylene blue (Merck, Germany) and Bengal rose B (Fluka, Switzerland) were used for coloring two grain fractions. At the start of each experiment, the two grain fractions were placed such that the initial interface was located in the middle of the drum; that is, grains of red color were loaded in the section between 0 and -10 cm, and the green colored grains were loaded between 0 and 10 cm with respect to the axial coordinate. After a certain number of rotations the process was stopped. A gelatin solution (20 g/l dissolved gelatin sheets, Deutsche Gelatin-Fabriken, Eberbach/Baden, Germany), was carefully poured over the load to solidify the bed. The solution hardened overnight at 5 °C. Subsequently, axial sections of 2 cm were sliced and pictures were acquired, using a webcam (Philips USB PC Camera) with an image resolution of 640 x 480 pixels. These pictures were analyzed to determine the relative concentrations of the red and green particles, by applying appropriate color threshold values, based on visual observation. The images we analyzed with MATLAB 5.3 with an image-processing toolbox. Using this method, accurate data were obtained, although variations in lighting (and thus the quality of the image) during acquisition of the pictures introduced some experimental errors.
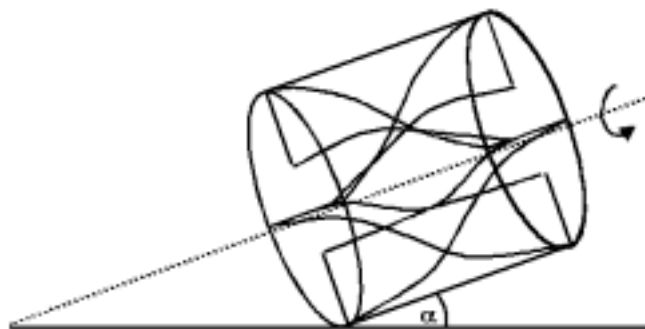
Figure 2. Design of the curved baffles in an inclined rotating drum ($\alpha = 20°$).

Results and Discussion

Granular mixing in a rotating drum

Mixing behavior in a rotating drum depends strongly on the solids flow regime, which may be quantified in terms of the Froude number (*Fr*):

$$Fr = \frac{\omega^2 R_d}{g}$$

which is defined as the ratio of the centrifugal and the gravitational forces, where g is the acceleration due to gravity, R_d is the drum radius and ω is the rotational speed (Blumberg and Schlünder, 1996). For SSF, the rotation rate is usually very low. Therefore, in this research mixing behavior was only studied at very low Froude numbers or rotation rates (0.5-2 rpm, corresponding to Fr = $3 \cdot 10^{-6}$-$1.1 \cdot 10^{-5}$), for which a slumping bed was obtained (Blumberg and Schlünder, 1996; Wightman and Muzzio, 1998). In this solids flow regime a solid body rotation of the bed was observed except for the top layer of the bed, where discrete avalanches of grains occured.

Mixing of particles in a 3D-rotating drum can be divided into two types of mixing processes, (1) radial mixing and (2) axial mixing. For slow radial mixing it appeared that the bed surface:volume ratio is an important design parameter. For constant particle size, this design parameter depends on the fill level (defined as the volume fraction of the total reactor occupied by the load) and the size of the drum. In this study, fill level ($\varepsilon = 0.25$) and drum size (4.2 dm^3) have been kept constant. The chosen fill level, $\varepsilon = 0.25$, is within the range (0.1 to 0.4) of commonly chosen fill levels for SSF (Hardin et al., 2000).

Simulations of 3D drum mixing: radial mixing

First, the radial mixing, predicted by 3D simulations, was compared with the behavior predicted by 2D simulations, which have been previously validated with experiments (Schutyser et al., 2001). In Figure 3, radial mixing progress is depicted in terms of entropy of mixing as a function of the number of rotations. For the 3D simulations averages along the axial direction are presented. From this figure we can conclude that radial mixing follows a similar trend for both the 2D and 3D models, although strong oscillations in the entropy of mixing were observed in the 3D simulations. These oscillations were due to the influence of the sidewalls of the drum on the flow, which was found by visualizing the simulated flow (Fig. 4). The particles near the wall rotated somewhat slower than the particles in the middle of the bed, which explains the existence of the 'tongue' of gray particles in the middle of the bed (Fig. 4). This behavior was also observed in our experiments, although less pronounced. Due to these
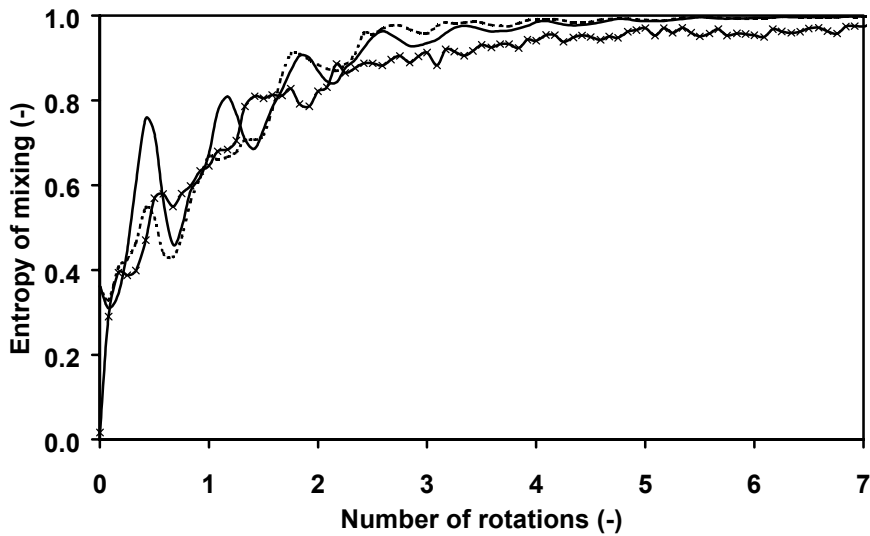
Figure 3. The entropy of mixing versus the number of rotations in a drum without baffles. Comparison between the predictions of the 2D and 3D discrete particle model for radial mixing. —— 3D mixing, -x-x- 2D mixing, - - - 3D mixing without the sections of the bed near the sidewalls.

Figure 4. Visualization of the 'tongue formation' during the initial mixing of two horizontal colored layers during the discrete particle simulation. This 'tongue formation' is due to the influence of the sidewalls on the solids flow in the rotating drum without baffles.

differences in flow behavior, the entropy of mixing depends considerably on the location in the drum along the horizontal axis. When the regions near the walls were omitted from the entropy calculations, the oscillating behavior disappeared almost entirely (Fig. 3). The entropy of mixing for the 3D simulations after many rotations approached unity closer than for the 2D simulations. This is due to the larger sample sizes (i.e., number of particles per grid cell), taken for the 3D case. The predicted initial entropy of mixing for the 2D simulations was close to zero, because the interface of the two colored layers incidentally coincided with a grid line. However, this should not be seen as a significant difference between the simulation results.
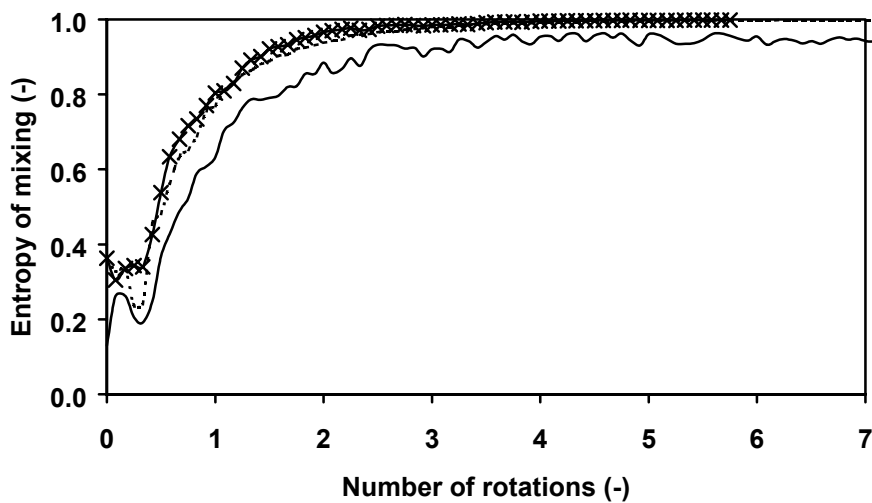
Figure 5. The predicted radial entropy of mixing curves for rotating drums with straight and curved baffles. - - - 3D with straight baffles, —— 2D with straight baffles, 3D -x-x- with curved baffles (simulation without particle rotation).

Small variations in the height of the initial interface due to the random packing of the settled particles in the drum determined the initial offset of the entropy.

Application of straight baffles in the drum gives similar radial mixing behavior in the 2D and 3D simulations (Fig. 5). In this case, the simulated flow of the particles near the sidewall did not differ from the bulk flow. Because the 2D model was extensively validated in previous research (Schutyser et al., 2001), we may conclude that the similar predictions for radial mixing behavior in both 2D and 3D support the validity of the 3D model. The differences between radial mixing in a drum with curved or straight baffles were found to be negligible (Fig. 5). Apparently, the expected difference in axial mixing behavior did not significantly influence the radial mixing behavior.

Simulations of drum mixing: axial mixing

No baffles

The 3D discrete particle simulations provided the opportunity to predict mixing behavior of the wheat grains along the horizontal axis of a rotating drum. The predicted axial mixing behavior was experimentally verified, using a solidification method and image analysis to obtain representative data on mixture composition along the horizontal axis of the drum. The conventional method (i.e., taking discrete samples) to characterize mixtures is not always very reliable (Wightman and Muzzio, 1998). Parameters such as sample size, number of samples, and the location of the sample points can affect the measured values considerably. Marsh et al. (2000), for example, experimentally studied axial mixing in a rotating SSF bioreactor, using a tracer method. In their study it was assumed that samples were representative for a whole

section of the bed. Discrete particle simulations show that radial gradients may occur, which makes the use of discrete samples less reliable, or at least causes a loss of information.

We compared the concentration profiles of two initially separated colored fractions along the horizontal axis for simulation and experiment after five and seven rotations (Fig. 6). Subsequently, dispersion coefficients for experiment and simulation were obtained, by fitting the concentration profiles with the solution of Fick's diffusion law [Eq. (10)]. It was found that the experimentally obtained, and simulated, concentration profiles of the colored wheat grains could be well described with Fick's diffusion law, when the first nine summation terms in Eq. (10) were taken into account. For five rotations, the dispersion coefficients were $7.1 \cdot 10^{-5}$ and $3.9 \cdot 10^{-5}$ for the experiments and the simulation, respectively; for seven rotations these values were $6.7 \cdot 10^{-5}$ and $3.4 \cdot 10^{-5}$. The average dispersion coefficients found were $7 \cdot 10^{-5}$ m^2/rev (experiment) and $4 \cdot 10^{-5}$ m^2/rev (simulation), respectively. From these results it appears that the discrete particle simulation model underestimated the axial mixing. However, it should be noted that there was an experimental error in the image analysis, which we estimated to be in the order of magnitude of 0.1. Such a relatively small deviation in the measured fractions of colored particles had a large effect on the dispersion coefficient for the low number of rotations used here. Thus, our conclusion is that discrete particle simulations can predict axial mixing with reasonable accuracy.

The simulation time for discrete particle simulations increases considerably when the number of particles in the system increases. In order to simulate one drum rotation of our system, containing 36000 particles, 48 hours of computation are required. Because axial mixing proceeds rather slowly, it is not practical to simulate the total number of rotations needed for complete mixing. Therefore, we used the dispersion model to extrapolate the experimental and simulation results and predict the axial concentration profiles after many more rotations. From the concentration profiles calculated with the dispersion model, the entropy of mixing of the system was calculated (Fig. 7). The numbers of rotations needed for complete mixing (i.e., entropy of mixing = 0.9) were estimated to be 122 rotations and 64 rotations, respectively, for simulation and experiment (Table I and Fig. 7). The twofold difference in the dispersion coefficient was reflected in this result.

Table I. Fitted dispersion coefficients and numbers of rotations needed for complete axial mixing calculated with Eq. 7 (entropy of mixing = 0.9).

Design	$D_{simulation}$ (m^{2}rev^{-1})	$D_{experiment}$ (m^{2}rev^{-1})	$N_{simulation}$ (-)	$N_{experiment}$ (-)
Without baffles	$4 \cdot 10^{-5}$	$7 \cdot 10^{-5}$	122	64
Straight baffles[1]	$1.6 \cdot 10^{-4}$	$5 \cdot 10^{-4}$	28	9
Curved baffles	ND	ND	3	3 - 4

[1] Calculated with the discrete particle model with particle rotation. ND, not determined.
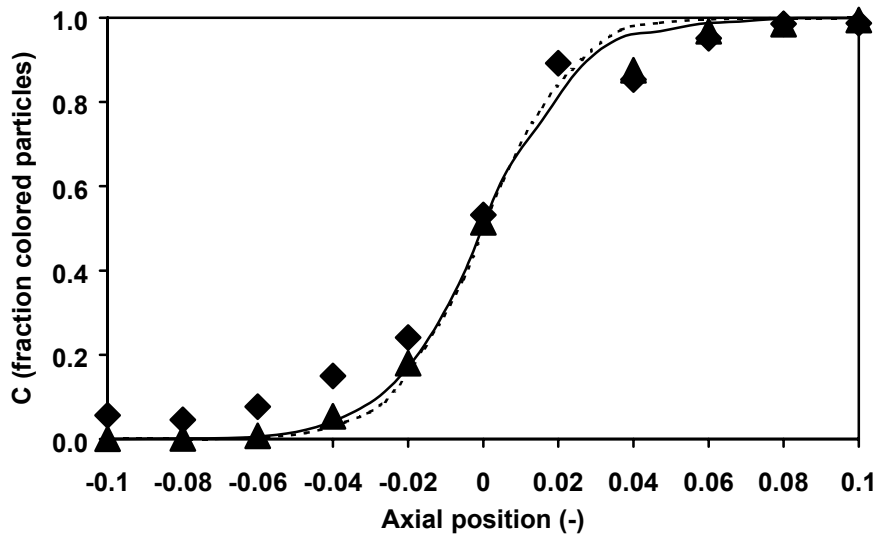
Figure 6. Comparison of concentration profiles found in experiments and predicted by the discrete particle model, after five and seven rotations for a drum without baffles (▲) experiment for N = 5, (◆) experiment for N = 7, - - - simulation for N = 5, ——— simulation for N = 7.
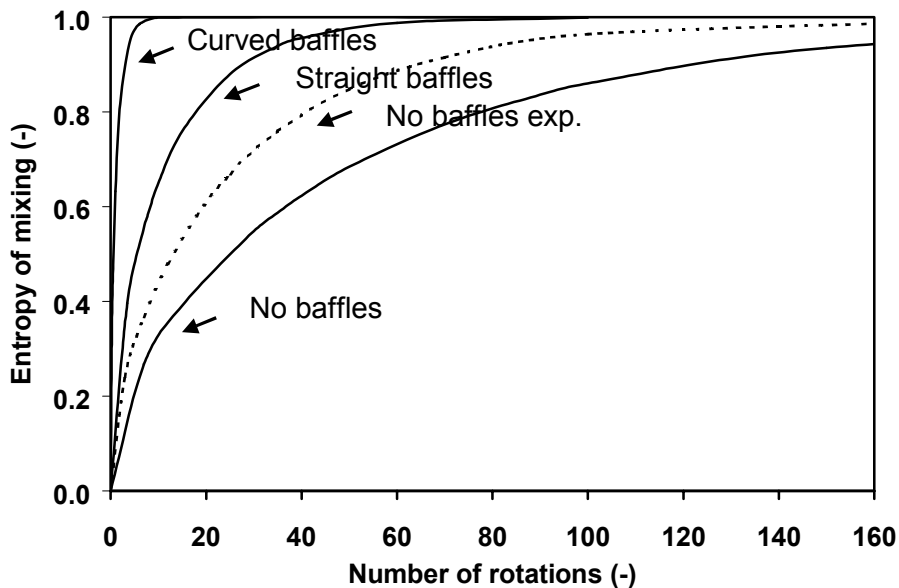
Figure 7. The entropy of mixing curve predicted with the axial dispersion coefficients derived from either the discrete particle model (closed lines) or the experiments (staggered line) for different drum designs. Only for the drum without baffles the entropy of mixing curve is shown with the axial dispersion coefficient derived from experiments.

Straight large baffles

The axial mixing in the drum with four straight baffles may be expected not to differ much from that in the drum without baffles, because the straight baffles are not designed to enhance axial particle movement. However, from the experiments it appears that mixing proceeded considerably faster when large straight baffles (66 % of the drum radius) were implemented (Fig. 8). In previous research it was found that these baffles have a large influence on the radial mixing behavior as they can disturb the solid body rotation and literally turn the bed (Schutyser et al., 2001). During mixing experiments in a drum with baffles it can be easily observed that the wheat grains move more rapidly at the surface of the bed than they do in a drum without baffles. This results in more and faster collisions between particles. In this way baffles enhance particle mixing in the radial, but also in the axial, direction of the drum.

Although the discrete particle model predictions for the radial mixing behavior in a drum with large baffles coincided with the experimental results, this was not the case for the axial mixing behavior. As in the 2D discrete particle simulations, the baffles were simulated as large arrays of partially overlapping particles, which rotated at the same rate as the drum. The predicted concentration profiles after 3.5 and 7 rotations are compared with duplicate experimental results in Figure 8. From this comparison it can be concluded that the simulated particle movement in the axial direction of the drum was much smaller than the movement in the experiments. The reason for the large difference between model predictions and experiments might be found in the assumptions we made in the discrete particle model. A wheat grain was modeled as a simple nonrotating, perfect sphere and its movements are described by specific interaction equations [Eqs. (1) and (2)]. In previous cases, these simplifications were found to be of minor significance and mixing behavior of the rotating drum system could thus be predicted
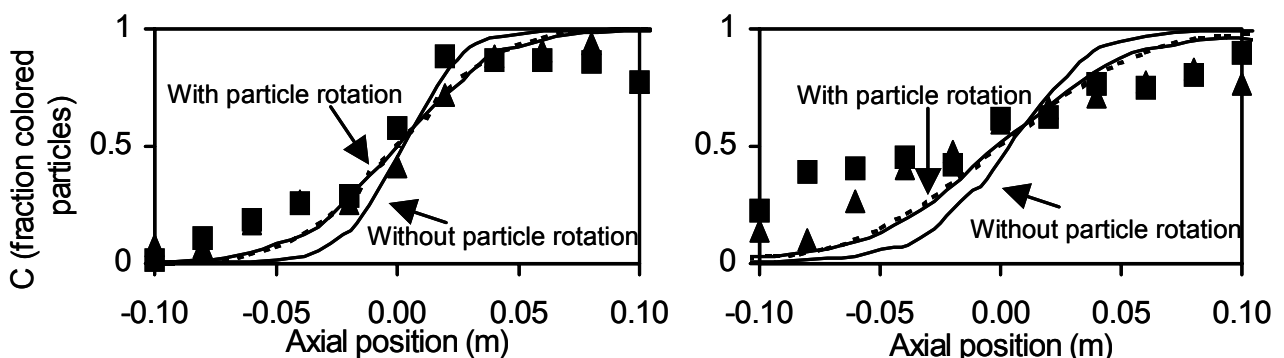
Figure 8. Comparison of experimentally found and predicted concentration profiles (by the discrete particle model) after 3.5 (left) and 7 (right) rotations for a drum with straight baffles (▲) and (■) are duplicate validation experiments, - - - is the fitted diffusion model on the simulation with particle rotation and —— are the simulation lines of the model with and without particle rotation.

accurately. However, in this case, the model may have to be extended to improve the accuracy; for example particle rotation may need to be included. To enhance dynamic movement of the particles during the avalanches and thus increase the axial mixing rate in the simulations, we incorporated rotation of particles in the model. In the discrete particle model used so far, rotational movements of the particles had not been taken into account. The concentration profiles obtained with the model, with and without rotation of particles, are depicted in Figure 8 for 3.5 and 7 rotations. It can be concluded that, for more accurate prediction of axial mixing in a drum with straight baffles particle rotation needs to be included in the discrete particle model. Because there is still a discrepancy visible between the model and the experiment (Fig. 8), more model improvements are in fact required. To further increase the accuracy of the model predictions, implementation of ellipsoidal instead of spherical particles would be reasonable. However, the big disadvantage of ellipsoidal particles is that the model becomes much more complicated and, as a result, simulations will require much more computation time. In most modeling studies of ellipsoidal particles only a relative small number of particles was considered (<1000) (Vu-Quoc et al., 2000). Implementing ellipsoidal particles in our model was thus not a practical option.

We also compared the predicted radial mixing behavior for the drum design with baffles, with and without particle rotation, and found no significant difference in radial mixing behavior. For accurate predictions of radial mixing behavior, model refinement is thus not necessary. This is also the case for predictions of axial mixing in a drum without baffles. In contrast, for accurate prediction of axial mixing in a drum with straight baffles, more research has to be conducted to determine the necessary details, such as particle shape, which need to be included in the discrete particle model. However, implementation of these details, needed to obtain accurate predictions, is very complicated and will also, undoubtedly, result in a large increase of computation time. Therefore, further research on the drum with straight baffles as a SSF fermenter, making use of a discrete particle model, will not be simple.

The remaining differences between model (with particle rotation) and experiment, as expressed in Figure 8, may thus be due to simplifications made in the model; for instance the assumption that particles are spherical instead of ellipsoidal. We also observed that at both ends of the drum (y < -0.08 and y > 0.08) the model predicts a more continuous flow downhill instead of the discrete avalanches we observe in the experiments. Such avalanches may promote axial dispersion. From duplicate experiments it can be concluded that the experimental results are reasonably accurate (Fig. 8). Differences between separate experiments may be due to the filling procedure, the gelatin slicing procedure and the image acquisition and analysis. However, we believe that the experimental errors contribute little to the differences between model and experiment.

In Table I the dispersion coefficient and the number of rotations for complete mixing (entropy = 0.9) are shown, which were obtained by fitting Fick's diffusion law [Eq. (10)] on the experimental data as well as the simulated concentration profiles. From these results, we conclude that the differences between the simulated and experimentally obtained values are larger for the drum with baffles than for the drum without baffles. This means that the discrete particle model more accurately predicts the axial mixing in the drum without baffles than in the drum with baffles, despite the inclusion of particle rotation in the model. For further research, for example heat and mass transfer in a rotating drum system, the model for the drum without baffles provides a better basis than the current model for the drum with straight baffles.

Curved baffles

Curved baffles (Fig. 2) are expected to enhance axial mixing. If a drum with such curved baffles is placed horizontally and rotates slowly, the grains are transported to one side of the drum. The transport continues until the angle of the bed with the horizontal axis is similar to the angle of repose ($\approx 35°$), and particles start to slide back. If the drum is placed under an angle of 20°, the angle of the bed with the axial axis of the drum is at most 15°, guaranteeing a more even distribution of material along the horizontal axis. It is possible to place the drum under a larger angle (close to 35°), but this would make the filling procedure in our experiments more difficult.

The baffles were again simulated by partially overlapping particle arrays, but here more particles were used, as the length of the curved baffle was larger than the straight baffle. From the simulations (without particle rotation) axial concentration profiles were obtained after several numbers of rotations (Fig. 9). These results show that axial mixing proceeds very rapidly in comparison with the former drum designs. From the shape of the concentration profiles it can also be concluded that the dominant mechanism for mixing is not random dispersion but rather convection. Therefore, it is not valid to use Fick's law to describe the axial mixing behavior. This is in contrast to the previous drum designs. After three rotations, the discrete particle model predicts an almost flat concentration profile, indicating that complete mixing has been achieved. The concentration profile after three rotations has also been obtained experimentally (Fig. 9). Figure 9 shows that the concentration profile of the experiment and the simulation are not equal, but in both cases a high degree of mixing was obtained (S_{exp}=0.81 and S_{sim}=0.90). From these results, we can conclude that, using this baffle configuration, total mixing performance of the rotating drum is enhanced considerably.

In comparison with the drum with straight baffles, the mixing behavior in this design with curved baffles appeared to be less dependent on particle rotation. This can be concluded as the predictions of the model without rotation and the experiments were very similar. The drum with curved baffles may therefore be easier to design with the discrete particle model, as complicated
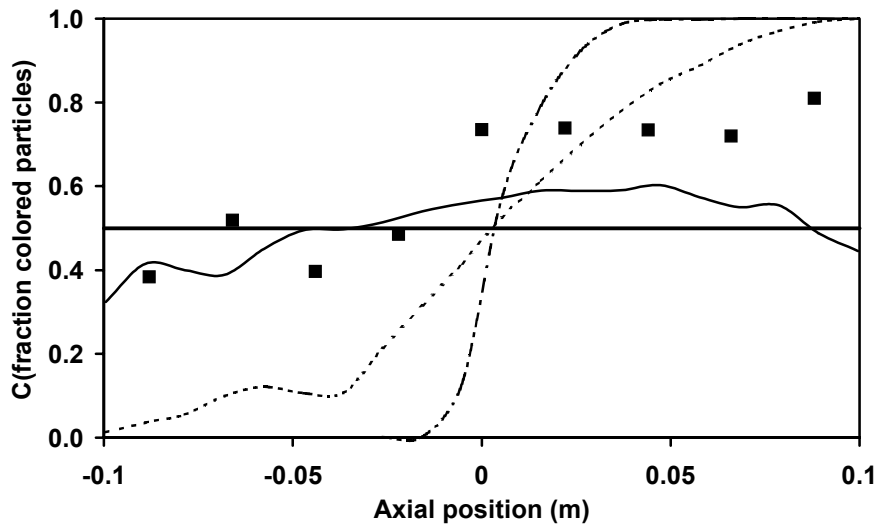
Figure 9. Concentration profiles in a rotating drum with curved baffles. Predicted concentration profiles by the discrete particle model after 0.25 (— - -), 0.5 (- - - -) and 3 (———) number of rotations. The experimentally determined concentration profile after three number of rotations (■).

model improvements are not necessary to improve the accuracy of the predictions. An additional advantage of the use of curved baffles is that continuous operation of the rotating drum might be applied (given that the drum is placed at an appropriate angle to the horizontal plane), as the baffles transport the mixed materials in the axial direction of the drum while providing radial mixing at the same time. In further studies not only will mixing in solid-state fermenters will be the subject of study, but also coupled heat- and moisture-transfer phenomena in SSF will be addressed.

Conclusions

Discrete particle simulations have provided more insight into understanding particle mixing behavior in three rotating drum designs, while offering detailed information concerning local phenomena. Concerning radial mixing behavior, we found similar results for 3D simulations and previous 2D simulations, which were extensively validated experimentally. This result confirms the validity of both discrete particle models. Concerning axial mixing behavior, we found that it was dominated by dispersion for a drum without baffles and a drum with straight baffles, as Fick's law could describe the concentration profiles during mixing of two initially separated colored fractions of wheat grain. The measured progress of axial mixing in the drum with straight baffles was somewhat faster than predicted by the simulation model. It was found that by including rotation of particles in the model, the predictions of the axial mixing behavior improved. This result indicates that, for a drum with straight baffles, particle rotation is

important for predicting the mixing behavior. This was not the case for radial mixing and axial mixing in the other drum designs. Improvement of the predictions of the discrete particle model for the drum with straight baffles—for example, by implementation of ellipsoidal particles—is not easy to accomplish. In future research, the current models of the drums without baffles and with curved baffles will provide a more reliable basis on which to study the coupled heat and mass transfer processes in SSF. The predicted axial mixing behavior in the drum with curved baffles was similar to the experimental results. This drum design is found to be less dependent on particle rotation. After three to four rotations, complete mixing was achieved for both radial and axial direction. Guaranteeing fast mixing, this drum design with curved baffles should be explored further for application in SSF or in other particle mixing processes.

Nomenclature

C	relative concentration ($kg \cdot m^{-3}$)
D	axial dispersion coefficient ($m^2 \cdot rev^{-1}$)
D^*	axial dispersion coefficient ($m^2 \cdot s^{-1}$)
$\vec{F}_n$	normal component of the contact force (N)
$\vec{F}_s$	tangential component of the contact force (N)
Fr	Froude number (-)
g	gravitation constant ($m \cdot s^{-2}$)
I	moment of inertia ($kg \cdot m^2$).
k_n	stiffness coefficient ($N \cdot m^{-1}$)
L_d	length of the drum (m)
m	mass (kg)
$\vec{M}$	total torque ($N \cdot m$)
N	number of rotations (-)
N_p	total number of particles in the system (-)
$N_{cel}(i)$	number of particles in cell i (-)
$\vec{n}_{ij}$	normal unit vector (-)
nix, niz	unit vectors of particle i in the x and z direction to the horizontal axis (-)
R_d	drum radius (m)
r_{ixz}	distance of particle i in the x-z direction to the horizontal axis (m)
r_p	particle radius (m)
r_y	distance of the particle in the y direction (m)
S	entropy of mixing (-)
S_o	entropy of a completely mixed system (-)
t	time (s)
v_{ix}, v_{iz}	velocities in x and z direction of particle i to the horizontal axis ($m \cdot s^{-1}$)
v_s	tangential velocity difference between particle and wall ($m \cdot s^{-1}$)

$\vec{v}_{rij}$	normal velocity difference (m·s^{-1})
$\vec{v}_{sij}$	tangential velocity difference (m·s^{-1}).
$x_1(i), x_2(i)$	fractions of the two colored particles in cell i (-)
y	position along the horizontal axis (m)
δ	computational overlap (m)
η_n	normal damping coefficient (kg·s^{-1})
μ_d	dynamic friction coefficient (-)
ω	angular velocity (rad·s^{-1})
γ_s	viscous friction coefficient (kg·s^{-1})

References

Allen MP, Tildesly DJ. 1987. Computer simulation of liquids. Oxford, Oxford University Press.

Blumberg W, Schlünder E-U. 1996. Transversale Schüttgutbewegung und konvektiver Stoffübergang in Drehrohren. Teil 1: Ohne Hubschaufeln. Chem Eng Proc 35:395-404.

Buchholtz V, Pöschel T, Tillemans H. 1995. Simulations of rotating drum experiments using non-spherical particles. Physica A 216:199-212

Cleary PW. 2000. DEM simulation of industrial particle flows: case studies of dragline excavators, mixing in tumblers and centrifugal mills. Powder Technol. 109:83-104.

Han B, Kiers JL, Nout RMJ. 1999. Solid-substrate fermentation of soybeans with *Rhizopus* spp.: Comparison of discontinuous rotation with stationary bed fermentation. J Biosc Bioeng 88:205-209.

Hardin MT, Mitchell DA, Howes T. 2000. Approach to designing rotating drum bioreactors for solid-state fermentation on the basis of dimensionless design factors. Biotechnol Bioeng 67:264-282.

Hogg R, Cahn DS, Healy TW, Fuerstenau DW. 1966. Diffusional mixing in an ideal system. Chem Eng Sci 21:1025-1038.

Hoomans, BPB. 2000. Granular Dynamics of Gas-Solid Two-Phase Flows. Ph.D. Thesis, University of Twente.

Iwai T, Hong C-W, Greil P. 1999. Fast particle pair detection algorithms for particle simulations. Int J Mod Phys 10:823-837.

Lacey, MC. 1954 Developments in the theory of particle mixing. J Appl Chem 4:257-268

Marsh AJ, Stuart DM, Mitchell DA, Howes T. 2000. Characterizing mixing in a rotating drum bioreactor for solid-state fermentation. Biotechnol Letters 22:473-477.

McCarthy JJ, Shinbrot T, Metcalfe G, Wolf DE, Ottino JM. 1996. Mixing of granular materials in slowly rotated containers. AIChE J 42:3351-3363.

Metcalfe G, Shinbrot T, McCarthy JJ, Ottino JM. 1995. Avalanche mixing of solids. Nature 374:39-41.

Mitchell DA, Krieger N, Stuart DM, Pandey A 2000. New developments in solid-state fermentation II Rational approaches to the design, operation and scale-up of bioreactors. Proc Biochem 35:1211-1225.

Nagel FJI, Tramper, J, Bakker, MSN, Rinzema, A. 2001. Temperature control in a continuously mixed bioreactor for solid-state fermentation. Biotechnol Bioeng 72:219-230.

Pandey A, Soccol CR, Mitchell DA. 2000. New developments in solid state fermentation: I-bioprocesses and products. Process Biochem 35:1153-1169.

Rao SJ, Bhatia SK, Khakar DV. 1991. Axial transport of granular solids in rotating cylinders. Part 2: Experiments in a non-flow system. Powder Technol 67:153-162.

Schäfer J, Dippel S, Wolf DE. 1996. Force schemes in simulations of granular materials. J Phys I 6:5-15.

Schutyser MAI, Padding JT, Weber FJ, Briels WJ, Rinzema A, Boom R. 2001. Discrete particle simulations predicting mixing behavior of solid substrate particles in a rotating drum. Biotechnol Bioeng 75:666-675.

Vu-Quoc L, Zhang X, Walton OR. 2000. A 3-D discrete element method for dry granular flows of ellipsoidal particles. Comput Methods Appl Mech Engrg 187:483-528.

Weber FJ, Tramper J, Rinzema A. 1999. A simplified material and energy balance approach for process development and scale-up of *Coniothyrium minitans* conidia production by solid-state cultivation in a packed-bed reactor. Biotechnol Bioeng 65:447-458.

Wightman C, Muzzio FJ. 1998. Mixing of granular material in a drum mixer undergoing rotational and rocking motions I. Uniform particles. Powder Technol 98:113-124.

Yamane K, Nakagawa M, Altobelli SA, Tanaka T, Tsuji Y. 1998. Steady particulate flows in a horizontal rotating cylinder. Phys Fluids 10:1419-1427.

Chapter 4

Numerical simulation and PEPT measurements of a 3D Conical Helical Blade Mixer: A high potential solids mixer for solid-state fermentation

Abstract

Helical-blade solids mixers have large potential as bioreactors for solid-state fermentation (SSF). Fundamental knowledge of the flow and mixing behavior is required for robust operation of these mixers. In this study predictions of a discrete particle model were compared to experiments with colored wheat grain particles and positron emission particle tracking (PEPT) measurements. In the discrete particle model individual movements of particles were calculated from interaction forces. It was concluded that the predicted overall flow behavior matched well with the PEPT measurements. Differences between the model predictions and the experiments with wheat grains were found to be due to the assumption that substrate particles were spherical, which was in the model. Model simulations and experiments with spherical green peas confirmed this. The mixing in the helical-blade mixer could be attributed to 1) the transport of particles up and down in the interior of the mixer, and 2) dispersion or micro-mixing of particles in the top region of the mixer. It appeared that the mixing rate scaled linearly with the rotation rate of the blade, although the average particle velocity did not scale proportionally. It may be that the flow behavior changes as a function of the rotation rate (e.g. changing thickness of the top region); further study is required to confirm this. To increase the mixing performance of the mixer, a larger blade or a change in the shape of the mixer (larger top surface/volume ratio) is recommended.

Introduction

Solid-state fermentation (SSF) involves the cultivation of fungi on moist solid substrates. SSF is an ancient technology that is used for the production of different fermented foods, such as sausages, cheese, Tempe, soy sauce and mushrooms. In the latest decades, numerous studies have been reported on potential new SSF products, such as for example aromas, organic acids, antibiotics and enzymes (Pandey, 1992; Robinson et al., 2001). Despite the large amount of research on SSF there are however relatively few new commercial applications. Various fermenter types, amongst others, packed beds, rotating drums, stirred beds and other solids mixers, have been applied for solid-state fermentation (Mitchell et al., 2000). However, despite a considerable amount of research on design and scale-up strategies for these fermenters, reliable operation of large-scale SSF fermenters is not straightforward. In order to facilitate robust operation of large-scale SSF, adequate control of temperature and moisture content and distribution is necessary. Because evaporative cooling is the most important cooling mechanism, dehydration of the substrate is inevitable. It is possible to compensate for this loss of water by addition of water during the fermentation (Nagel et al., 2001). To distribute the water in the bed, mixing action is required. Although mixing will facilitate robust process control during SSF, possible detrimental effects of mixing on fungal growth have to be considered. Ideally, the mixing would have to be gentle, not influencing fungal growth, and efficient, removing gradients in temperature and moisture content.

The production of high-value products by SSF, such as pharmaceuticals and food ingredients, requires that the design of the fermenter complies with FDA and GMP guidelines (Nagel, 2002). Equipment with mixing facilities that meets these requirements includes amongst others commercially available solids mixers, such as for example orbiting-screw mixers and helical-blade mixers. From practical experience it was known that these mixers exert low shear forces on the solids, which may be advantageous for SSF. Recently, Oostra et al. (in prep.) successfully explored the application of a pilot-scale helical-blade solids mixer for solid-state cultivation of the fungus *Coniothyrium minitans*. Although these solids mixers have a long history of application in food and pharmaceutical industry, most knowledge on scale-up behavior and design was obtained by trial and error. This implies that a time-consuming experimental design study is required for new applications.

In previous research we developed a mechanistic discrete particle model to study the mixing behavior of solid substrate particles (wheat grains) in a conventional rotating drum fermenter (Schutyser et al., 2001, Schutyser et al., 2002). This fermenter system was mainly chosen for its geometric simplicity and its suitability for the evaluation of mixing performance. Rotating drum fermenters have a long history of use, but mass and heat transfer between the headspace and the

bed are regarded to be poor in comparison with systems in which forced aeration through the bed is applied, e.g. stirred beds (Mitchell et al., 2000). Although the rotating drum may not be the best bioreactor concept available, modeling of this system provided fundamental insight and new tools. In this paper we report the extension of this discrete particle model to the geometry of a helical blade solids mixer.

Because it was unpractical to simulate the entire mixing process of a wheat grain bed in a pilot-scale solids mixer, a geometrically scaled-down transparent version of the mixer was constructed to validate the model predictions. Experiments and simulations were conducted with colored fractions of wheat grains to investigate the flow and mixing behavior in this solids mixer. Because accurate experimental data of the flow and mixing could not be obtained via these measurements, positron emission particle tracking (PEPT) experiments were conducted as well. With PEPT the movements of a radioactively labeled tracer particle could be followed without disturbing the flow behavior. To study the effect of the particle shape on the flow behavior in the mixer, also spherical green peas were used in the experiments.

Model development

Discrete particle model

In previous papers we presented discrete particle models for two-dimensional (2D) and three-dimensional (3D) rotating drum designs (Schutyser et al., 2001; Schutyser et al., 2002). In this modeling approach motion of particles is predicted by calculating all forces acting on each individual particle. Inter-particle, particle-wall and gravitational forces are included (Schutyser et al., 2002).

The normal interaction force ($\vec{F}_n$) is described by:

$$\vec{F}_n = \left(-k_n \delta - \eta_n \left(\vec{v}_{rij} \cdot \vec{n}_{ij} \right) \right) \vec{n}_{ij} \tag{1}$$

in which k_n is the stiffness coefficient (N·m^{-1}), η_n is the normal damping coefficient (kg·s^{-1}), $\vec{v}_{rij}$ is the normal velocity difference (m·s^{-1}), $\vec{n}_{ij}$ is the normal unit vector (-).

The tangential force ($\vec{F}_s$) is described by:

$$\vec{F}_s = -\min\left(\left| \gamma_s \, v_{sij} \right|, \left| \mu_d F_n \right| \right) \cdot \text{sign}(\vec{v}_{sij}) \tag{2}$$

in which γ_s is the viscous friction coefficient (kg·s^{-1}), μ_d is the dynamic friction coefficient (-), $\vec{v}_{sij}$ is the tangential velocity difference (m·s^{-1}).

The values of the parameters in equations 1 and 2 were assumed to be identical for the wheat grains and the green peas and are shown in Table I (Schutyser et al., 2001). From the resulting force on each particle, new positions and velocities were calculated by integration of Newton's equation of motion. Updating of forces and calculation of new positions and velocities were performed at 20 µs intervals. Contact detection and subsequent inter-particle force calculations are responsible for the larger part of the total computational effort during simulation. Sophisticated contact detection algorithms may be used to limit the amount of calculations (Allen and Tildesly, 1985). In this study, a linked cell method was used, which was found to provide optimum computational performance for simulation of large particle systems (Schutyser et al., 2002).

In the discrete particle model, the wheat grains were modeled as spherical particles. The implementation of, for example ellipsoidal particles was not considered, as relatively large systems (> 1000 particles) cannot be evaluated within reasonable computation time (Vu-Quoc et al., 2000). Despite our use of spherical particles, most predictions of the mixing behavior in different rotating drum designs were found to be accurate, when compared to the validation experiments with moist autoclaved wheat grains (Schutyser et al., 2001; Schutyser et al., 2002).

Table I. Simulation parameters

Description	Value
Stiffness coefficient	$k_n = 125$ N·m^{-1}
Damping coefficient	$\eta = 0.079$ kg·s^{-1}
Viscous friction coefficient	$\gamma = 1.0$ kg·s^{-1}
Dynamic friction coefficient	$\mu = 0.5$

Helical blade mixer

The helical blades in the model and the transparent scaled-down mixer were geometrically identical to the blade present in a pilot-scale mixer from Hosokawa (NL) that is used for solid-state fermentation in our laboratory. To simulate the helical-blade mixer, a mathematical description of the geometry of the blade was needed. Therefore we measured the absolute height of the spiral after 0, 0.5, 1, 1.5, 1.75 turns [0-3.5π rad], starting from the bottom of the blade. The helical blade was a continuous spiral with a pitch (i.e. height of one turn of the blade) that increased with height. The blade width was varied between 10 and 20 mm and the blade thickness was equal to the diameter of one particle (4.9 mm). The blade is modeled as a large array of overlapping particles. A polynomial function was used to describe the height of

the blade (z in mm) as a function of the turns of the spiral, starting at the bottom with 0 rad (β in rad):

$$z(\beta) = -a_0 + a_1\beta + a_2\beta^2 + a_3\beta^3 \qquad (3)$$

in which: a_0 .. a_3 are fit parameters. The following values were obtained for the fit parameters: a_0 .. a_3= 100.35 (mm), 9.098 (mm/rad), -0.605 (mm/rad^2), 0.088 (mm/rad^3). The corresponding x and y coordinates of the blade are described by the following equations:

$$x(\beta) = r(\beta) \cdot \cos(\beta) \qquad (4a)$$

$$y(\beta) = r(\beta) \cdot \sin(\beta) \qquad (4b)$$

where $r(\beta) = \dfrac{R_{D\max} - R_{D\min}}{L_D} \cdot \left(z(\beta) + \dfrac{1}{2}L_D \right) + R_{D\min}$

in which: $R_{D\max}$ and $R_{D\min}$ are the maximum and minimum radii of the cone, L_D is the height of the cone, and $r(\beta)$ is the distance between the central axis and the wall at a certain height, $z(\beta)$. The point of origin was defined exactly in the middle of the solids mixer (Fig.1). The vertical central axis and the three side arms were also modeled by straight arrays of overlapping particles (Fig. 1).

During simulation of the helical blade mixer filled with particles, the spiral is rotated. Therefore all blade particles need to be rotated around the central axis:

$$x(\beta,t) = r(\beta) \cdot \cos(\omega t - \beta) \qquad (5a)$$

$$y(\beta,t) = -r(\beta) \cdot \sin(\omega t - \beta) \qquad (5b)$$

in which: ω is the rotation rate of the blade (rad/s), and t is time (s).

To obtain a smooth surface of the blade 8230 overlapping particles were used for modeling the blade. For example to model a 10 mm wide blade, 5 overlapping particles (diameter = 4.9 mm) were used in the model across the width. Division of the displacement of the blade particles and the integration time step yielded the velocities of the blade particles. Only normal forces were considered in the interaction of bulk particles and blade particles.

The interaction force between a particle and the bottom or top wall of the cone consisted of a repulsive normal force in the z-direction and a friction force in the x-y plane. The normal interaction force that was calculated between a particle and the sidewall of the cone was based on the following computational overlap (δ) between the wall and the particle:

$$\delta = \frac{\sigma}{2} - \left(r_\beta - \sqrt{x^2 + y^2} \right) \cdot \cos(\alpha) \qquad (6)$$
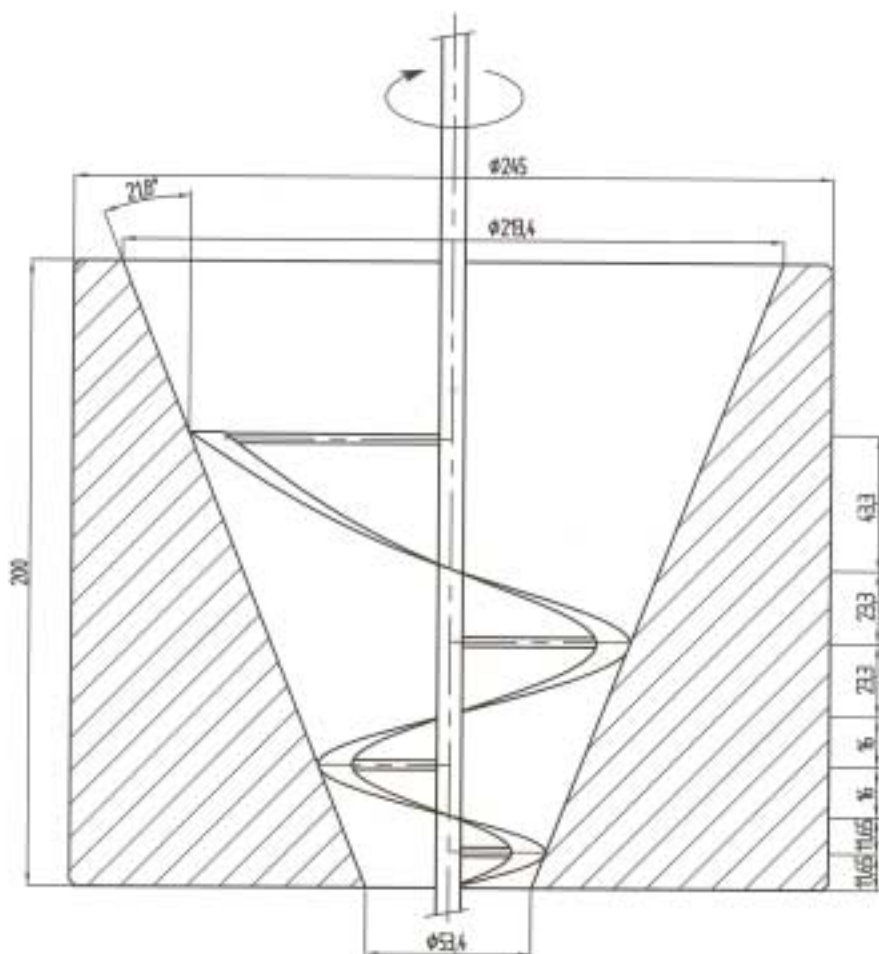
Figure 1. Design of the down-scaled helical blade mixer (sizes in mm).

in which: σ is the diameter of the particle, α is the angle of the wall with the vertical axis, 21.8° (Fig. 1).

Materials and methods

Mixer design

A transparent (Perspex) downscaled helical-blade mixer was constructed for this study (Fig. 1). The mixer was geometrically scaled down (1:3) from an industrial helical-blade mixer (Hosokawa, The Netherlands). The design of this large helical blade mixer is based on a long history of experience of Hosokawa. The total vessel volume and the bed volume of the large mixer were 84.5 L and 41.6 L, respectively, whereas the total and bed volumes of the small mixer were 3.1 L and 1.5 L. The maximum and minimum radii of the cone of the small mixer (R_{Dmax} and R_{Dmin}) were 106.7 and 26.7 mm, respectively; the height of the cone (L_D) was 200

mm. Two blade widths were used in the small mixer, viz. 10 and 20 mm. The thickness of the blade was 1 mm.

Experimental conditions

The wheat grains were treated according to the standard procedure applied with substrate particles for SSF. The whole-wheat grains were soaked for 2.5 h in excess tap water of 60 °C. Subsequently, the soaked grains were sieved and autoclaved for 1 h at 121 °C to obtain a final average weight of 72 mg per grain (0.8 kg water / kg dry matter). The (spherical) green peas were only soaked for 2.5 hours and not autoclaved, to obtain a final weight of 515 mg per pea. Both wheat grains and green peas were obtained from a local supplier. The mixer was filled with 960 grams of particles, which resulted in a bed height of 145 mm, just below the highest side arm. Methylene blue (Merck, Germany) and Bengal rose B (Fluka, Switzerland) were used for coloring particles. For validation purposes the experimental mixing performance was studied by mixing a bottom layer consisting of red colored grains and a top layer of green colored grains.

Simulation

Green peas are spherical and larger than wheat grains. The number of particles that were involved in the simulation therefore varied according to the type of particles (wheat grains or green peas) and the helical blade (small or large) that were simulated. The small helical blade contained 8230 particles while the large helical blade contained 16230 particles (d_p=4.9 mm). To obtain similar fill levels for the wheat grains (d_p=4.9 mm) and the green peas (d_p = 9.4 mm), 13248 and 1864 particles (excluding the helical blade particles) were used for simulation of the grains and the peas, respectively. Simulation conditions are shown in Table II. For visualization of the model we used AVS/Express 5.0, UK.

Positron emission particle tracking (PEPT) measurements

PEPT is a non-invasive measurement technique used to track the motion of a single tracer particle for a period of time. This technique has been successfully applied to study solids mixing in numerous systems, such as fluidized beds (Hoomans et al., 2001) and mixers (Conway-Baker et al., 2002; Parker et al., 1997; Stewart et al., 2001). A tracer particle is used that contains a radioisotope, which decays by a form of beta-decay producing a positron. Once emitted from the nucleus, the positron annihilates with an electron, releasing energy in the form of two 511 keV γ-rays which are emitted back-to-back (180°). The γ-rays are detected simultaneously by two sensitive cameras that are placed according to Figure 2 (Parker et al., 2002). The position of the tracer particle can be calculated from the intersection point after detecting multiple successful annihilation vectors (Fig 2).

Table II. The operation conditions that were used in the six PEPT experiments and in the six discrete particle simulations that were conducted

Case Number	Substrate	Rotation speed (rpm)	Ribbon Size (mm)
1	wheat grains	5	10
2	wheat grains	1	10
3	wheat grains	5	20
4	wheat grains	1	20
5	peas	5	10
6	peas	5	20
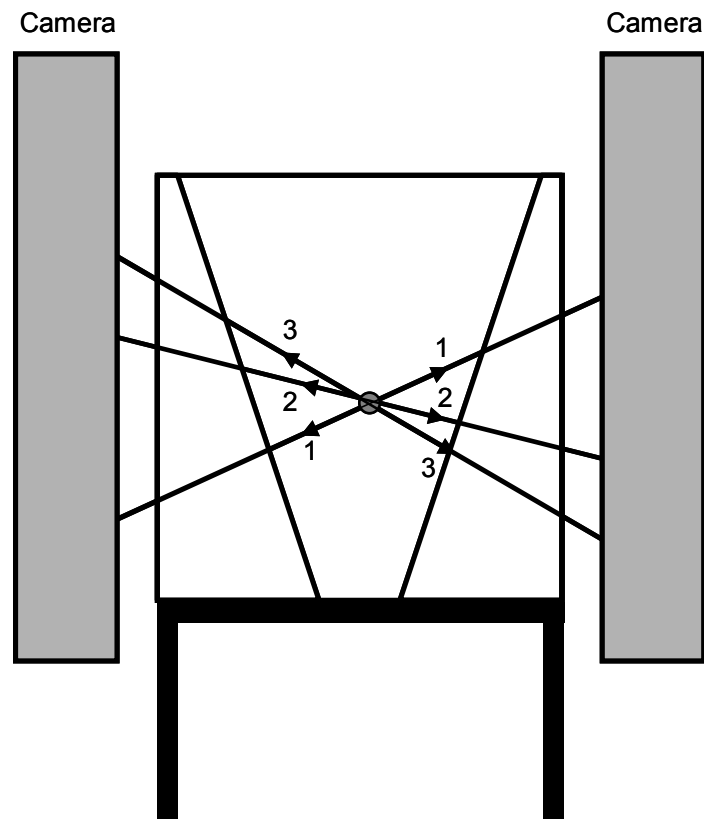
Figure 2. Position of the solids mixer between the two cameras. The particle position is reconstructed after detecting multiple successful annihilation vectors.

In this research we applied the radioisotope ^{18}F, which could emit 511 keV annihilation photons and had a half-life of 109 minutes. A tracer particle that contained ^{18}F gave about 74% valid events in total and a high accuracy of detected locations. ^{18}F is produced from distilled water by direct irradiation, using a 33 MeV ^{3}He beam from the Birmingham Radial Ridge Cyclotron.

The tracer particle was produced according to the following procedure. Firstly, a resin particle was labeled with ^{18}F. The resin particle (d=600μm) was made from quaternary amines in

hydroxide form. After replacement of the hydroxide ions by the ^{18}F atoms, the resin particle became a γ-ray emitter. The resin particle was inserted in a small hole in the wheat grain or pea. Some glue was used to seal the hole. Several PEPT experiments were performed with different conditions (Table II).

Post-processing of the PEPT and the simulation data

From the PEPT measurements we obtained the positions of a single tracer particle during a long time of mixing. To visualize the motion of the tracer particle, we used software developed by D. Parker at Birmingham University. From the simulations we obtained positions and velocities of all particles in the mixer for only a short period of mixing (12 blade rotations). To compare the experiments and the model predictions we performed post-processing.

From the raw data obtained from the PEPT measurements we could calculate the particle velocities via the "six-point" method (Stewart et al., 2001). The use of several data points instead of two reduces the effect of the measurement error. From these calculations we obtained the velocity of the tracer particle at every position along its path. The particle velocities simulated in the discrete particle model could be obtained directly from the output of the simulation.

Velocity histograms were constructed by calculating the percentage of velocities that were detected between 0 and 50 mm/s with a bin-width of 1 mm/s. To construct the velocity maps, the system was divided into a grid of 7x7 mm^2 cells and the average velocity was calculated in each cell. Vector plots that were mainly used for comparison were constructed from the radial velocities. The advantage of using the radial velocity is that the comparison is based on all data produced during the PEPT measurement and the simulation. Radial velocity vector plots were mirrored along the vertical axis to get a better overview of the flow inside the mixer.

To characterize the degree of mixedness we calculated the entropy of mixing (Schutyser et al., 2001). The calculation of the entropy of mixing is based on the definition of a grid (I,J,K) across the mixer. In each cell (i,j,k), the entropy of mixing is determined and subsequently the entropy of mixing of the whole system is calculated by addition of the entropy of mixing of all cells:

$$S = \frac{1}{S_0} \sum_i \left(x_1(i,j,k) log(x_1(i,j,k)) + x_2(i,j,k) log(x_2(i,j,k)) \right) \frac{N_{cel}(i,j,k)}{N} \tag{7}$$

in which S_o is the entropy of a completely mixed system, which depends on the fraction of colored particles in the system, $x_1(i,j,k)$, $x_2(i,j,k)$ are the fractions of the colored particles in cell i,j,k, $N_{cel}(i,j,k)$ is the number of particles in cell (i,j,k), N is the total number of particles in the system. The size of the grid should be chosen such that each grid cell contains a significant number of particles (Schutyser et al., 2001).
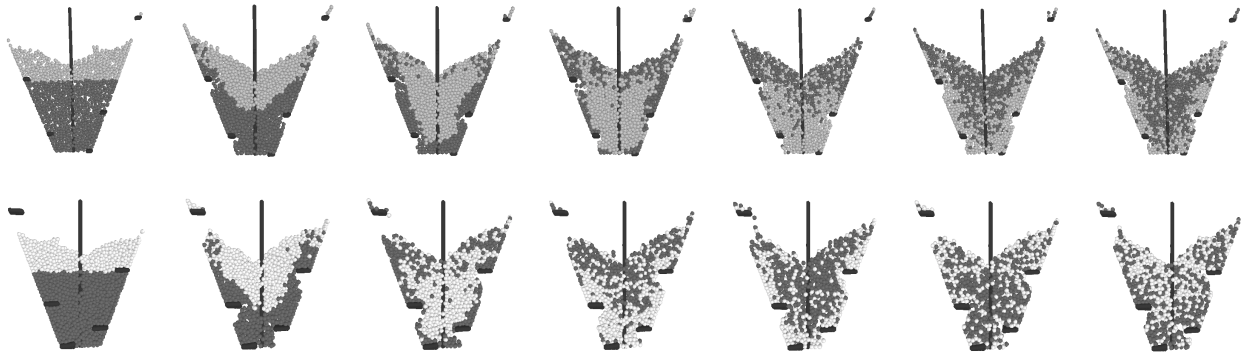
Figure 3. The simulated flow behavior inside the mixer is visualized by mixing of two horizontally colored layers of grains for the small (first row) and the large blade. Conditions are according to case number 1 and 3 (Table II). Snapshots are shown after 0, 2, 4, 6, 8, 10 and 12 blade rotations.

Results and Discussion

General flow behavior in the helical blade mixer

During experiments it could be observed that particles, which were transported to the top of the bed by the helical blade, migrated to the middle of the bed towards the central axis before disappearing downwards into the bulk. Hence, the expected flow inside the helical-blade mixer is that particles move downwards in the region near the central axis and move upwards somewhat quicker in the region near the wall due to the moving helical blade.

The simulated flow behavior of the granular medium inside the helical-blade mixer was visualized with the help of two horizontal layers of grains with different colors. Figure 3 shows subsequent snapshots of a vertical cross-section of the simulated bed through the central axis, for the small (10 mm) and the large ribbon (20 mm). Initially, it can be observed that the light gray particles descend through the interior of the mixer. At the same time, dark gray particles are transported up along the walls of the mixer along with the helical blade. The particle movements along the walls are expected to be faster than the movements in the middle of the bed as the volume of the first region is smaller. For the large blade similar but faster transport is observed. During the initial up and down transport of the two colored fractions in the mixer, it is observed that the interface between the two fractions remains quite clear (Fig. 3). This indicates that only few individual particles are exchanged between the two layers moving in opposite direction and thus little dispersion occurs. At the top of the bed particles migrate from the wall towards the central axis to move downwards again. Dispersion or micro-mixing appears to occur predominantly during this migration process. Mixing of the two colored fractions can be clearly observed when dark gray particles of the bottom layer enter the top region of the mixer, after 4-6 rotations (Fig. 3). The model predictions also show that after 12 rotations of both the small and large blade, the bed is still not mixed entirely (Fig. 3).
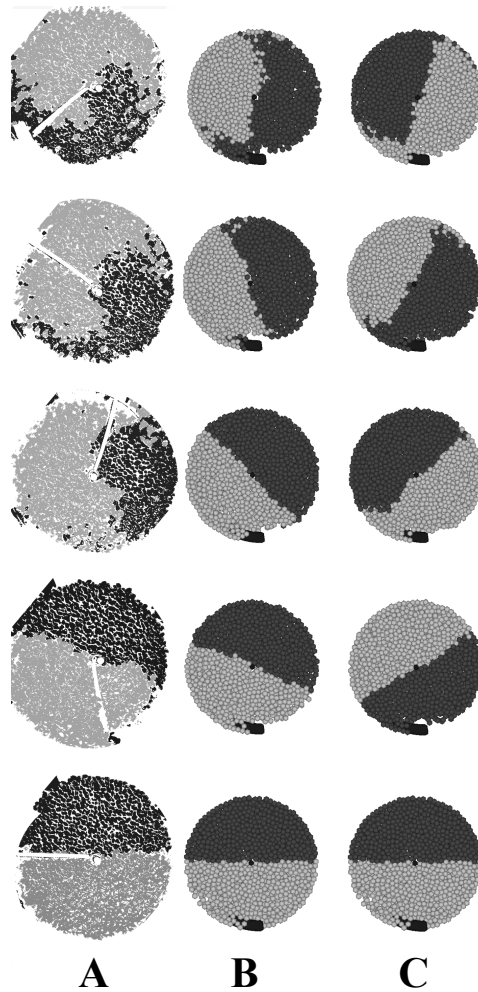
Figure 4. The flow behavior, which is observed from the top of the mixer, is visualized with two colored layers of grains. Conditions are according to case number 1 (Table II). The blade is rotating clockwise. **a** The experimental observations after 0, 0.67, 2.3, 3.1 and 3.9 rotations of the blade. **b** Simulation of the flow *with friction* between the wall and the particles after 0, 1, 2, 3 and 4 rotations. The ribbon on the top of the bed is visible as a black area **c** Simulation of the flow *without friction* between the wall and the particles after 0, 1, 2, 3 and 4 rotations.

A qualitative comparison shows broad agreement between the mixing patterns predicted by the model and the experimentally observed mixing patterns that were reported above. Model predictions also indicated that micro-mixing occurs slowly and mainly at the top surface of the bed.

Influence of model parameters on flow behavior

We investigated the influence of different parameters on the flow behavior of the particle bed in the mixer. During these investigations we observed that friction forces significantly influenced the simulated flow behavior. As an example, Figure 4 shows the effect of wall friction on the flow behavior. This figure depicts subsequent snapshots of the top view of the mixer, in which we mixed two layers of wheat grains with different colors. We show snapshots for the

experiment and for model predictions with and without friction between the particles and the wall. In the simulations without wall friction, the particles cannot dissipate kinetic energy at the wall of the mixer and therefore the bed turns more rapidly around the vertical axis together with the helical blade. The simulation with wall friction shows better agreement with the experimental observations, in which the bed only turns around the central axis at a slow rate. Normal interaction forces did not influence the simulated flow behavior and also the implementation of a small variation in the particle diameter did not significantly affect the results (results not shown).

Initially, we neglected the presence of the central axis and the side-arms during development of the model. We found, however, that the central axis and the supporting side-arms significantly influenced the flow behavior (in particular the highest and largest side-arm). In absence of the highest side-arm we found unrealistic accumulation of particles, packed along the wall from the top of the bed to the top of the mixer. The side-arm was found to disturb the formation of such structures, which were also not found in our experimental setup. Therefore, in subsequent simulations the central axis and all side-arms were included.

PEPT measurements

To obtain statistically reliable data from the PEPT measurements it was necessary to observe the tracer particle multiple times in all different regions in the mixer. This requirement was checked via occupancy plots that showed the total hits of the tracer particle in a certain region of the mixer. A cubic grid across the system defined these regions. Because the particles spend most time in the core of the mixer, highest occupancy was found in the regions near the core of the mixer. Low occupancies were mainly found near the wall of the mixer and at the top surface near the wall, although no regions in the bed were found that showed zero occupancy.

Figure 5 shows typical one-dimensional plots for the X, Y and Z direction of the motion of the tracer particle. These plots were obtained during a mixing experiment with wheat grains, and the large blade rotating at 5 rpm. The plots show that the movements in the X and Y direction show larger amplitude when the tracer particle is at the top of the bed. This is reasonable since the mixer has a conical shape and particles in the top of the mixer are thus less restricted in the X and Y direction. The plot of the motion in the Z direction shows that the particle oscillates vertically with a high frequency (about $1/12$ sec^{-1}) and small amplitude during its movement up and down in the mixer. It appears that each time the spiral passes near the particle (each rotation = 12 sec.) it is lifted and subsequently it moves downwards. XYZ-plots were also made for several randomly located particles from the simulation during 144 seconds (12 rotations). It was found that these particles exhibited similar movements during mixing including the fast up- and down movements in the Z-direction each 12 sec (results not shown).
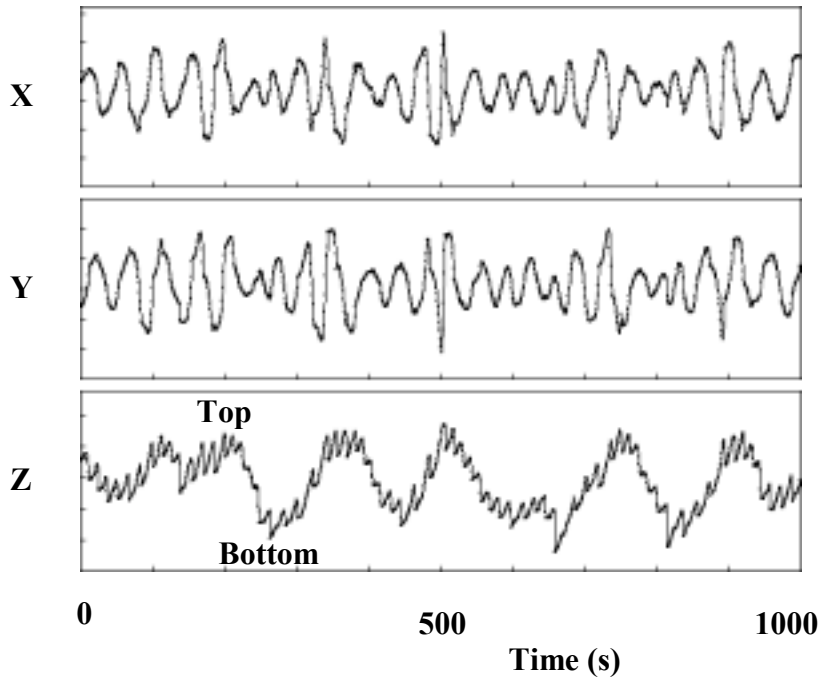
Figure 5. The x, y and z position of the radioactive labeled tracer particle during 1000 seconds mixing. Conditions are according to case number 3 (Table II).
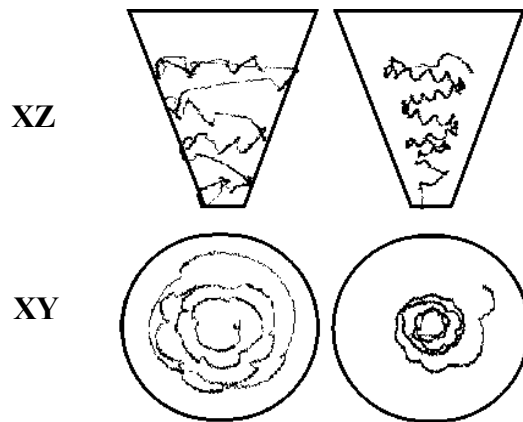
Figure 6. The motion of the tracer particle during upwards motion (left half of the diagram) and downwards motion (right half of the diagram). Sideview (XZ) and Topview (XY). Conditions are according to case number 1 (Table II).

In Figure 6 we plotted the movements of the tracer particle in two planes (side- and top view). These plots show how the particle moves in two distinct regions, viz. in the middle of the bed and near the wall of the mixer. From these plots it also appears that particles near the central axis make circular movements, though with a smaller amplitude than near the wall. In the plots of the side view, small movements in the Z-direction can be observed again. Thus, the blade does not only induce reactor-scale flow, but also a small-scale turbulence around the blade

itself. This may imply that the blade induces larger strain on the particles than necessary, which may negatively influence the fermentation performance.
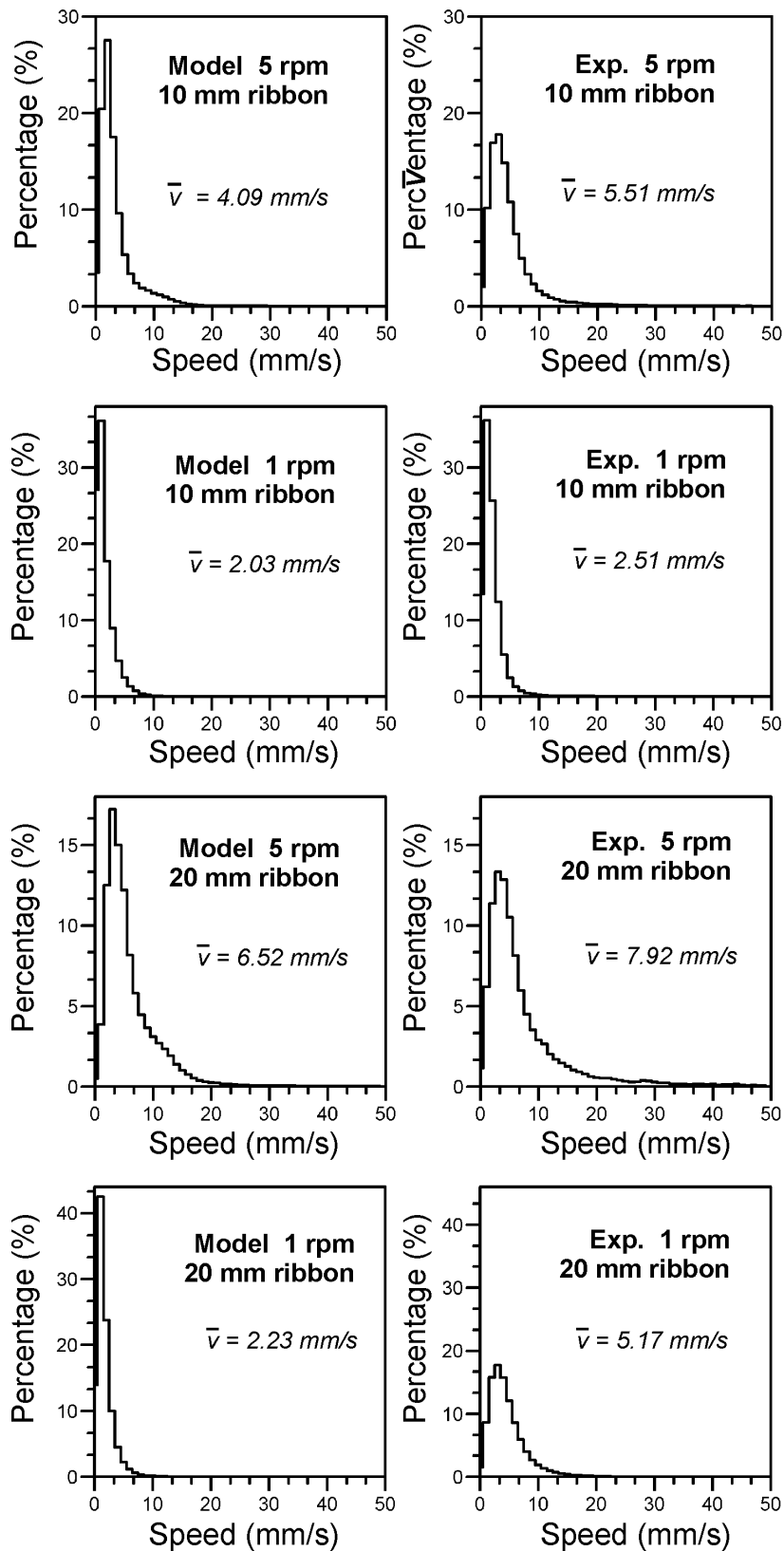
Velocity calculations

Figure 7 shows the velocity distribution histograms for the PEPT experiments with wheat grains, for the small and large blades and two different speeds. Also the corresponding histograms for the model simulations with identical conditions are shown. From the velocity distribution it can be concluded that the majority of the velocities that were detected were small, while a few percent of the detections indicate that some particles in the bed move at a large velocity. These few particles probably move fast at the top of the bed or in the small region near the wall of the mixer.

The histograms of the PEPT experiments and the model agree reasonably well, except for the large blade rotating at 1 rpm. The average velocities that were calculated for model and experiment are in the same order of magnitude and also the velocity distributions are comparable. The main difference between the model and the experiment is the somewhat larger velocities that were found during the experiments. This might be caused by the simplifications introduced in the model, especially concerning the friction forces.

One would expect that the mean particle velocity in the mixer is a factor five larger for a rotation rate of 5 rpm than it is at 1 rpm. Figure 7 shows that the mean velocities differ only by a factor two. This may be partially explained by the fact that particle movements in the mixer not only result from direct contact with the blade, but also from gravitational forces. Therefore, the particle velocities near the top surface of the bed might be influenced more by gravitation than those in the interior of the bed. We checked this by comparing the ratio between the particle velocities in the top region and near the central axis (in the middle of the bed) for blade rotation rates of 1 and 5 rpm. It was found that the ratio was 2.2 in the top region and 4.2 in the interior of the bed. This would suggest that the mixing rate does not scale linearly with the rotation rate of the helical blade, because dispersion of particles or micro-mixing mainly occurs at the top of the bed.

We compared the radial velocity vector plots that were obtained from the PEPT measurements and the simulations. Figure 8 shows the vector plots of mixing experiments and simulations with wheat grains for a small blade and a large blade, both rotating at 5 rpm. It can be concluded that the overall flow pattern inside the mixer is captured well by the model. A small region near the wall is again observed in which particles are quickly transported upwards. In the center of the bed, particles are moving downwards at a low speed.

Figure 7. Velocity distribution histograms from the model predictions and the PEPT measurements for cases 1-4 (Table II). The calculated average speed is displayed in mm/s.
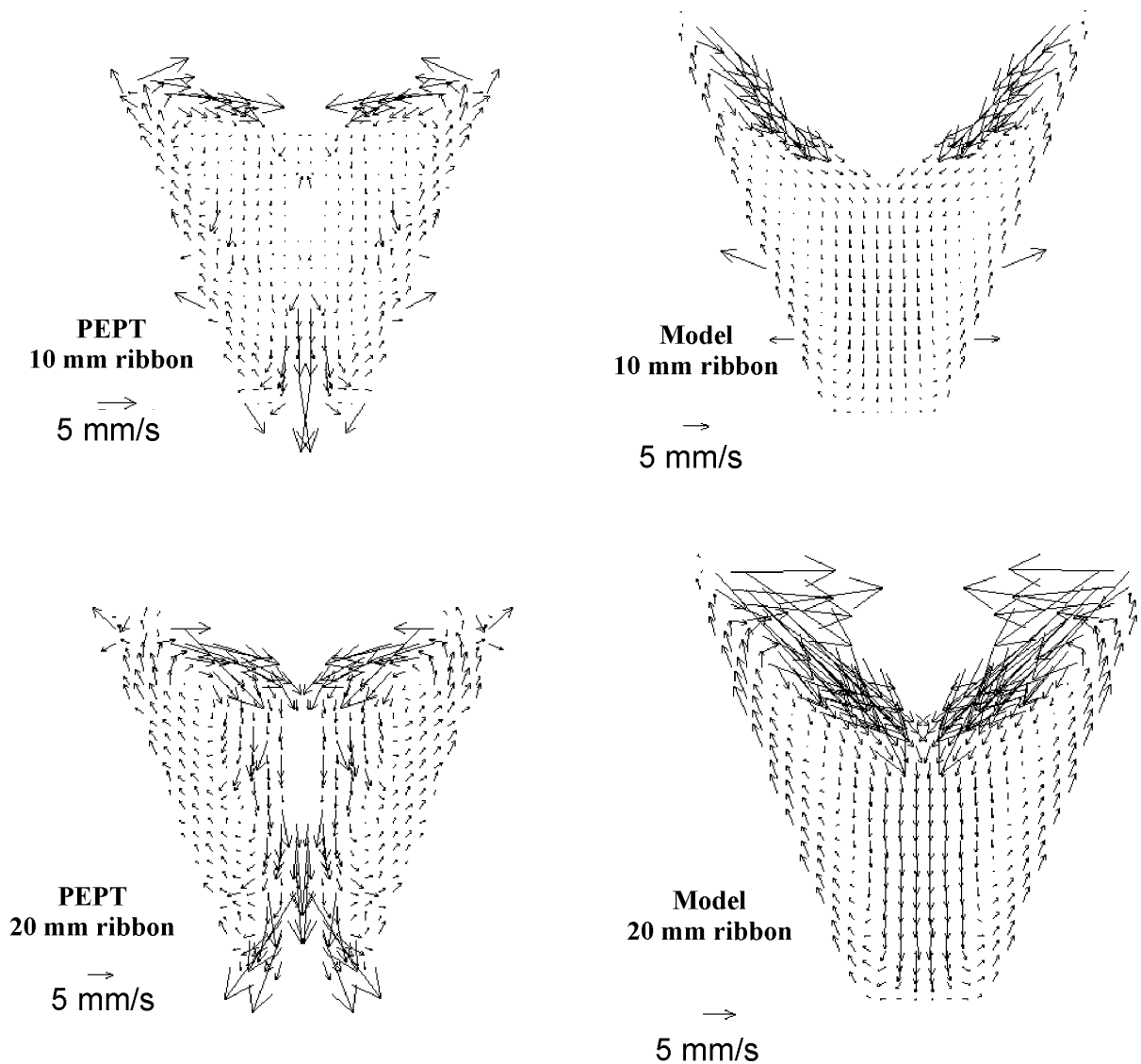
Figure 8. Velocity vector plots from the model predictions and the PEPT experiments for the wheat grains and a rotation rate of 5 rpm, cases 1 and 3 (Table II).

For the large blade it is logical that the region near the wall is larger and particles in the middle of the bed have to move down more rapidly. The most remarkable difference is that the slope of the particle bed at the top of the mixer is larger in the simulation than in the PEPT experiments.

The explanation for this difference in bed slope at the top of the bed was found when PEPT experiments and simulations were performed with spherical peas instead of ellipsoidal wheat grains. Figure 9 shows the vector plots of mixing experiments and simulations with green peas for a small and a large blade, both rotating at 5 rpm. From these results it was concluded that the model predicts the slope of the bed surface correctly. Especially the vector plot of the experiment with the large blade shows the increased slope that is found in the simulations. For
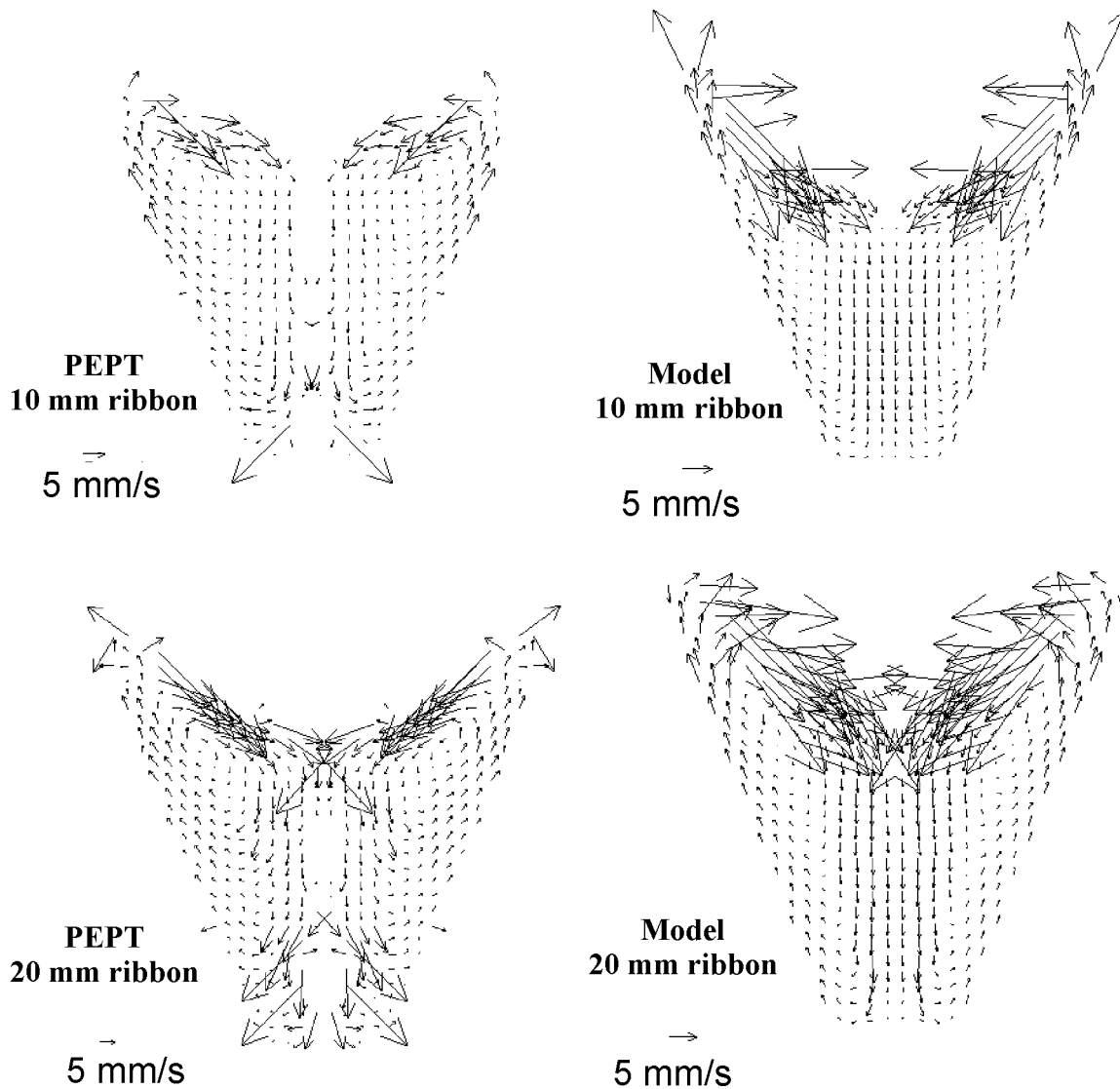
Figure 9. Velocity vector plots from the model predictions and the PEPT experiments for the green peas and a rotation rate of 5 rpm, cases 5 and 6 (Table II).

the measurements with the small blade the surface seems to be less steep again, but this may be attributed to a too short duration of the PEPT experiment. These results show that the particle shape, in addition to the friction forces, influences the slope of the bed in the mixer. The important message is that the dependency of the mixing rate on the particle shape makes the reactor design complicated: as the substrate is changed, performance of the reactor may decrease. Although the overall flow behavior of the wheat grains in the mixer is well predicted with the spherical particle approach, it may be worthwhile to implement ellipsoidal or irregularly shaped particles for specific applications. However, the computational effort involved will be so large that parallel computing will be necessary to solve such calculations within reasonable time. To illustrate: the computation times needed for the problems in this

study (see Table II) were 14 days for case 1 and 70 days for case 2, on a single-processor alpha workstation (XP1000).

In addition to the PEPT measurements we also obtained images (with a webcam) of the top view of the bed during mixing of two horizontal layers of wheat grains with different colors. We aimed at comparing these images with similar results obtained from simulations. However, it was impossible to obtain accurate data from these experiments. The PEPT measurements indicated that the model predicted the overall flow behavior well, except for the slope of the bed surface. It could therefore be concluded that the PEPT technique gives a good overview of the flow behavior, while image analysis of the bed surface did not yield accurate data.

Predicted entropy of mixing

To further verify the effect of different process parameters on the mixing behavior in the helical-blade mixer, we calculated the entropy of mixing as a function of the number of rotations of the helical blade (Fig. 10). Two horizontal layers of grains with different colors were used. To validate the approach with two horizontal layers, we also checked the mixing of two vertical layers with different colors (Fig. 11). We found that there are initially significant differences between the calculated entropies of mixing, as could be expected. After a while the entropy of mixing curves approach each other, which indicates that both methods give similar results. These results confirm the validity of the results that were based on the mixing of two horizontal layers.

It is important to choose the correct mesh size for the calculation of the entropy of mixing. For the helical-blade mixer we used a grid with cubic cells with a width of $2 \cdot d_p$, which is equivalent to about eight particles in a cell. From Figure 3 it was concluded that the bed was not entirely mixed after 12 rotations for both the small and the large blades. From Figure 10 it can also be concluded that the mixing proceeds very slowly and after 12 rotations the bed is still not mixed entirely, because the entropy of mixing still increases. To estimate the total number of rotations needed for complete mixing, a simulation with 60 blade rotations was performed (small blade, 5 rpm, wheat grains). It was found that the entropy of mixing remained constant at a value of 0.87 after 30-40 rotations of the blade. We visualized vertical cross-sections of the bed after several numbers of blade rotations and observed no visible change in mixedness after 40 rotations; the bed was entirely mixed after 30-40 rotations.

The entropy of mixing curves show fast initial mixing, while mixing proceeds slowly after about 4-6 rotations. The fast initial change in entropy of mixing is mainly due to the transport of the two layers up and down the mixer. The reason for this entropy increase is that the interface area between the two layers increases and therefore overlaps with many grid cells. After about 4-6 rotations, dispersion of dark and light gray particles at the top surface begins (micro-
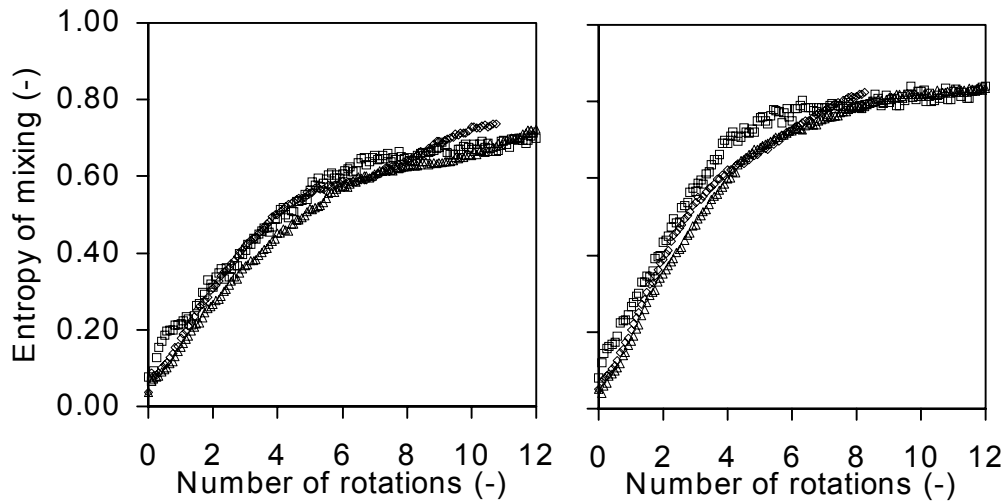
Figure 10. The entropy of mixing versus the number of rotations of the blade. The grid size used for the entropy of mixing calculation was $2 \cdot d_p$. (left) small blade: Δ case 1, $\square$ case 2 and $\diamond$ case 5 (right) large blade: Δ case 3, $\square$ case 4 and $\diamond$ case 6.
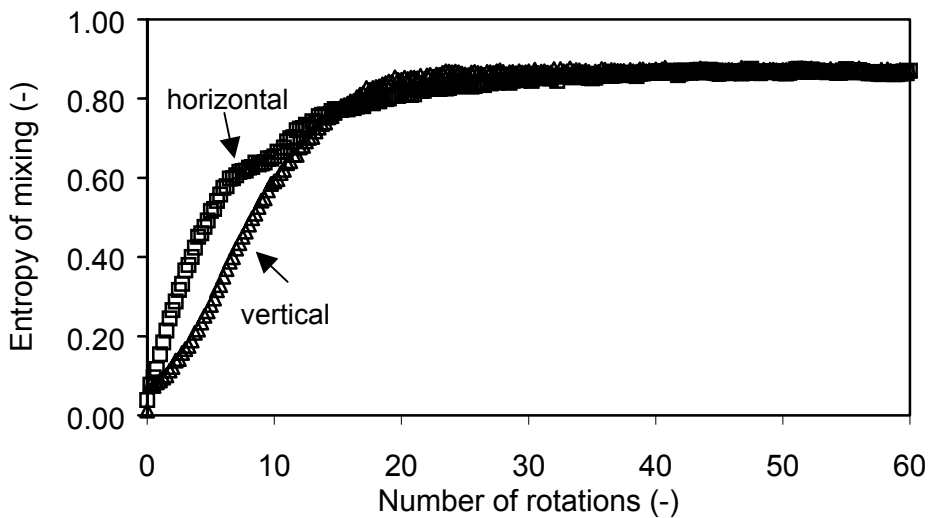
Figure 11. The entropy of mixing curve starting with two horizontally colored layers ($\square$) and starting with two vertically colored layers (Δ) for case 1 (grid size $2 \cdot d_p$).

mixing). Accordingly, the entropy of mixing changes due to the mixing at the top surface of the bed, and this mixing proceeds more slowly. During SSF in a helical-blade mixer, micro-mixing is needed to remove spatial gradients in for example temperature entirely. If the mixing period applied is too short, regions with higher temperatures may persist, which may negatively affect the fermentation (Schutyser et al., 2003).

Because the mixing progress is only dependent on the number of rotations of the blade, this would imply that the mixing rate scales linearly with the flow up and down in the mixer. Ellis et

al. (1994) observed similar mixing behavior in the Z-blade mixer. However, from the velocity histograms (Fig. 7) we concluded that the average particle velocity in the bed did not scale proportionally with the rotation rate of the blade. Therefore, it would not be logical that the mixing scales linearly with the rotation rate of the blade, especially not after 4-6 rotations when micro-mixing at the top surface is the dominant mixing mechanism. An additional change in flow behavior should be involved that enhances mixing, because the average particle velocity at the top surface only increases by a factor 2.2 when the rotation rate is changed from 1 to 5 rpm. The change in flow behavior could for example be an increase in the thickness of the top region. Further study is required to investigate this phenomenon in more detail.

The difference between the entropy of mixing curve for the small and the large blade can be explained by the fact that more particles are transported to the surface per rotation with the large blade (Fig. 10). The simulated mixing progress for wheat grains and green peas is also similar, which is reasonable since the flow patterns coincided well (Figs. 8 and 9). In practice, however, differences may be observed due to the difference in shape between the wheat grain and the green pea, because, particle shape affects flow behavior at the top surface of the substrate bed, according to the PEPT measurements.

When designing a helical-blade mixer it is important to know that micro-mixing occurs mainly at the top surface of the bed in the mixer. To improve the mixing performance of the helical blade mixer, the width of the blade could be increased or the design of the vessel could be changed. If the angle of the wall of the mixer (21.8º, see Fig. 1) is increased and/or the height of the mixer is decreased, the ratio of the top surface area to the volume of the bed is larger and mixing performance could be improved. When scaling up helical-blade mixers, mixing performance will rapidly decrease as the top surface / volume ratio of the bed becomes smaller. This effect could be partially compensated by using a relatively large blade or by reducing the height or increasing the angle of the wall of the mixer.

Conclusion

The discrete particle model developed for the helical-blade mixer captured the bulk flow behavior of the mixer adequately, compared to the results of the PEPT measurements. The main difference between the experiments and the model predictions was the slope of the top surface of the wheat grain bed. This deviation of the surface slope could be attributed to particle shape effects, because the model predicted the correct surface slope for a bed with spherical particles (green peas). This implies that the choice of substrate is an important parameter in the design of this mixer.

The flow inside a conical helical-blade mixer could be divided into three main zones: a small region near the wall in which particles are rapidly transported upwards, a larger region near the central axis in which particles move downwards and the top surface region in which particles migrate towards the central axis. It was found that micro-mixing occurred mainly in the top region of the mixer and not during the up and down transport in the interior of the mixer. The mixing rate scaled linearly with the rotation rate of the blade, which was in contrast to the fact that the average particle velocities only increased with a factor two when the rotation rate of the blade was increased from 1 to 5 rpm. This linear scaling of the mixing rate with the rotation rate of the blade may be explained by an additional change in flow behavior that enhances mixing with increasing rotation rate, for example an increasing thickness of the top layer.

It was found that by using a helical blade with a larger width, the total amount of particles transported per rotation is increased and thus also the mixing rate. Another possibility to improve the design of the mixer and to have better performance during scale-up of these mixers is to increase the ratio of the top surface area and the volume of the bed.

Acknowledgement

References

Allen MP, Tildesly DJ. 1987. Computer simulation of liquids. Oxford: Oxford university press. 385 p.

Conway-Baker J, Barley RW, Williams RA, Jia X, Kostuch J, McLoughlin B, Parker DJ. 2002. Measurement of the motion of grinding media in a vertically stirred mill using positron emission particle tracking (PEPT). Min Eng 15:53-59.

Ellis SP, Gray KR, Biddlestone AJ. 1994. Mixing evaluation of a Z-blade mixer developed as a novel solid-state bioreactor. Trans IChemE 72:158-162.

Hoomans BPB, Kuipers JM, Salleh MM, Stein M, Seville JK. 2001. Experimental validation of granular dynamics simulations of gas-fluidised beds with homogenous in-flow conditions using Positron Emission Particle Tracking. Powder Technol 116:166-177.

Mitchell DA, Krieger N, Stuart DM, Pandey A. 2000. New developments in solid-state fermentation II Rational approaches to the design, operation and scale-up of bioreactors. Process Biochem 35:1211-1225.

Nagel, FJI. 2002. Process control of Solid-State Fermentation. Ph.D. Thesis, WUR.

Nagel FJI, Tramper J, Bakker MSN, Rinzema A. 2001. Model for on-line moisture content control during solid-state fermentation. Biotechnol Bioeng 72:231-243.

Pandey A. 1992. Recent process developments in solid-state fermentation. Process Biochem 27:109-117.

Parker DJ, Dijkstra AE, Martin TW, Seville JPK. 1997. Positron Emission particle tracking studies of spherical particle motion in rotating drums. Chem Eng Sci 52:2011-2022.

Parker DJ, Forster RN, Fowles P, Takhar PS. 2002. Positron emission particle tracking using the new Birmingham positron camera. Nuclear Instruments And Methods In Physics Research Section A Accelerators Spectrometers Detectors And Associated Equipment 477:540-545.

Robinson T, Singh D, Nigam P. 2001. Solid-state fermentation: a promising microbial technology for secondary matabolite production. Appl Microb Biotech 55:284-289.

Schutyser MAI, Padding JT, Weber FJ, Briels WJ, Rinzema A, Boom R. 2001. Discrete particle simulations predicting mixing behavior of solid substrate particles in a rotating drum. Biotechnol Bioeng 75:666-675.

Schutyser MAI, Weber FJ, Briels WJ, Boom RM, Rinzema A. 2002. Three-dimensional simulation of grain mixing in three different rotating drum designs for solid-state fermentation. Biotechnol Bioeng 79:284-294.

Schutyser MAI, Weber FJ, Briels WJ, Rinzema A, Boom RM. 2003. Heat and water transfer in a rotating drum containing solid substrate particles. Biotechnol Bioeng 82:552-563

Stewart RL, Bridgwater J, Zhou YC, Yu AB. 2001. Simulated and measured flow of granules in a bladed mixer - a detailed comparison. Chem Eng Sci 56:5457-5471.

Vu-Quoc L, Zhang X, Walton OR. 2000. A 3-D discrete element method for dry granular flows of ellipsoidal particles. Comp Meth Appl Mech Eng 187:483-528.

Chapter 5

Heat and water transfer in a rotating drum containing solid substrate particles

Abstract

In previous work we reported on the simulation of mixing behavior of a slowly rotating drum for solid-state fermentation (SSF) using a discrete particle model. In this investigation the discrete particle model is extended with heat and moisture transfer. Heat transfer is implemented in the model via interparticle contacts and the interparticle heat transfer coefficient is determined experimentally. The model is shown to accurately predict heat transfer and resulting temperature gradients in a mixed wheat grain bed. In addition to heat transfer, the addition and subsequent distribution of water in the substrate bed is also studied. The water is added to the bed via spray nozzles to overcome desiccation of the bed during evaporative cooling. The development of moisture profiles in the bed during spraying and mixing are studied experimentally with a water-soluble fluorescent tracer. Two processes that affect the water distribution are considered in the model: the intraparticle absorption process, and the interparticle transfer of free water. It is found that optimum distribution can be achieved when the free water present at the surface of the grains is quickly distributed in the bed, for example by fast mixing. Alternatively, a short spraying period, followed by a period of mixing without water addition, can be applied. The discrete particle model developed is used successfully to examine the influence of process operation on the moisture distribution (e.g., fill level and rotation rate). It is concluded that the extended discrete particle model can be used as a powerful predictive tool to derive operating strategies and criteria for design and scale-up for mixed SSF and other processes with granular media.

Introduction

Solid-state fermentation (SSF) is defined as the cultivation of microorganisms on moist solid substrates with air as a continuous phase. During the last decade Western food industries have explored the possibilities for the production of novel food products and ingredients (e.g., aromas) with SSF (Pandey et al., 2000). Unfortunately, the development of large-scale SSF systems is complex (Mitchell et al., 2000). One of the most critical issues is the removal of metabolic heat during large-scale SSF. On a small scale, conductive cooling contributes considerably to the removal of heat. On a large scale, conduction is insufficient, unless additional cooling surface is installed in the fermentor, as has been done in the Zymotis (Roussos et al., 1993) and the Plafreactor (Suryanarayan et al., 2001, US patent nr. US 6,197,573 B1) designs. However, we believe that these conductively cooled systems require high capital investments and are cumbersome to fill, empty and clean. If a continuously mixed SSF system is used, the bed volume that can be cooled via conductive cooling is larger than for static systems, but it is still too small for most industrial applications. Therefore, evaporative cooling is the only option for both static and mixed SSF systems on an industrial scale.

Evaporation and incorporation of water in the cytoplasm of the microorganisms cause desiccation of the substrate, which will have an adverse effect on microbial growth (Nagel et al., 2001). In static systems, desiccation can also result in channeling and total loss of process control, even before the water activity drops to a critical level (Weber et al., 2002). Only mixing can prevent the adverse effect of evaporation: It prevents or disrupts the mycelium network that binds the substrate particles together and is needed to achieve homogeneous distribution of water added to compensate for evaporation, etc. Nagel et al. (2002) found that the fermentation rate in a continuously mixed paddle mixer, which was cooled by evaporation, increased significantly when water was sprayed as a fine mist on top of the bed.

However, the available knowledge about the influence of mixing on temperature and moisture gradients is insufficient to accurately control the gradients during mixed SSF. We believe that the development of mathematical models that give more fundamental insight in mixing and the effect of mixing on the local gradients, can be of great support for rational design of SSF with discontinuous mixing (Schutyser et al., 2001, 2002). In previous research we developed a discrete particle model that could successfully predict the mixing of substrate particles in various rotating drums (Schutyser et al., 2002). In this modeling approach, forces on and subsequent trajectories of each individual substrate particle are calculated.

In this study we focus on the extension of this model with conductive heat transfer and the distribution of sprayed water in the bed during mixing. The model that results form this work can be used as a predictive model to set up design and scale-up criteria for mixed SSF. The predicted heat transfer is validated by measuring the development of temperature gradients in

time in the bed by heating up and cooling down the walls of the drum. In modeling the distribution of sprayed water in the bed we distinguish between absorption of water by individual grains and transfer of water between neighboring grains. The model is validated with the use of a fluorescent tracer in the sprayed water.

Mathematical Model

A two-dimensional (2D) discrete particle model was used, originally developed to predict radial mixing in rotating drums (Schutyser et al., 2001). The model can provide accurate predictions of mixing by calculating the movements of an array of particles from forces acting on each individual particle. The forces include gravitation, interactions between particles and interactions between particles and the fermentor walls. This discrete particle model was used as a basis for incorporating heat and mass transfer models, to be able to predict the coupled heat and mass transfer phenomena during mixing in a rotating drum. It should be emphasized that the discrete particle approach can also be extended to three dimensions and to other geometries (Schutyser et al., 2002). In principle, the heat and mass transfer models developed in this study can therefore also be applied to other mixed particle systems.

Some details of the 2D discrete particle model are given in what follows. For more information concerning the modeling approach we refer to previous work (Schutyser et al., 2001). The wheat grains are modeled as perfect spheres (diameter 4.9 mm). Mixing predictions have been found to be accurate despite this simplification. During simulation, contacts between particles are detected at very small time intervals (20 µs). When particles are in contact, interaction forces are calculated. To minimize the computational time spent on contact detection, we used a neighbor-list (Allen and Tildesly, 1987). Finally, the newtonian equations of motion are integrated to obtain the new velocities and positions for each particle.

The interaction forces consist of a repulsive force combined with a dissipative force, which determines the force in the normal direction ($\vec{F}_n$),

$$\vec{F}_n = \left(- k_n \delta - \eta_n \left(\vec{v}_{rij} \cdot \vec{n}_{ij} \right) \right) \vec{n}_{ij} \tag{1}$$

where k_n is the stiffness coefficient ($N \cdot m^{-1}$), δ is the computational overlap (m), η_n is the normal damping coefficient ($kg \cdot s^{-1}$), $\vec{v}_{rij}$ is the velocity difference ($m \cdot s^{-1}$) and $\vec{n}_{ij}$ is the normal unit vector (-).

and a tangential or shear force ($\vec{F}_s$), using a combination of a viscous and a dynamic friction.

$$\vec{F}_s = -\min\left(\left|\gamma_s\,v_{sij}\right|, \left|\mu_d F_n\right|\right) \cdot \text{sign}(\vec{v}_{sij})$$

(2)

where γ_s is the viscous friction coefficient (kg·s^{-1}), μ_d is the dynamic friction coefficient (-), $\vec{v}_{sij}$ is the relative tangential velocity (m·s^{-1}).

Modeling conductive heat transfer

In the current study we focus only on the modeling of conductive heat transfer without aeration. Aeration is applied during SSF to supply the microorganisms with oxygen and often to remove metabolic heat by evaporation of water from the substrate bed (evaporative cooling). The heat and mass transfer processes that occur during SSF interact in a complex way. The flow of the air phase and the subsequent heat and mass transfer processes will be modeled in the future to study their complex interactions.

Studies of heat transfer phenomena in rotating drums (for SSF) have been frequent (Boateng and Barr, 1996; Ding et al., 2001; Oostra et al., 2000). By using a novel discrete particle approach we can study the rate of heat transfer between individual particles in a mixed rotating drum system. Integration towards the total reactor scale is then straightforward. A clear advantage of this modeling approach is that it can be easily used to predict heat transfer rates for different reactor geometries, because the thermal conductivity of air (0.025 Wm^{-1}K^{-1} at T=20 ºC) is small compared with the conductivity of the solids (Table I). Heat transfer via evaporation of water from the bed to the headspace might also be expected. In the Appendix we compared the initial heat flux from the bed to the top wall of the headspace due to evaporation to the heat flux from the bed to the wall due to conduction. We estimated that the conductive heat flux between the bed and the wall is 64 times larger than for evaporation. The heat transfer to the headspace may thus be neglected in our modeling approach.

Table I. The measured thermal conductivity (λ) of a moist wheat grain bed (0.77 kg w / kg DM) and the heat transfer coefficient (α) for particle-particle contact, obtained from the same experiments.

Ambient Temperature [°C]	λ [Wm^{-1}K^{-1}]	α [s^{-1}]
22.0	0.121	0.0130
25.5	0.123	0.0140
34.7	0.130	0.0146
42.3	0.142	0.0150

The extension of the discrete particle model presented herein takes into account heat transfer via particle-particle contact in the bed. Only a few studies have been conducted on this topic (Hunt, 1997; Vargas and McCarthy, 2001). Vargas and McCarthy (2001) followed a similar modeling approach, to investigate heat conduction in a packed bed of cylinders.

The contribution of convection to the heat transfer other than the mixing of the particles is neglected (i.e., no transport of water vapor); the interstitial air has a low thermal conductivity compared to the wheat kernels and is considered stagnant. The heat transfer takes place via the contact points of two adjacent wheat grains. The characteristics of the conducting medium, which represent the contact area between contacting particles and the specific heat capacity of the grains, are assumed constant and included in the heat transfer coefficient, α (s^{-1}). The heat transfer for a single particle is modeled by:

$$T_{t+dt}^i = T_t^i + \sum_{l}^{n_c} \alpha (T_t^j - T_t^i)dt \qquad (3)$$

T_{t+dt}^i is the predicted temperature of particle i at time $t = t+dt$, T_t^i is the temperature of particle i at time t, α is the heat transfer coefficient (s^{-1}), and n_c is the number of neighboring particles (dimensionless).

If wheat grain i is in contact with the wall of the drum, a different heat transfer coefficient, α_{wall} (s^{-1}), is applied for this contact. In this case the equation for heat transfer for particle i becomes:

$$T_{t+dt}^i = T_t^i + \sum_{l}^{n_c} \alpha (T_t^j - T_t^i)dt + \alpha_{wall}(T_{wall} - T_t^i)dt \qquad (4)$$

Modeling mass transfer of sprayed water

Only few investigations have been done on the distribution of sprayed liquid in mixed particle systems. Recent work has involved the distribution of liquid during (spray) granulation (Goldschmidt, 2001; Litster et al., 2001). During granulation, the liquid serves as a binder for agglomeration of powder into larger granules and liquid distribution should be well controlled in order to obtain the desired agglomerate sizes. Goldschmidt et al., (2001) developed a discrete particle model to describe the process of fluidized-bed granulation (Goldschmidt, 2001). In this granulation model, powder particles and liquid droplets are both modeled as particles and collisions between the two species are considered. In our modeling approach, the solid substrate particles are modeled as particles, whereas the much smaller water droplets are not. In the model, water is always assumed to be 'attached' to a substrate particle. This is allowed, because the water droplets are very small ($d = 100$ μm) compared with the wheat grains ($d = 4.9$ mm), and the presence of the water droplets does not visibly influence the flow behavior of the bed. Because it has been observed that the addition of a relatively small amount of water to the
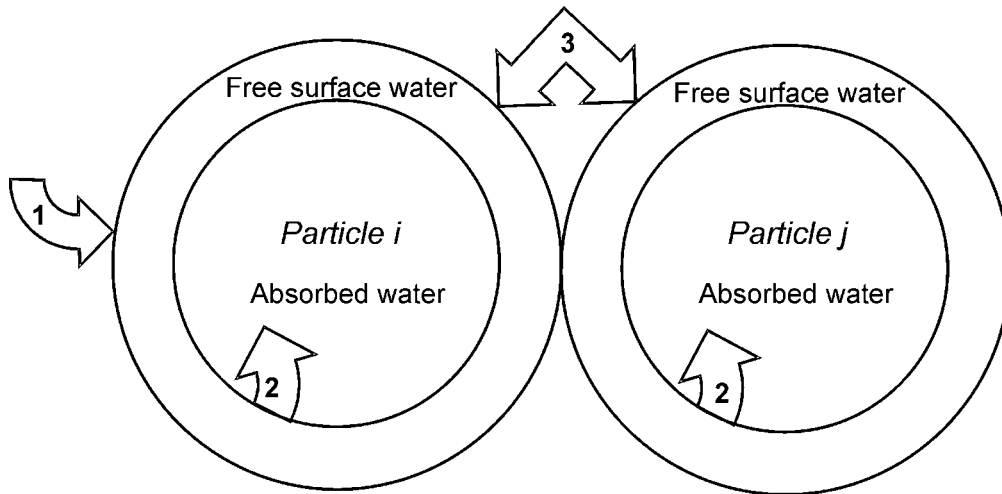
Figure 1. Scheme of the moisture distribution model for two particles (*i* and *j*). Particle *i* is located at the surface of the bed. Two varying water fractions are distinguished; the absorbed water and the free surface water. The different water transport processes are depicted as open arrows (1) the addition of water (2) the absorption of water by the grains (3) the transfer of water between two grains.

system does not influence particle movements, interparticle forces due to liquid bridge formation do not have to be taken into account. This differs from discrete particle simulations for particles that are cohesive in the presence of a liquid (Mikami et al., 1999; Muguruma et al., 2000; Yang and Hsiau, 2001).

To model the water distribution of the sprayed water throughout the mixed substrate bed we distinguish three different processes: (1) external addition of water to the particles, (2) absorption of water by individual particles, (3) transfer of water between neighboring particles. We assume that the water already absorbed by the wheat grain is not transferred to a neighboring particle. The transfer of water between particles can only take place via the fraction of the water that is freely present on the surface of a particle, which, for convenience, is called 'free surface water volume'. The precise location of the water on the surface is not considered, but it may be envisaged as a film on the surface of the particles. In the model, for each particle we distinguish for each particle two varying water volumes: (1) the absorbed volume, and (2) the free surface water volume (Fig. 1). It should be emphasized that the substrate particles, wheat grains, already contain water due to the pretreatment in all experiments (app. 0.8 kg water / kg DM). This absorbed water, already present at the start, is not taken into account in the absorbed water volume in the current model.

Experimental data indicated that the absorption process can be divided into two cases (a and b). If the amount of total water is below a critical value ($V_{abs,0}$), the water present at the surface is absorbed instantaneously into the particle (case a). If this critical volume is exceeded, absorption takes place at a constant rate (case b). This rate is derived from experimental data. This process is mathematically described by the following three equations:

$$V^i(t) = V^i_{abs}(t) + V^i_{free}(t) \tag{5}$$

$$V^i_{free}(t) = 0 \qquad\qquad \text{if} \quad V^i(t) < V_{abs,o} \tag{5a}$$

$$\frac{dV^i_{free}(t)}{dt} = -k_{abs} \qquad\qquad \text{if} \quad V^i(t) > V_{abs,o} \tag{5b}$$

where V^i is the total water volume of particle i (ml), V^i_{abs} is the absorbed water volume of particle i (ml), V^i_{free} is the free water volume of particle i (ml), t is the time (s), and k_{abs} is the absorption rate (ml·s^{-1}).

The excess of free water transferred from one particle to a neighboring particle can be received by the neighboring particle in three different ways: (1) the neighboring particle can receive all free water in its absorption volume; (2) the neighboring particle can receive part of the water in its absorption volume; or (3) the two particles share the free water. The direct absorption of free water by neighboring particles has higher priority than the equal distribution of free water among the particles. Only if the absorbed volumes of all neighboring particles are equal to or larger than $V_{abs,0}$, the rest of the free water is distributed among the particle itself and its neighbors. Distribution of water between a particle and its neighboring particle is thus only possible if the absorbed volumes of all neighboring particles are equal or larger than $V_{abs,0}$ (Fig. 1). It is noted herein that, in the algorithm, the direction of transfer of water via absorption might be sensitive to the sequence of particles considered during the calculation. In the algorithm, the sequence of calculation is determined mainly by the identity number (1..N) of each particle. Because we can assume that the particles are randomly spread in the bed, the direction of the calculation sequence is random and thus does not determine the predicted moisture gradients.

The transfer of water occurs via equal distribution of water between neighboring particles. The rate, at which this distribution is calculated, is a parameter in the model, u (sec^{-1}). In this way, each $1/u$ or dt seconds calculations are performed for all particles. An example calculation is shown for the distribution of free water, initially present at particle i, among particle i and its neighbors (Eq. 6). Note that particle i has multiple neighbors j and that the new values for the free water volumes are defined at $t + dt$.

$$V^i_{free}(t + dt) = V^i_{free}(t + dt) + \frac{V^i_{free}(t)}{nb^i + 1} \tag{6a}$$

$$\forall j \in nb^i :$$

$$V^j_{free}(t + dt) = V^j_{free}(t + dt) + \frac{V^i_{free}(t)}{nb^i + 1} \tag{6b}$$

where nb^i is the number of neighbor particles and $\forall j \in nb^i$ includes all neighbors. Of course, particle i and its neighbors may also receive additional free water from other neighboring

particles. If this is the case, a summation is made of all the free water received to obtain the new free water volume after calculation.
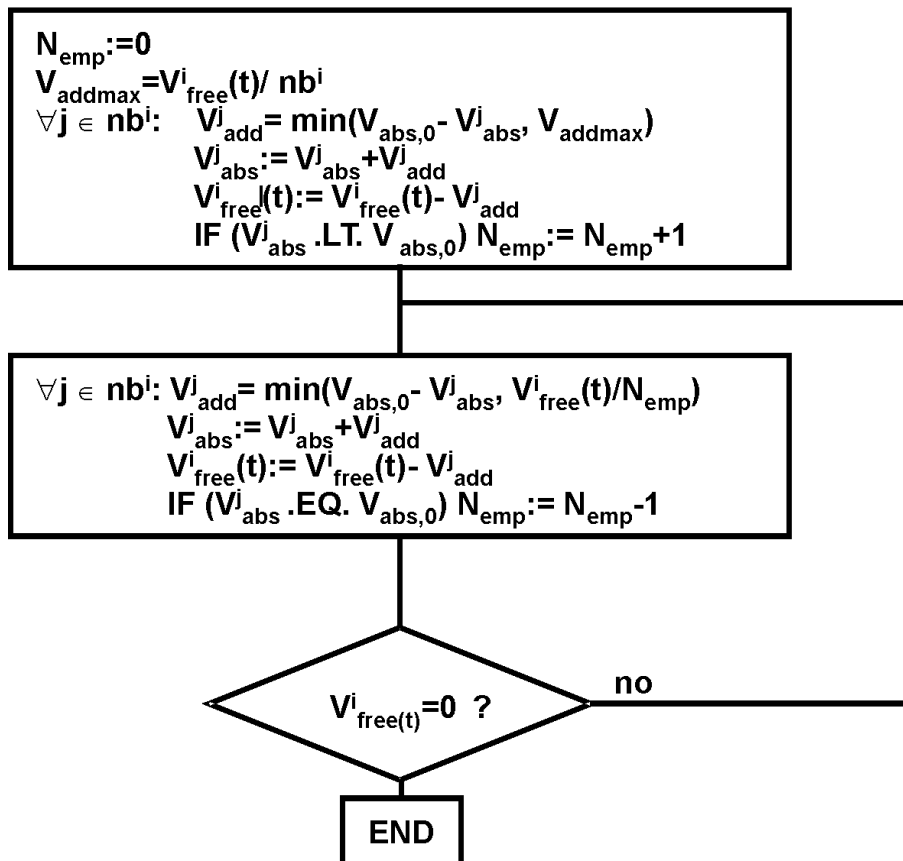
Schemes 1 and 2 give an overview of the calculation procedure of the model described. We distinguish three categories, which are calculated subsequently: A) particles at the surface that receive water, B) particles touching the wall, C) remaining particles or bulk particles. Schemes
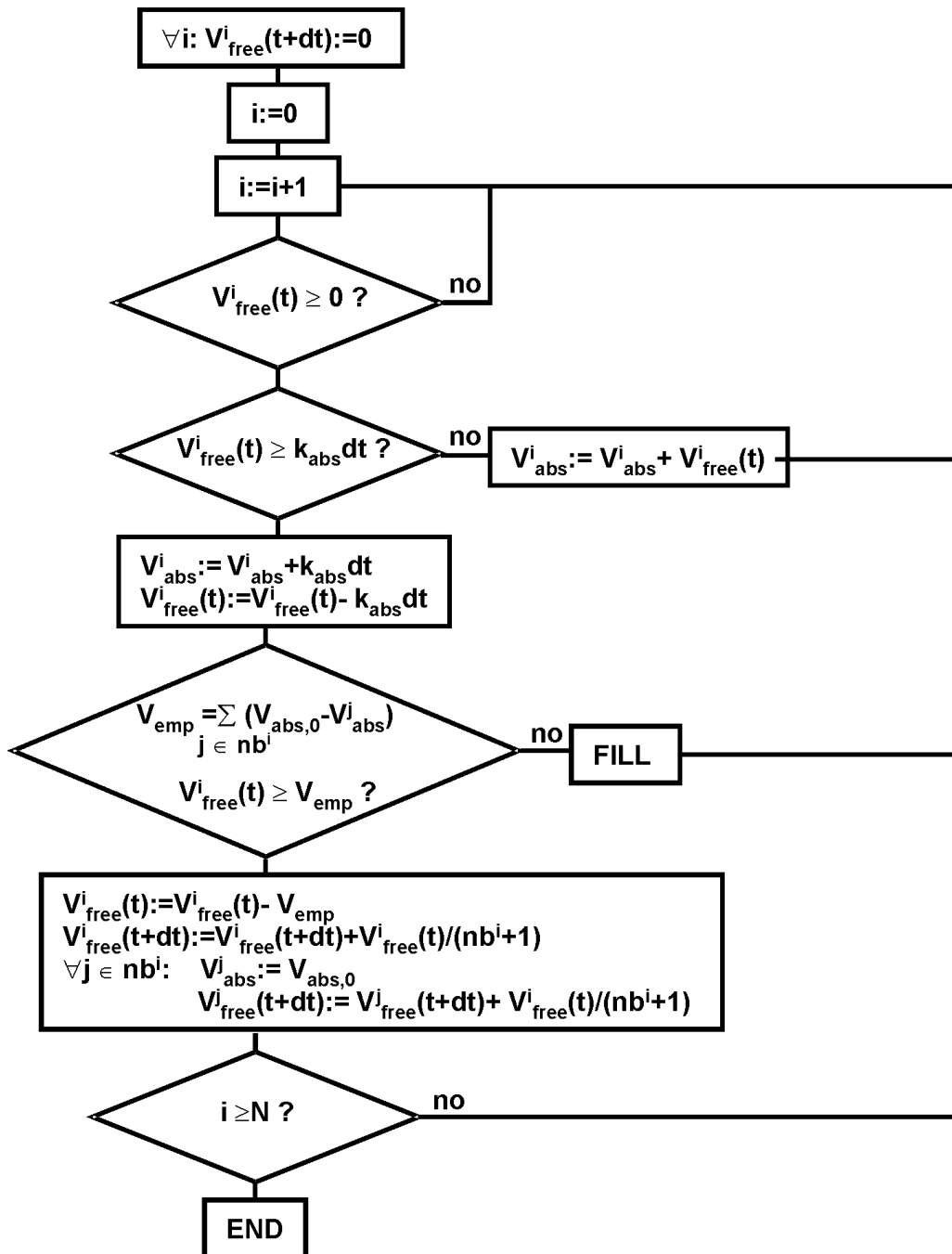
Scheme 1. The numerical procedure for calculation of absorption and moisture transfer between the grain particles. The scheme is slightly different for particles that receive water directly from the spray nozzles. The FILL procedure is shown in Scheme 2.

1 and 2 show only the calculation procedure for bulk particles. The only difference between category A and B is that direct absorption of sprayed water has to be calculated (Eq. 5). In the calculation of the amount of sprayed water that is received by surface particles, it is taken into account that the surfaces of some particles are more and some are less shielded by surrounding particles. Subsequently, absorption for the particles on the surface that received water is calculated and excess of free water is distributed among the neighbors. For the particles along the wall, the excess of free water is not distributed among the neighbors, because it is assumed that the particles steadily move with the wall of the drum and therefore transfer of free water is negligible. Finally, absorption and transfer of free water for the other particles (that did not directly receive water) is calculated. It should be emphasized that for the calculation of the new free water volumes only those free water volumes resulting from the previous updating (i.e., dt seconds ago) are used so as to avoid transfer of free water due to the calculation procedure.

FILL

$N_{emp} := 0$
$V_{addmax} = V^i_{free}(t) / nb^i$
$\forall j \in nb^i: \quad V^j_{add} = min(V_{abs,0} - V^j_{abs}, V_{addmax})$
$\qquad\qquad V^j_{abs} := V^j_{abs} + V^j_{add}$
$\qquad\qquad V^i_{free}(t) := V^i_{free}(t) - V^j_{add}$
$\qquad\qquad IF\ (V^j_{abs} .LT. V_{abs,0})\ N_{emp} := N_{emp} + 1$

$\forall j \in nb^i: V^j_{add} = min(V_{abs,0} - V^j_{abs}, V^i_{free}(t)/N_{emp})$
$\qquad\qquad V^j_{abs} := V^j_{abs} + V^j_{add}$
$\qquad\qquad V^i_{free}(t) := V^i_{free}(t) - V^j_{add}$
$\qquad\qquad IF\ (V^j_{abs} .EQ. V_{abs,0})\ N_{emp} := N_{emp} - 1$

$V^i_{free(t)} = 0\ ?$ **no**

END

Scheme 2. The numerical FILL procedure, in which the neighboring particles of particle i that contain space for water absorption are filled with free water of particle *i*.

Materials and methods

Experimental conditions

The wheat grains were treated according to the standard procedure applied for substrate particles for SSF. The whole wheat grains were soaked for 2.5 h in excess tap water of 60 °C. Subsequently, the soaked grains were sieved and autoclaved for 2 h at 121 °C.
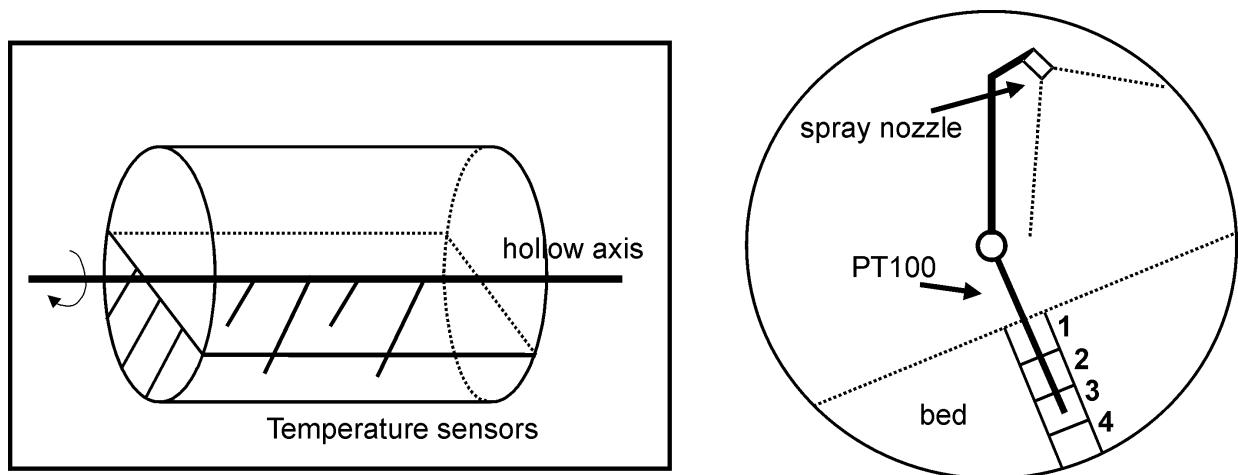
Set-up of the rotating drum reactor

The reactor consisted of an aluminum cylinder (thickness of the wall 2 mm) with two side plates, made of polycarbonate (Lexan), with the following dimensions: internal diameter 30 cm, length 40 cm, and an internal volume of 28.3 L (Fig. 2). The drum rotated around the horizontal axis at constant rate (0.5 or 1 rpm). The drum was driven by a Watson-Marlow drive (Type 505DU, Cornwall, UK) fitted with a factor 10 gear-wheel transmission for sufficient torque on the axis. On the (non-rotating) horizontal axis, four temperature sensors (Pt-100 Ω Tempcontrol, NL) were mounted (adjustable in height) that penetrated the grain bed. The average wall temperature was obtained from two temperature sensors. The drum reactor was placed in a temperature-controlled cabinet. The temperatures were monitored with a PC using Fieldpoint hardware and Labview software (both from National Instruments, NL).

For the moisture transfer experiments two spraying nozzles (Bète PJ8*5-1/8, Spraybest, NL) were placed in a position to obtain optimal coverage of the higher half of the surface of the bed (Fig. 2). The feed water was supplied via the hollow axis and pressurized by a gear-wheel pump (Verder 2040, NL). During the spraying of water, the bed was continuously mixed (1 rpm).

The fill levels—that is, the ratio of the volumes of the substrate bed and the drum (ε)—were restricted to 33% and 40%, common for SSF in rotating drums (Schutyser et al., 2002).

Thermal conductivity measurements

Thermal conductivity measurements of moistened wheat grains were conducted with a non-steady probe method (Haneghem van, 1981). A metal cylinder was filled with moistened wheat grains and placed into a thermostatted bath. A needle-shaped probe, containing a heating wire and a temperature sensor, was inserted into the material (Fig. 3). The temperature response ($\Delta T \approx 1$ °C), due a stepwise increase of the heat production by the heating wire, was measured for 200 seconds. Because of the small temperature rise it was assumed that the only mechanism for heat transfer would be conductive heat transfer, which is a method described accurately by van Haneghem (1981). Measurements were conducted in duplicate at four different temperatures ranging from 22 to 45 °C. From these obtained temperature profiles the thermal conductivity of

Figure 2. Experimental set-up of the rotating drum reactor, front- and side-view. The front-view shows the 4 temperature sensors. The side-view shows the position of the spraying nozzles and the temperature sensors (that are mounted on the non-rotating hollow axis) during experiments with a mixed bed. Also the four sampling regions for examining the moisture distribution are shown.
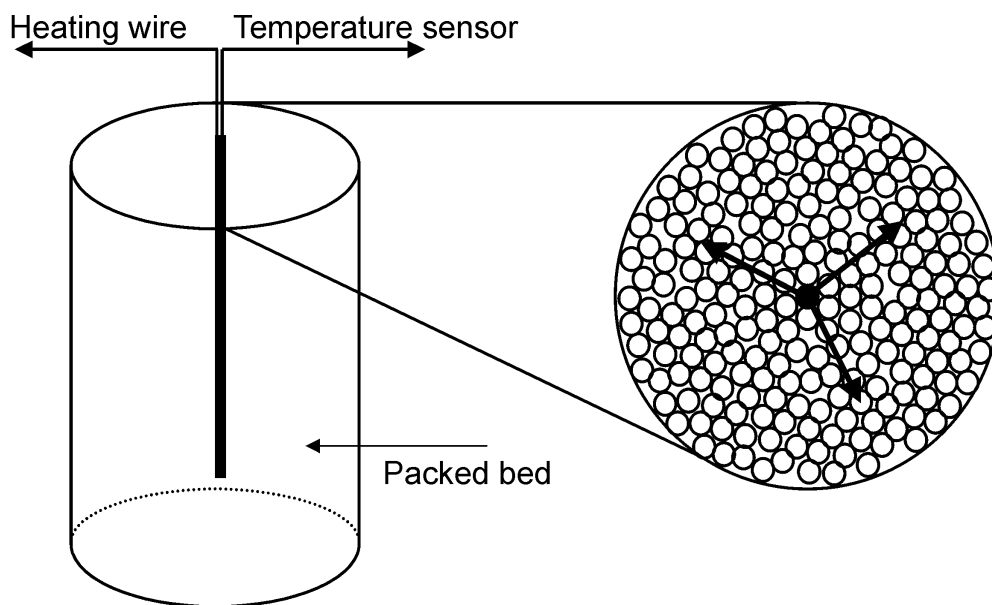
Figure 3. Left: experimental set-up for measuring the interparticle heat conduction coefficient. Right: Two-dimensional top-view of the cylinder, arrows indicate heat transfer in radial direction. Discrete particle simulations (2D) were conducted of this section to calculate the interparticle heat conduction coefficient.

the wheat grain bed (λ) could be calculated as a function of the temperature (Haneghem van, 1981).

To obtain a local heat transfer coefficient ($\alpha(T)$), we simulated the experiment with a 2D discrete particle simulation. A 2D simulation of the radial heat transfer in the measuring device was appropriate, because the heat transfer in the axial direction was negligible. In this simulation the pen was simulated as a small particle with a diameter of 2 mm and the wheat

grains as particles with a diameter of 4.9 mm. The pen particle was located in the middle of the bed (Fig. 3). The temperature rise in the pen was modeled according to the following equation:

$$dT = \frac{Q_l}{A\rho c_p} \cdot dt \qquad (6)$$

where dT is the temperature rise due to the increased energy dissipation; Q_l is the heat production of the pen per unit length and is calculated from the known conductivity resistance (119.333 Ω/m) and the applied current (50 mA) ($Q_l = RI^2$); $A\rho c_p$ is the heat capacity of the pen per surface area ($A = \pi r^2$ (m^2), $r = 1\cdot10^{-3}$ (m); $\rho c_p \approx 3\cdot10^6$ (Jm^{-3}K^{-1}); $A\rho c_p \approx 10$ (Jm^{-1}K^{-1})).

When heat transfer and heat production for the pen particle are taken into account the temperature response in the pen can be calculated according to:

$$T_{t+dt}^i = T_t^i + \frac{Q_l}{A\rho c_p}dt + \sum_1^{n_c}\alpha(T_t^j - T_t^i)dt \qquad (7)$$

The heat transfer coefficient was obtained by fitting the experimental temperature response with the predicted temperature profile.

Tracer experiments to study moisture distribution

To validate the model predictions of the evolution of moisture gradients in the bed in time during mixing, we conducted tracer experiments. A tracer was used in the sprayed water, because the amount of water added to the bed is very small compared with the water initially present; therefore, an analysis based on total water contents would thus not be practical. Because it is not possible to measure the tracer concentrations on-line (in contrast to temperature) on different locations in the bed, we used a gelatin solution (20 g/L) to solidify the bed after the spraying period. This procedure was also used in previous research to study mixing in different rotating drum designs and has been described in more detail by Schutyser et al. (2002). The disadvantage of this method is that many experiments must be conducted to determine the extent of development of the moisture gradients in time. Three locations were chosen along the horizontal axis and, at those locations, four or five equidistant samples were taken of the solidified bed in the radial direction perpendicular to the surface of the bed (Fig. 2). Two of the three locations were situated 5 cm from the sidewalls and one was situated in the middle of the drum. Because of the three different locations and because of the simple geometry of the drum we obtained triplicate measurements.

Initial experiments showed that of the tracers tested: Methylene blue (Merck, Germany), Bengal Rose B (Fluka Switzerland), Na$_2$SO$_4$ (Merck, Germany) and Rhodamine wt solution (Yorkshire chemicals plc, England), Rhodamine wt was most suitable. To extract the Rhodamine wt from a solidified wheat grain sample, the sample was put in a flask with 100 mL of demineralized

water. The flask was then shaken for 2 hours in an orbital shaker. Then 1.5 mL liquid was pipetted from the flask in an Eppendorf and centrifuged for 2.5 min at 5000 rpm. The fluorescence of 1 ml of supernatant was examined for its intensity in a Luminescence spectrometer (Model LS50NB, Perkin Elmer) with excitation and emission wavelengths of 557 nm and 581 nm, respectively (Marsh et al., 2000).

To correlate the amount of tracer, measured from a sample to the amount of tracer (recovery) that was actually added to the sample, we constructed a calibration curve by adding a series of different tracer amounts to 36 g of pretreated grains. Subsequently, we added the gelatin solution, let it harden in the fridge, and then followed the extraction procedure and measured the tracer concentration.

Methods of Calculation for Heat and Moisture transfer

For accurate calculation of the particle trajectories with the discrete particle model, a small time step (20 µs) is required. This small time step is not needed for modeling the heat transfer, as the characteristic time for this process is much larger. If the same time step (i.e., 20 µs) would be applied, this might even lead to inaccurate results due to rounding-off errors, as the temperature difference between two particles would then be very small. For efficient detection of (conducting) contacts between particles we made use of the neighbor-list (Allen and Tildesly, 1987). Temperatures were updated with every neighbor-list update, but at least within each 0.1 sec. It may be that some contacts were not taken into account in the heat transfer calculations, since the contact between two particles may possibly have existed for <0.1 sec. Because particle velocities were low in the bed, only relatively small errors are expected to be introduced in this way. The heat conduction and particle mixing calculations were thus calculated simultaneously using a different time step. However, because the time scale for heat conduction in a mixed bed (~2 hrs) is much larger than for mixing itself (~8 min), calculations remained extensive.

For calculation of the moisture transfer in the mixed bed we made therefore use of the concept of post-processing. A large data file was constructed, containing calculated positions of the particles with an interval of 1 s. In this way, several simulations could be performed easily and rapidly. Also here it is important to realize that not all contacts can be taken into account in the moisture transfer, as contact between particles may last for <1 sec. It was assumed that the short contacts do not contribute significantly to the process of moisture transfer.

The sprayed water in the model was distributed among the particles at the surface of the upper half of the bed and the particles in direct contact with the wall, because the nozzles were spraying partially on the upper half of the bed and on the wall (Fig. 2). To compare the experimental results and the model predictions a program routine was written to obtain the total added water in equivalent regions in the model as in the experiments (Fig. 2). Because in the

experiments free water cannot be distinguished from absorbed water, comparison of model and experiment was based on the sum of both water volumes.

Results and Discussion

Heat conductivity experiments and simulations

Figure 4 shows the measured and simulated temperature response to a stepwise increase in heat production by the heating wire, in the probe with an ambient temperature of 34.7 °C. During the first 30 s, a small difference between the simulated and the experimentally obtained temperature response was observed. The reason for this difference is that the number of heat-conducting contacts was relatively small and therefore small (random) differences between the model and the experiment initially have a considerable effect on the temperature curve. From these simulations, we obtained values for the heat transfer coefficient (α) as a function of temperature (Table I). These results show an increase in the thermal conductivity of the bed with increasing temperatures. In Table I also provides heat conduction coefficients (λ) of the same wheat grain bed with a moisture content of 0.77 kg water per kg dry matter (for four different temperatures). Both coefficients, α and λ, reflect the conductive properties of the medium, but are defined in a different way.
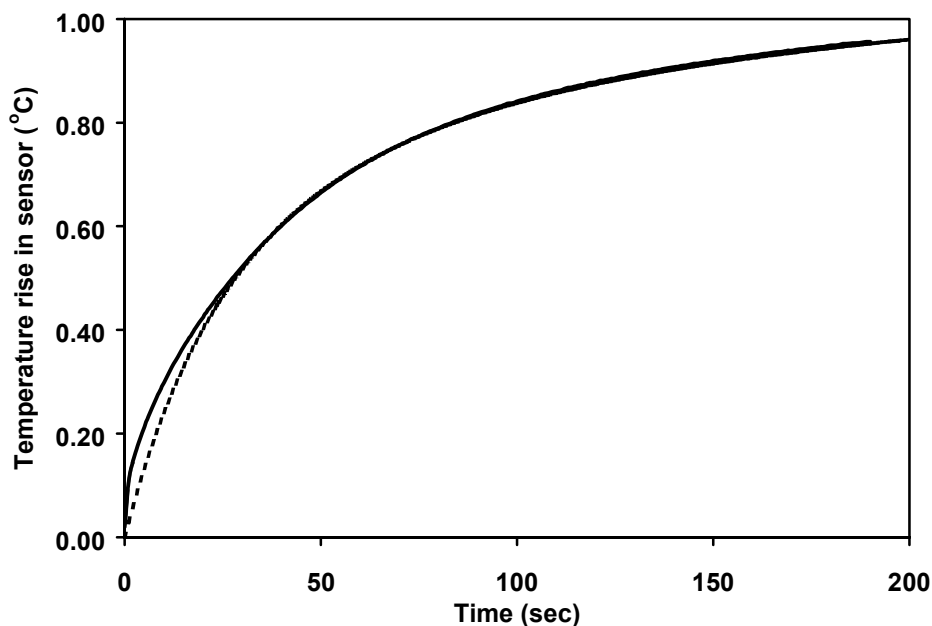
Figure 4. Experimental (-----) and simulated (- - -) temperature response in the probe after an increase in heat production. These simulations are performed to obtain the interparticle heat transfer coefficient (α).

Heat conduction in a static and a mixed bed in a rotating drum

Simulations and experiments were conducted for a non-mixed or static bed (ε=33%), which was heated up and cooled down by changing the temperature of the incubator (Fig. 5a and b). The heat transfer coefficient for the wheat grains used in the simulations was obtained from independent measurements, as described earlier. The heat transfer coefficient between the particle and the wall was unknown and was obtained from the experiments with a static bed. The wall temperature in the simulations was set identical to the measured averaged wall temperatures. From Figure 5a and b it can be concluded that the simulations predict a similar increase or decrease in bed temperature for both cases as that found in the experiments.

The heat transfer coefficient describing the heat transfer between the particles and the wall (α_{wall} = 0.003 s^{-1}) was obtained by fitting the measured temperature response in a static bed with the model predictions. For reasons of simplicity it was assumed to be independent of temperature. The α_{wall} value obtained was then used to predict heat transfer in a mixed rotating drum (0.5 rpm, ε=33%). It was found that, for both cases (cooling and heating up), an identical heat transfer coefficient could be used. Simulations and measurements, similar to those for the static bed, were conducted for a mixed grain bed (Fig. 6a and b). The simulated temperature curves matched the experimental results accurately.

The results show that the extended model is capable of describing heat transfer in a mixed rotating drum. Because the discrete particle model can be adapted to different reactor geometries, the heat transfer model can, in principle, be used to predict heat transfer in other reactor designs. In addition to prediction of temperature gradients, the effect of different process parameters, such as drum diameter and rotation rate, may also be predicted and generic design rules can be based on these simulations.

Moisture distribution of sprayed water in a rotating drum

Absorption of water

In the model, we describe (1) the absorption process into the particle and (2) the accumulation of free water on the surface of the particles due to mechanical interaction between particles. In an independent experiment we characterized the absorption process. Samples of a few pretreated wheat grains were put in a beaker with water for a known period of time. The weight of the grains was determined before and after this period. Because the free surface water was removed from the grains with a paper tissue, the difference in weight was equal to the absorbed water. In Figure 7, the absorbed water volume is shown as a function of time. It was found that the increase in absorbed volume in time could be described with an initial offset and a line with a constant slope. It was assumed that the initial offset was equal to the volume of the macropores, present on the surface of the grains.
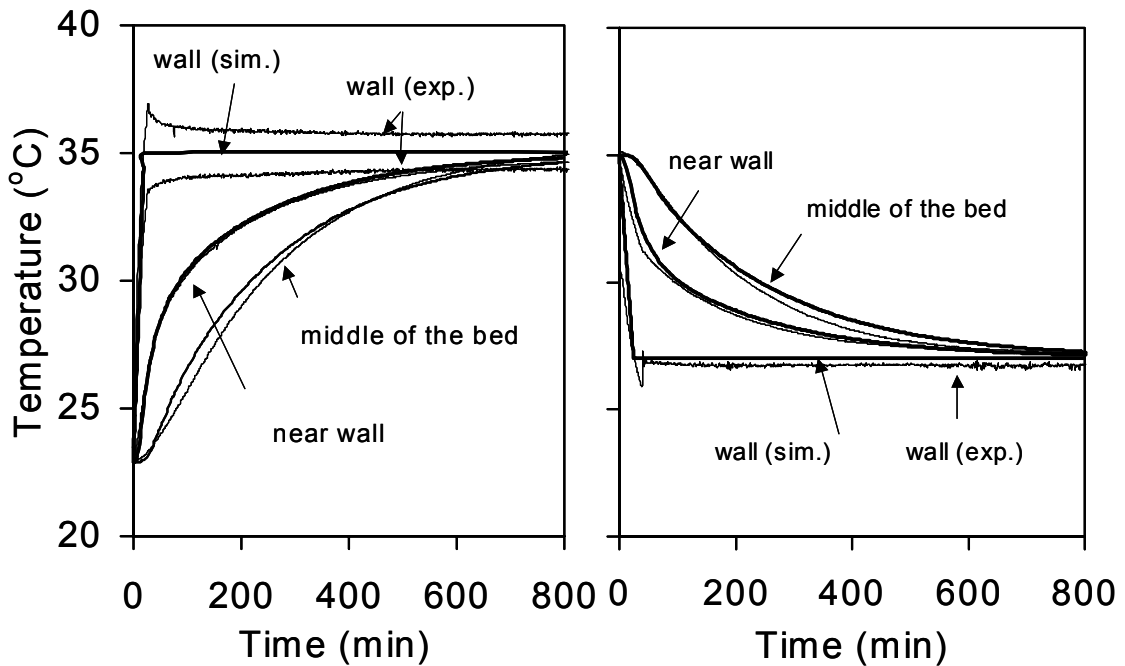
Figure 5. Left: Simulated and experimental temperature curves in a heated static bed. The thick lines are the simulated temperatures and the thin lines the experimentally determined temperatures. Right: Simulated and experimental temperature curves in a cooled static bed. The thick lines are the simulated temperatures and the thin lines the experimentally determined temperatures.
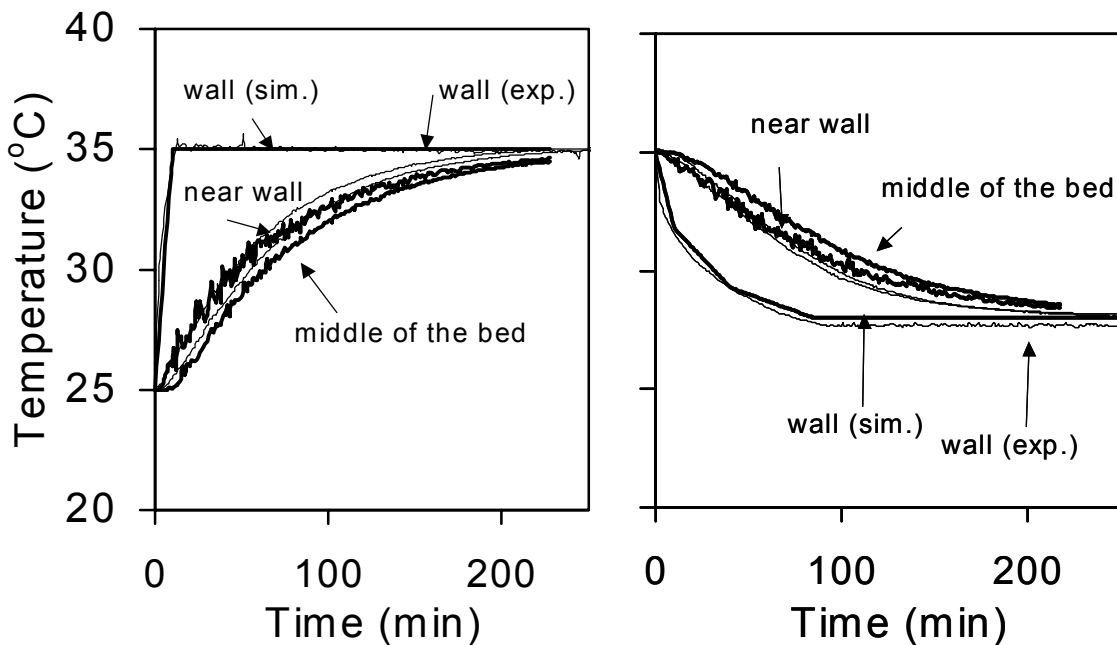
Figure 6. Left: Simulated and experimental temperature curves in a heated mixed bed. The thick lines are the simulated temperatures and the thin lines the experimentally determined temperatures. Right: Simulated and experimental temperature curves in a cooled mixed bed. The thick lines are the simulated temperatures and the thin lines the experimentally determined temperatures.

Subsequent absorption occurred at a constant rate due to diffusion of water into the core of the wheat grain. It should be emphasized that only the initial absorption can be assumed to occur at a constant rate, because, after a long period of time, a maximum absorbed volume of water should be reached. Nevertheless, 1000 s is long enough for our process.
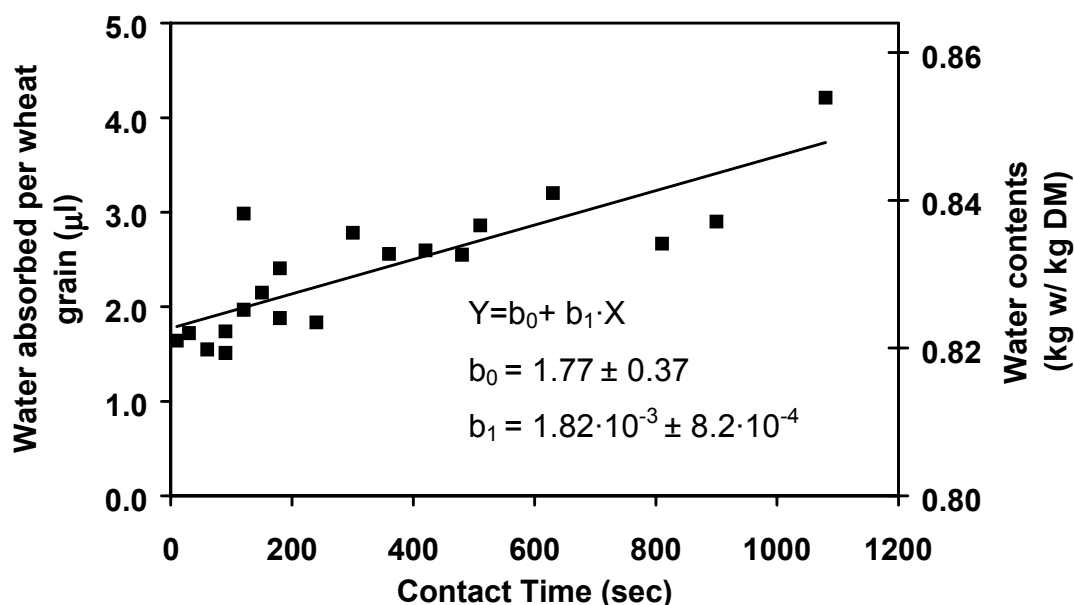
Figure 7. The absorbed water volume per pre-moistened wheat grain (initially 0.8 kg w / kg DM) versus absorption time. The points represent the experimental data and from the trend line the model parameters are determined, the offset, $V^i_{abs,0}$ (b_0) and the slope, k_{abs} (b_1). The 95% confidence intervals of the two parameters are shown.

Tracer

The tracer must satisfy three requirements: (1) it should dissolve well in water; (2) it should not be specifically adsorbed by the solid matrix of the wheat grains; and (3) it should be possible to extract the tracer and to accurately measure its concentration in a sample. Four tracer compounds were checked for these requirements.

Rhodamine wt was found to satisfy the requirements best. No significant adsorption was detected and the recovery of Rhodamine wt after extraction was high (80 %). It was also found that the sensitivity of the fluorescence measurements was high. We concluded that Rhodamine wt is suitable for use as a tracer for measuring moisture gradients in a mixed wheat grain bed with water addition. The only problem that could occur was that the addition of gelatin solution to solidify the bed might disturb the Rhodamine wt distribution in the bed. To prevent such a disturbance a 1-h delay was inserted (to allow the sprayed water to be absorbed) before pouring the gelatin solution on top of the bed. Another precaution was that the gelatin solution was

poured in eight fractions to allow subsequent hardening of different gelatin layers, and thus to prevent flow or diffusion of partially extracted dye to other regions in the bed due to the presence of the liquid gelatin solution.

Development of moisture gradients during water addition

The tracer method with Rhodamine wt allowed us to study the evolution of the moisture profile during addition of water in a rotating drum. To obtain more insight into the development of moisture gradients due to the spraying of water, multiple experiments were performed after different numbers of rotation. The spraying rate and the rotation rate were kept constant during these experiments, at 1.95 ml/sec and 1 rpm, respectively. The spraying rate was chosen to be as low as possible, taking into account the minimum flow needed for correct operation of the spraying nozzles. In Figure 8, experimental data are shown for different periods of spraying. The period of spraying was restricted to a maximum of 160 s, because addition of more water resulted in free-flowing water, which accumulated at the bottom of the drum. The moisture profiles depicted in Figure 8 show that the difference between the water concentrations in the middle of the bed and at the top and bottom of the bed increased in time. This result indicates that the distribution of the water throughout the bed occurred at a lower rate than the addition of the water at the surface of the bed. Faster mixing or a lower spraying flux could be applied to prevent formation of such gradients. Another option would be to continue mixing after water addition.

The accuracy of the measurements was reasonable; the variance in the triplicate measurements is shown with error bars for one case (160 s) in Figure 8. The main source of experimental error was the distribution of water sprayed by the two nozzles over the surface of the bed. In the current setup, completely homogeneous distribution of the sprayed water along the horizontal axis of the drum was not accomplished. In the middle of the drum the amount of added water was, on average, slightly lower than near the walls due to less coverage by both nozzles.

The spray rate applied in the model was equal to the flow rate in the experiments multiplied by the ratio of the numbers of particles in the model (only two-dimensional) and in the experiment (ε=33%, 1137/86051; ε=40%; 1364/102985). In Figure 8, the predicted moisture profiles are shown for the same spraying periods as in the experiments. The data points were obtained at the same locations as in the experiments (Fig. 2). A comparison of the model predictions and the experimental results shows good agreement between both.

Except for the rate at which the distribution of free water (u) is calculated, all parameters in the model were known or were obtained from independent experiments (e.g., the absorption rate).
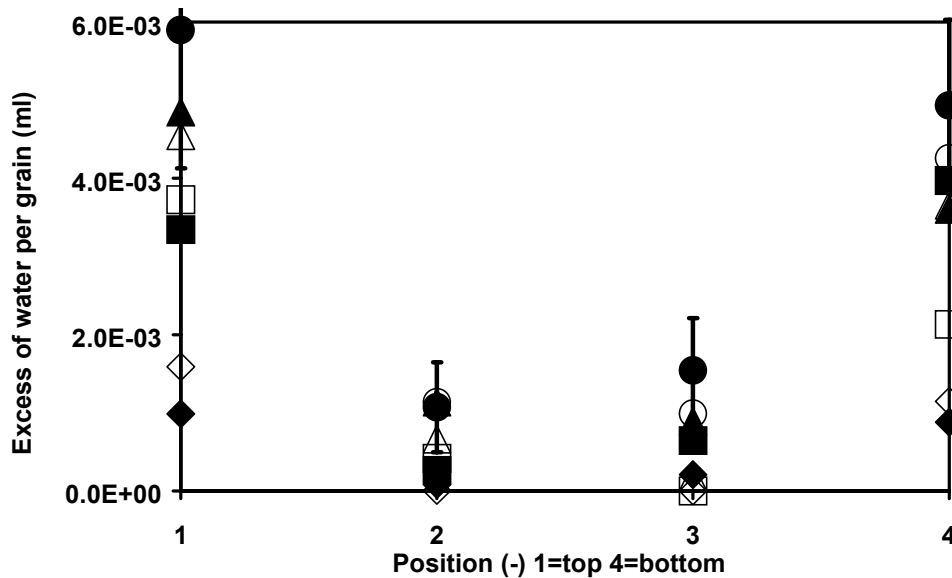
Figure 8. Experimental and model predicted moisture profiles obtained after ◆ 40 (model) and 45 (experiment), ■ 80, ▲ 120, ● 160 seconds of continuous spraying. The error bars show the variance of the triplicate measurements (only shown for 160 sec.). Closed symbols indicate experimental values and open symbols model predictions.

The rate of distribution was initially set to 1 s^{-1}. This initial value was found to give accurate predictions. A rate of distribution of 2 s^{-1} was not able to describe the experimental results.

Removal of moisture gradients by mixing after water addition

A possible approach to obtain optimum distribution of sprayed water in the bed is to spray water at a very low rate on a continuously mixed bed. In this way, each particle would receive the required extra water when it passes the surface. Because there is a minimum flow rate required for operation of the spraying nozzles this is not possible in the current set-up, although it might be applicable for large-scale fermentors. However, during continuous mixing, the damage to substrate and fungi may be considerable. Another approach may be to mix at high rotation rates (>>1 rpm) only during the addition of water. However, if this approach is chosen, the possible damage (due to the large shear rates during intensive mixing) to substrate and fungi should be considered. The most common approach in SSF is to spray for a relatively short time interval, followed by a period of mixing without addition of water. Nagel et al. (2002) applied mist addition with a specified time interval to control the water content in the bed during continuously mixed SSF in a paddle mixer. During the period of mixing without addition of water, free water at the surface of particles is distributed further in the bed and moisture gradients that developed during spraying are removed.

Experiments were conducted to study the removal of the gradients by distribution of the water by mixing, after spraying for a short time interval (80 s). Moisture profiles were measured after

different periods of additional mixing (Fig. 9). It can be seen that the parabolic shape of the moisture profile obtained directly after 80 s of spraying slowly disappears. After four rotations (or 240 s) the local moisture concentrations were about equal to the average water content of the substrate bed (i.e., the moisture gradients were removed). The model predicts the reduction of the moisture gradients with a similar rate as observed in the experiments (Fig. 9).

The reduction in the moisture gradients (Fig. 9) does not necessarily imply that all particles finally contain the same amount of water, because the samples obtained in experiments and in simulations average the water contents of several wheat grains. To avoid large differences between individual grains, fast mixing and thus distribution of free surface water is important. If the free surface water is not distributed quickly, the water will be absorbed locally and transfer of water to other particles impeded. To show the necessity for rapid distribution of free water among the wheat grains, the variance of the excess of water between individual wheat grains was checked (results not shown). It was found that the variance was minimal when mixing grains in a beaker immediately after addition of water.

In Figure 10, different water volumes, summed for the whole bed, are depicted for continuous spraying and for a short spraying period followed by mixing only. The total amount of water (excluding the water initially present) present in the system was equal to the water supplied during the experiment. During continuous spraying, the absorbed volume and the free water volume initially increase. After some time, the absorbed volume leveled off, whereas the free water volume continued to increase. This can be explained by the limited absorption rate of the substrate particles. If only a short period of spraying is applied followed by mixing only, the free water volume slowly would decrease until all water is absorbed. If all water in the system is absorbed, mixing would not help to level out differences of excess of water between individual wheat grains.
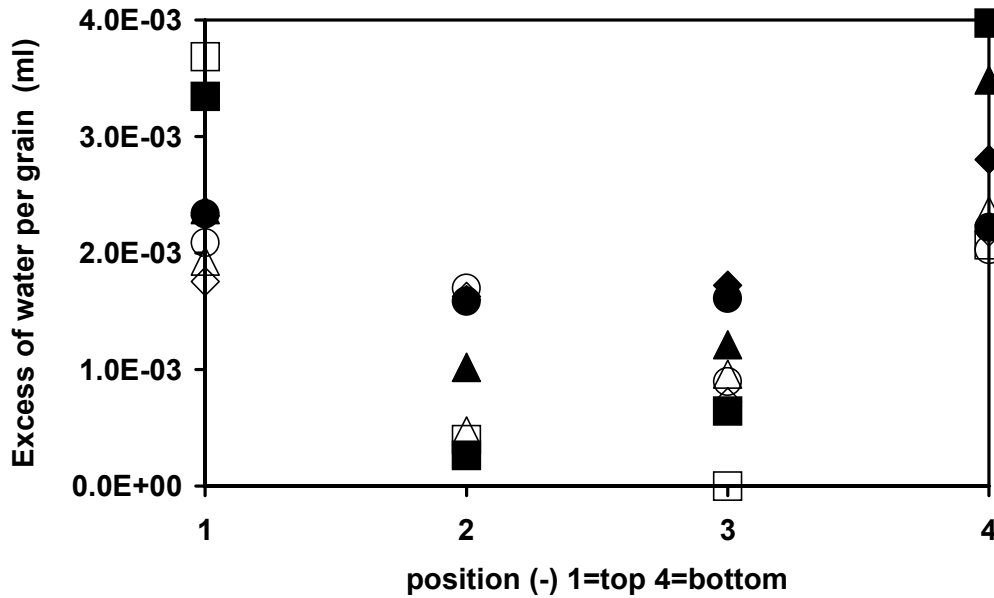
Figure 9. Experimental and model predicted moisture profiles for a short water spray period (80 s) followed by a variable period of only mixing. The profiles are shown for ■ 80, ▲ 180, ● 240, ◆ 480 seconds. The spraying period is 80 seconds, and the remaining time continuous mixing without spraying is applied. Closed symbols indicate experimental values and open symbols model predictions.
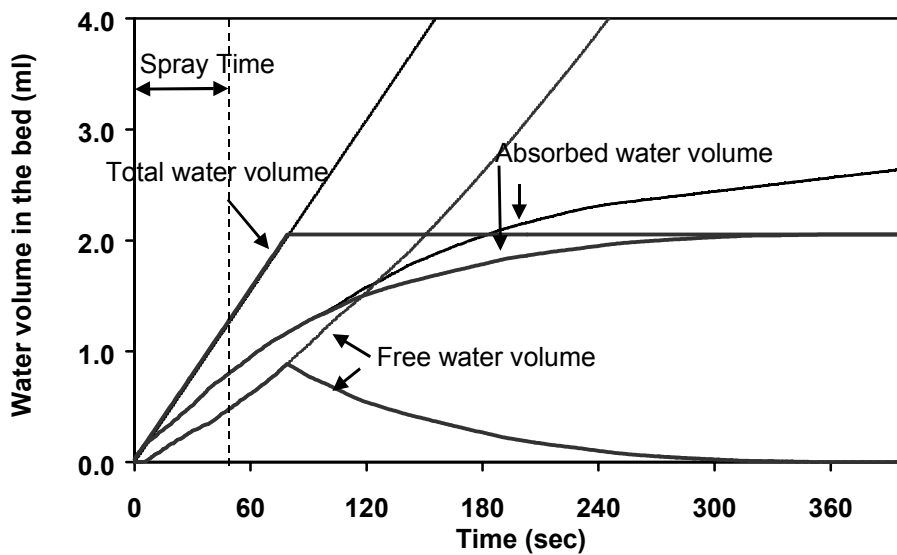
Figure 10. The volumes of the various water fractions in the substrate bed as predicted by the 2D model in time, for the continuous spray experiment (thin lines) and the spray experiment followed with a period of only mixing (thick lines).

Influence of process parameters on the water distribution in the bed

The influences of two process parameters (i.e., rotation rate and fill level) on water distribution were studied. If a larger rotation rate is applied during mixing it can be expected that the free water would be better distributed among the grains in the bed. In Figure 11 simulated moisture profiles are shown for a mixed bed (5 rpm) with continuous spraying. It can be concluded that, at an increased rotation rate, the transfer of the water to the middle of the bed would increase. An increased rotation rate is thus favorable for better water distribution. This result is logical, because we know from previous research that the number of rotations needed for complete mixing of the particles are identical for different rotation rates (Schutyser et al., 2001). As stated earlier, at increased rotation rates, the more favorable distribution may not outweigh the larger shear forces.

The effect of the fill level was studied to obtain more insight into the scaling-up effects of the water distribution process. It is expected that an increase in fill level would have a negative influence on the water distribution, because the ratio of the surface area and the volume of the bed decreases at higher fill level. The effect of fill level was experimentally examined by determining the moisture profiles with a higher fill level, $\varepsilon=40\%$ (Fig. 12a). Also, for the higher fill level, model predictions and experiments were in agreement (Fig. 12). To make a valid comparison between the different fill levels, the spray rate was increased for the higher fill level (based on the increased weight of the bed; 2.54 mL s^{-1} for $\varepsilon=40\%$ and 1.95 mL s^{-1} for $\varepsilon=33\%$). Because of the increased bed height, five samples (on three different locations along the axial axis) instead of four were taken from the bed. The moisture profiles obtained at a fill level of 40% (Fig. 12) were different from those obtained with a fill level of 33% (Fig. 9). The main difference between the two fill levels was the difference in moisture profile for the largest two timepoints: for $\varepsilon=33\%$ between 240 and 480 s, and for $\varepsilon=40\%$ between 300 and 480 s. For the lowest fill level we found that the difference between the moisture profiles for these timepoints was very small, whereas the difference for the higher fill level was significant. From these result it can be concluded that the increased bed volume had a negative influence on the distribution of the free water during mixing, and thus that a increased number of rotations would be needed to obtain a homogeneous distribution of water in the bed. More quantitatively, it can be concluded that for fill levels of 33% and 40%, distribution is achieved after roughly four rotations (240 s) and eight rotations (480 s), respectively.

We have shown that the discrete particle model is a powerful modeling tool to predict the water distribution after water addition in a rotating fermentor. In future work, this model will be used to derive general operating rules regarding moisture distribution under different process conditions (e.g., fermentor scale and geometry). Other work will focus on the implementation of different processes that occur during SSF, such as heat and mass transfer during evaporative

cooling and the effect of mixing on fungal growth and vice versa. If these processes are implemented in the model, this will facilitate rational design and scale-up of SSF fermentors.
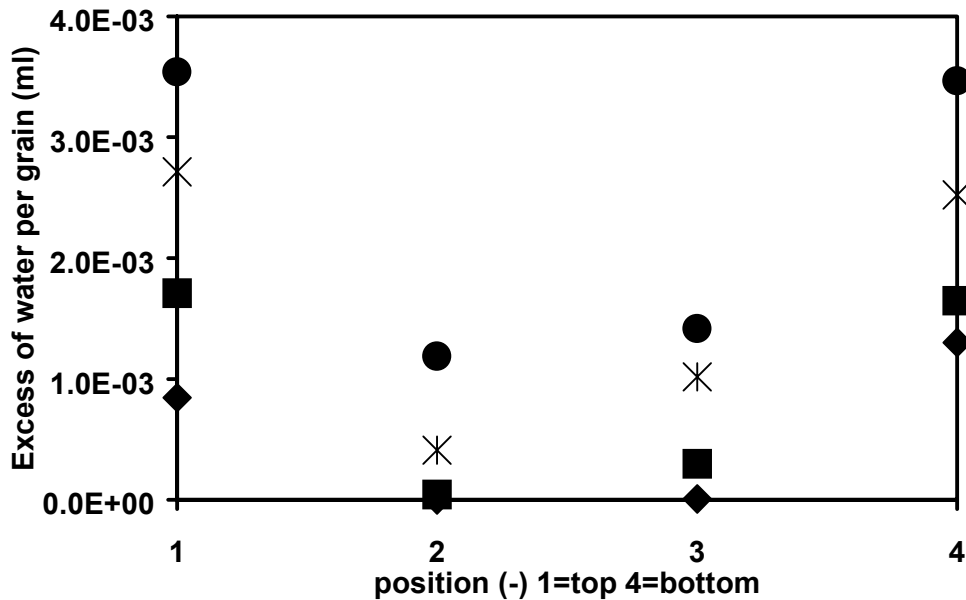
Figure 11. The effect of a higher rotation rate of the drum on the moisture transfer, predicted with the model during continuous spraying. The fill level is equal to 0.33. The profiles are shown for ◆ 40, ■ 80, ✕ 120, ● 160 seconds of continuous spraying.
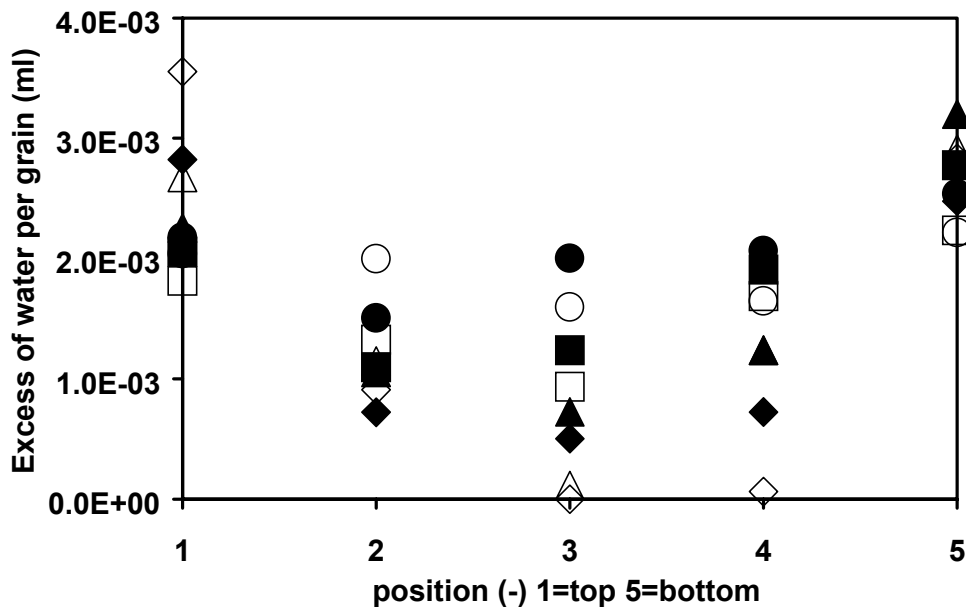
Figure 12. Experimental and model predicted moisture profiles for a short spray period (80 s) followed by a variable period of only mixing. The fill level is equal to 0.4. The profiles are shown for ◆ 80, ▲ 150, ■ 300, ● 480 seconds of continuous spraying. Closed symbols indicate experimental values and open symbols model predictions.

Conclusions

The extended discrete particle model successfully predicted the heat transfer in a static and mixed rotating drum filled with substrate particles. Heat transfer was modeled for individual contacts between wheat grains and a heat transfer coefficient was obtained experimentally. Different experiments and simulations were conducted to study the evolution of moisture profiles during spraying and mixing. The predictions of the discrete particle model, describing absorption and interparticle transfer of water, were in agreement with the experimental results. To obtain optimum distribution of water, a high rotation speed of the drum is favorable; the free water on the surface is then quickly transferred to the middle of the bed, before absorption of free water has taken place. Because of the larger shear forces at larger rotation rates, it may be preferable to spray for a short period, followed by a period with mixing (without addition of water) to distribute the excess of water. It was found that an increased fill level negatively influenced the distribution of water. Finally, it can be concluded that the discrete particle model, including heat and moisture transfer can be used to set up general operating rules and design and scale-up criteria for mixed SSF.

Acknowledgements

Appendix

Initial heat flux from top of bed to top wall of headspace.

Due to differences in temperature of the air in the headspace near the top wall and the bed, it is expected that heat transport due to evaporation takes place. We compare the contribution of this heat flux to the heat flux via conduction from the bed to the wall. To calculate the heat flux due to evaporation we compare the vapor pressure of the air near the bed surface at 35 ºC to the vapor pressure at the average height above the substrate bed ($\frac{1}{2} R_d = 0.075$ m) at 27 ºC.

The water vapor pressure (p_w) is calculated by the following Antoine equation:

$$p_w(T) = 10^{\left(10.06252 - \frac{1650.27}{T - 46.814}\right)} \tag{A1}$$

where T is the temperature (K). Subsequently, the heat flux (N''_{vap}) is given by:

$$N''_{vap} = \frac{2 \cdot D}{R_d} \cdot \left(\frac{p_w(T_{bed})}{R \cdot T_{bed}} - \frac{p_w(T_{wall})}{R \cdot T_{wall}} \right) \cdot \Delta H_w \tag{A2}$$

where D is the diffusion coefficient of water in air (10^{-5} m^2 s^{-1}), R is the gas constant (8.314 J mol^{-1} K^{-1}) and ΔH_w is the heat of evaporation ($4.5 \cdot 10^4$ J kg^{-1}). The heat flux with T_{wall} = 300 K and T_{bed} = 308 K that results from the calculation is 4.5 W m^{-2}.

Initial heat flux from bed to wall

The heat flux from the bed to the wall is calculated according to:

$$N''_{cond} = \alpha_{wall} \cdot \left(T_{bed} - T_{wall} \right) \tag{A3}$$

where α_{wall} is the heat conduction coefficient ($Wm^{-2}K^{-1}$). The value of this coefficient is estimated from the $\alpha_{wall,\,p}$ ($3 \cdot 10^{-3}$ s^{-1}) that was determined in this study for individual particles:

$$\alpha_{wall=} \frac{\alpha_{wall,p}}{A_{pw}} \cdot m_p \cdot c_{pp} \tag{A4}$$

where A_{pw} is the heat exchange surface area of a single grain with the wall ($\pi r^2 = 1.9 \cdot 10^{-5}$ m^2), m_p is the mass of a grain ($7.2 \cdot 10^{-5}$ kg) and c_{pp} is the heat capacity of a wet grain (3137 J kg^{-1} K^{-1}). The heat conduction coefficient that results is 36 W m^{-2} K^{-1}. The heat flux that results from Eq. A3 is then 288 Wm^{-2}. With these calculations we show that the heat flux due to evaporation is about 64 times smaller than due to heat conduction, and thus that the heat transport due to evaporation can be assumed to be negligible.

References

Allen MP, Tildesly DJ. 1987. Computer simulation of liquids. Oxford, United States: Oxford University Press.

Boateng AA, Barr PV. 1996. A thermal heat model for the rotary killn including heat transfer within the bed. Int J Heat Mass Transfer 39:2131-2147.

Ding YL, Forster RN, Seville JK, Parker DJ. 2001. Some aspects of heat transfer in rolling mode rotating drums operated at low to medium temperatures. Powder Technol 121:168-181.

Goldschmidt MJV. 2001. Hydrodynamic modelling of fluidised bed spray granulation. Ph.D. Thesis, University of Twente, Enschede, The Netherlands.

Hunt ML. 1997. Discrete element simulations for granular material flows: Effective thermal conductivity and self-diffusivity. Int J Heat Mass Transfer 40:3059-3068.

Litster JD, Hapgood KP, Michaels JN, Sims A, Roberts M, Kameneni SK, Hsu T. 2001. Liquid distribution in wet granulation: dimensionless spray flux. Powder Technol 114:32-39.

Marsh AJ, Stuart DM, Mitchell DA, Howes T. 2000. Characterizing mixing in a rotating drum bioreactor for solid-state fermentation. Biotechnol Lett 22:473-477.

Mikami T, Kamiya H, Horio M. 1999. Numerical simulation of cohesive powder behavior in a fluidized bed. Chem Eng Sci 53:1927-1940.

Mitchell DA, Krieger N, Stuart DM, Pandey A. 2000. New developments in solid-state fermentation II Rational approaches to the design, operation and scale-up of bioreactors. Proc Biochem 35:1211-1225.

Muguruma Y, Tanaka T, Tsuji Y. 2000. Numerical simulation of particulate flow with liquid bridge between particles (simulation of centrifugal tumbling granulator). Powder Technol 109:49-57.

Nagel FJI. Tramper J, Bakker MSN, Rinzema A. 2001. Model for on-line moisture content control during solid-state fermentation. Biotechnol Bioeng 72:231-243.

Nagel FJI. 2002. Process control of Solid-State Fermentation. Ph.D. Thesis, Wageningen University, Wageningen, The Netherlands.

Oostra J, Tramper J, Rinzema A. 2000. Model-based biorector selection for large-scale solid-state cultivation of *Coniothyrium minitans* spores on oats. Enzyme Microb Technol 27:652-663.

Pandey A, Soccol CR, Mitchell DA. 2000. New developments in solid state fermentation: I-bioprocesses and products. Proc Biochem 35:1153-1169.

Roussos S, Raimbault M, Prebois J-P, Lonsane BK. 1993. Zymotis, a large scale solid state fermenter. Appl Biochem Biotechnol 42:37-52.

Schutyser MAI, Padding JT, Weber FJ, Briels WJ, Rinzema A, Boom R. 2001. Discrete particle simulations predicting mixing behavior of solid substrate particles in a rotating drum. Biotechnol Bioeng 75:666-675.

Schutyser MAI, Weber FJ, Briels WJ, Boom R, Rinzema A. 2002. Three-dimensional simulation of grain mixing in three different rotating drum designs for solid-state fermentation. Biotechnol Bioeng, 79:284-294.

van Haneghem IA. 1981. Een niet-stationaire naaldmethode (warmtegeleiding, warmtecapaciteit, contactweerstand). Ph.D. Thesis, Wageningen Agricultural University, Wageningen, The Netherlands.

Vargas WL, McCarthy JJ. 2001. Heat conduction in granular materials. AIChE J 47:1052-1059.

Weber FJ, Oostra J, Tramper J, Rinzema A. 2002. Validation of a model for process development and scale-up of packed-bed solid-state reactors. Biotechnol Bioeng 77:381-393.

Yang SC, Hsiau SS. 2001. The simulation of powders with liquid bridges in a 2D vibrated bed. Chem Eng Sci 56:6837-6849.

Chapter 6

Substrate aggregation due to aerial hyphae during discontinuously mixed solid-state fermentation with *A. oryzae*: Experiments and Modeling

Abstract

Solid-state fermentation (SSF) is prone to process failure due to channeling caused by evaporative cooling and the formation of an inter-particle mycelium network. Mixing is needed to break the mycelium network and to avoid such failure. This paper presents the first attempt to quantify and predict the effect of mycelium bonds on particle mixing and *vice versa*. We developed a novel experimental set-up to measure the tensile strength of hyphal bonds in SSF: *A. oryzae* was cultivated between two wheat dough disks and the tensile strength of the aerial mycelium was measured with a texture analyzer. Tensile strength at different incubation times was related to oxygen consumption, to allow a translation to a rotating drum with *A. oryzae* cultivated on wheat grain. We performed several discontinuously mixed solid-state fermentations in the drum fermentor and measured the number and size of grain-aggregates remaining after the first mixing action. We integrated data on mycelium tensile strength into a previously developed two-dimensional discrete particle model that calculates forces acting on individual substrate particles and the resulting radial particle movements. The discrete particle model predicted the quantity and size of the aggregates remaining after mixing successfully. The results show that a first mixing event in SSF with *A. oryzae* is needed to break mycelium in order to avoid aggregate formation in the grain bed, and not to distribute water added to compensate for evaporation losses, or smooth out temperature gradients.

MAI Schutyser, P de Pagter, FJ Weber, WJ Briels, RM Boom, A Rinzema. In press, Biotechnol Bioeng

Introduction

Solid-state fermentation (SSF) can be considered as an alternative to submerged fermentation (SmF). In SSF, microorganisms are cultivated on moist solid substrates with air as a continuous phase. SSF offers perspectives for production of novel food products and ingredients, but SSF is not widely applied, mainly because there is a lack of technological knowledge about the design and scale-up of SSF systems. This lack of knowledge is especially apparent for mixing in SSF. There are very few systematic studies of mixing in SSF, and the available reports have shown conflicting results and do not provide clues on the mechanisms behind the reported success or failure. Given the large number of combinations of substrate, microorganism and fermentor layout that can be applied in SSF, it is extremely difficult to provide general guidelines. We believe that only mechanistic modeling can help to formulate such guidelines. In previous studies, we addressed modeling of the movement of particles, moisture and heat during mixing in rotating drums that can be used for SSF (Schutyser et al., 2001, 2002, 2003). In this investigation, we address the effect of fungal mycelium on mixing. We mainly used the fungus *Aspergillus oryzae*, which is commonly used in SSF for the production of soy-sauce (Nagel et al., 2001b).

Mixing is needed in SSF with substrates that shrink upon drying and fungi that form abundant aerial mycelium. Weber et al. (2002) demonstrated that during cultivation of *A. oryzae* on wheat grain in an unmixed packed-bed fermenter, the combination of shrinkage of the substrate due to evaporation of water, and the formation of a mycelium network between the grains caused channeling and failure of temperature control via forced aeration. In a study by Fernández et al. (1996) the pressure drop in a packed-bed fermentor was reduced by intermittent mixing, presumably by breaking up a dense network of mycelium in the pores between particles. Aggregation of substrate particles due to mycelium has also been suggested to play an important role during operation of discontinuously mixed rotating drum fermentors for SSF, but unfortunately quantitative data were not provided (Mitchell et al., 2000; Pandey, 1991).

Some reports have indicated that the bed of solid substrate can be mixed continuously without detrimental effects. For example, Oostra et al. (2000) found that continuous mixing did not impede spore formation of *Coniothyrium minitans* cultivated on oat grain. Nagel et al. (2001b) studied continuously mixed SSF with *A. oryzae* cultivated on wheat grain in a paddle mixer. They concluded that continuous mixing improves process control, because it allows addition and distribution of water during fermentation, reduces gradients in the bed and improves heat transfer to the fermentor wall. They also concluded that continuous mixing does not have a negative impact on the fermentation: Respiration rates were comparable to those in unmixed cultures. Nagel et al. (2001b) also observed that the fungus grew primarily inside the wheat

grain during continuously mixed SSF; hardly any mycelium was observed on the grain surface and the amount of aerial mycelium was negligible (F.J.I. Nagel, personal communication).

In contrast, Han et al. (1999) studied the effect of intermittent mixing on enzyme production during cultivation of *Rhizopus* on soybeans and concluded that intermittent mixing may negatively affect enzyme production. Compared with the work of Nagel et al. (2001b) there are four differences: the morphology of the fungus, the structure and firmness of the solid substrate, the fermentor layout and the mixing regime. This, of course, makes it impossible to derive general guidelines from any of these studies.

Recently, Rahardjo et al. (2002) published results that may shed some light on the detrimental effects of mixing reported in some studies. They showed that aerial hyphae contributed up to 75% to the oxygen uptake rate in cultures of *A. oryzae* on a wheat-flour model substrate. The development of aerial hyphae is also favorable for biomass production (Y.S.P. Rahardjo, personal communication). The reason for the high respiration rate of aerial mycelium is the rapid diffusion of oxygen in the air-filled pores (Rahardjo et al., 2002). It might be that mixing results in a decrease in respiration rate in SSF, because aerial hyphae are broken or simply pressed tightly together in a wet layer against the particle surface, where they face oxygen diffusion limitation.

The dilemma we face is that aerial hyphae are undesirable for proper process control during SSF, whereas they are desirable for biomass production. As a compromise, discontinuously mixed SSF may be preferred: Aerial growth is allowed until the aggregation of particles due to the formation of hyphal bonds becomes critical for process control and then the bed is mixed to prevent channeling. Discontinuous mixing may also reduce both damage inflicted on the substrate and operating and investment costs. The latter is evident from the construction of many Koji plants and malting factories: Given the enormous size of the bed it is impossible to mix all solids simultaneously; instead mixing screws mounted on a trolley or an arm moving over the bed mix the solids intermittently.

Because discontinuously mixed SSF is an attractive operating strategy, our focus in this study was on correlating the tensile strength of the hyphal bonds between substrate particles to the forces that can be exerted during mixing. The aim of the mixing action is to break up the network of aerial mycelia and prevent that aggregates remain after mixing. Fig. 1 presents a schematic example of the course of such a discontinuously mixed SSF: Mixing is initiated when the tensile strength of the hyphal bonds exceeds a critical value that would preclude disruption of the bed into single particles and small aggregates. The exponential increase of the hyphal bond tensile strength is hypothetical, but could occur either because there is exponential growth, or because the aerial hyphae gradually recover after a mixing event.

To measure the tensile strength of the hyphal bonds between the grains we developed a novel experimental set-up. Other fungi that were also studied with this novel experimental set-up were *Rhizopus oligosporus* and *Aspergillus niger*, two fungi that form abundant aerial mycelium just as *A. oryzae* does, and *Aspergillus sojae*, which forms no aerial hyphae.
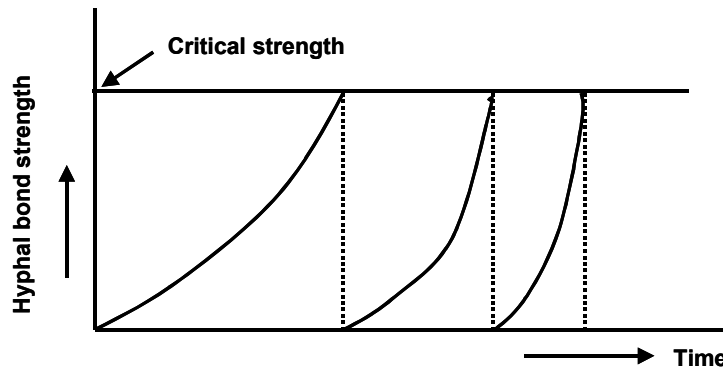
Figure 1. The average hyphal bond tensile strength between grains in the substrate bed plotted versus time for a discontinuously mixed SSF, in which mixing events are triggered by the critical hyphal bond tensile strength.

Discrete particle modeling

In previously published work, we developed a discrete particle model for a rotating drum fermentor predicting the two-dimensional mixing behavior of wheat grains (Schutyser et al., 2001). In this modeling approach, forces on and subsequent trajectories of each individual particle were calculated. In this study, we extended the discrete particle model and implemented the presence of hyphal bonds. Subsequently, we simulated the breakage of hyphal bonds and thus breakage of large aggregates in the substrate bed by mixing action.

In the discrete particle model the wheat grains are modeled as spherical particles. It was found that the model could accurately predict the radial mixing behavior of wheat grains in a rotating drum fermentor despite this simplification. This discrete particle model was extended with hyphal bonds between particles to study their effect on the mixing behavior. We chose a 2D modeling approach to avoid long computation times. This modeling strategy is feasible, because the horizontally rotating drum has no driving force for axial particle movement other than dispersion at the bed surface. It is also reasonable to assume that radial mixing is mainly responsible for the disruption of aggregated wheat grains, because axial mixing occurs at a much lower rate in a rotating drum fermentor without baffles (Schutyser et al., 2002).

In the discrete particle model, movements of particles are predicted from forces acting on each individual particle. These forces include gravitation and interactions between particles and between particles and the wall. In the force calculations we distinguish normal and tangential or shear forces. For more detailed information about the model and the parameters we refer to

Schutyser et al. (2001). The forces are evaluated at very brief time intervals (20 μs) and, subsequently, new particle velocities and positions are calculated by integration of the Newtonian equations of motion.

Extended discrete particle model with fungal growth

In this study, we modeled the breakage of aggregates of substrate particles (d=4.9 mm) that are held together by hyphal bonds of *A. oryzae* formed during SSF. Discrete particle models have been applied before to investigate the fracture and fragmentation of aggregates of powders (d= 5-30 μm) (Mishra and Thornton, 2001; Ning et al., 1997; Thornton et al., 1999). These aggegrates consisted of fine powder particles bound together by inter-particle molecular forces. Discrete particle models have also been used to analyze wet granulation processes, in which particles (d=0.25-1 mm) are glued together into larger aggregates by a binder solution (Goldschmidt, 2001; Mishra et al., 2002). Mishra et al. (2002) modeled the wet granulation process in a rotating drum, in which adhesive forces are responsible for aggregation and breakage of aggregates can occur due to the mixing action. Depending on the bond tensile strength, equilibrium in terms of aggregate size was reached during continuous mixing. Because of the similarity to these studies of physical aggregates, we expect that the discrete particle modeling approach can be applied to model the breakage of aggregates during SSF. The difference between this study and the previous studies is the nature of the bonds.

To model the hyphal bonds we applied a relatively simple approach. The attraction force between two particles increased linearly with the distance between the particles (Hookian force). The attraction force was zero when the distance between the particle surfaces was 0 mm and equal to the tensile strength when the distance was 1 mm (i.e. 10 % of the distance between the centers of the particles). The distance of 1 mm was found to be the critical length at which the maximum force was measured during tensile strength measurements (Fig. 5). Due to the mixing action the two bound particles may be forced to move away from each other. The distance increased only when the sum of the other forces acting on the particles exceeded the attraction force exerted by the hyphal bond between the particles. The bond was assumed to break if the distance exceeded 1 mm. The tensile strength of all bonds was normally distributed around the average tensile strength derived from independent measurements, with a variance of 10%. The reason for applying this variance in tensile strength was that small variations may occur due to differences in local growth conditions. During further investigations we observed that the simulated behavior of aggregates that had bonds with varying tensile strength (i.e. normally distributed) was similar to the behavior of aggregates that had bonds with equal tensile strength.

The extended discrete particle simulation generates a data file that contains the positions and velocities of each particle at different timepoints. A second file contains information about particles that have hyphal bonds. At the start of the simulation, bonds are defined between all particles separated from each other by $\leq$ 1 mm. The number of bonds created depends on the number of particles (N=1137) and on the initial configuration of the particles; in our case, we obtained 3077 bonds. This number of bonds is approximately 90% of what would be expected on the basis of a 2D dense packing of spheres. The identification numbers of corresponding particles that have a bond are stored in two arrays (length 3077) during simulation. A second array of the same length is created to store the force exerted by the bond.

After simulation, we conducted data postprocessing in order to count the number and size of the aggregates that exist during and after the mixing period. The postprocessing procedure used information on existing bonds (stored for different time intervals in the data file) to determine which particles formed an aggregate during simulation. Each aggregate was appointed a different color for visualization. It was also possible to appoint a similar color for aggregates of equal size.

Materials and Methods

Microorganisms

Aspergillus oryzae CBS 570.64 and *Rhizopus oligosporus* NRLL 5905 were grown for 7 days at 30ºC on malt-extract agar (Oxoid, CM 59, UK). *Aspergillus niger* CBS 131.52 and *Aspergillus sojae* ATTC 11906 were cultivated for 7 days at 30 ºC on potato-dextrose agar (Oxoid, CM 139). Stock solutions of spores were obtained by flooding the agar plates with 10 or 20 mL (only for *A. oryzae*) solution containing 1 g neutralized bacteriological peptone (Oxoid, L34), 8.5 g NaCl, 0.5 g Tween-80 (Merck, GE) per 1 L demineralized water and gentle scraping of the plate. After harvesting, the spore suspension was filtered through sterile glass wool to discard remaining mycelium. Glycerol (23% [v/v], final concentration) was added to the spore suspension, which was subsequently stored at -80ºC. The spore concentrations in the suspensions were determined using an electronic particle counter (Casy 1, Schärfe-System, Reutlingen, GE)

Substrate preparation for fermentation

The wheat grains were obtained from a local supplier and were stored at room temperature. The wheat grains were soaked for 2.5 hrs in excess tap water at 60ºC. After sieving, the soaked grains were autoclaved for 1.5 hrs at 121 ºC. The initial moisture content of the substrate was 0.8 kg H_2O/kg DM.

Sandwich cultivation of wheat dough disks

Wheat dough disks (d = 47.5 mm and height = 18 mm) were prepared from wheat flour, as described by (Nagel et al., 2001a). Equal masses of wheat flour and demineralized water were homogeneously mixed to obtain a final moisture content of 1.0 kg H_2O / kg DM. To obtain the wheat flour, whole wheat grains were milled in a mill (Retsch, NL). The wheat dough disks were glued in plastic petri-dishes (d = 60 mm and height = 15 mm, 628102 Greiner, Austria) with agar (technical agar 2%, Oxoid). The wheat disks were inoculated by homogeneously spreading 100 µl ($5 \cdot 10^4$ spores) of spore suspension over the disk with a sterile bent glass rod. Two glued, inoculated wheat disks were subsequently placed on top of each other to form a sandwich (Fig. 2). Four iron spacer bars (d = 0.5 or 1 mm, length = 60 mm) were placed between the two wheat disks to create a distance of 1, 1.5 or 2 mm, to allow development of aerial hyphae and transport of oxygen between the two disks. The sandwiches were put in a plastic container placed in a temperature-controlled cabinet (35ºC). To prevent dehydration of the wheat disks moistened and filter-sterilized air was passed through the container (100 mL/min).

We measured the tensile strength of the aerial hyphae forming bonds between two wheat dough disks with a texture analyzer (XT2i HR, Stable Micro Systems, NL). During these experiments the wheat dough disks were pulled (in the normal direction) apart at a constant velocity (0.1 mm/s). The lower petri-dish was mounted on the table of the texture analyser, while the upper petri-dish was attached to a pulling hook (Fig. 2). The force needed to maintain a constant velocity was recorded as a function of the distance.

Oxygen consumption measurements

Three wheat disk sandwiches were placed in a closed glass jar to measure the oxygen consumption during incubation. The jar was aerated with an airflow rate of 50 mL/min using a mass flow controller (Brooks Instruments BV, NL). To prevent dehydration of the wheat disks the air was moistened with a bubble column filled with demineralized water. Before the moistened air entered the jar it was filter-sterilized with a 0.2-µm hydrophobic membrane (Sartorius, Midisart 200, GE). The oxygen concentration of the outlet air, which was dehumidified using a condenser, was analyzed with an oxygen analyzer (Xentra 4100, Servomex, NL).
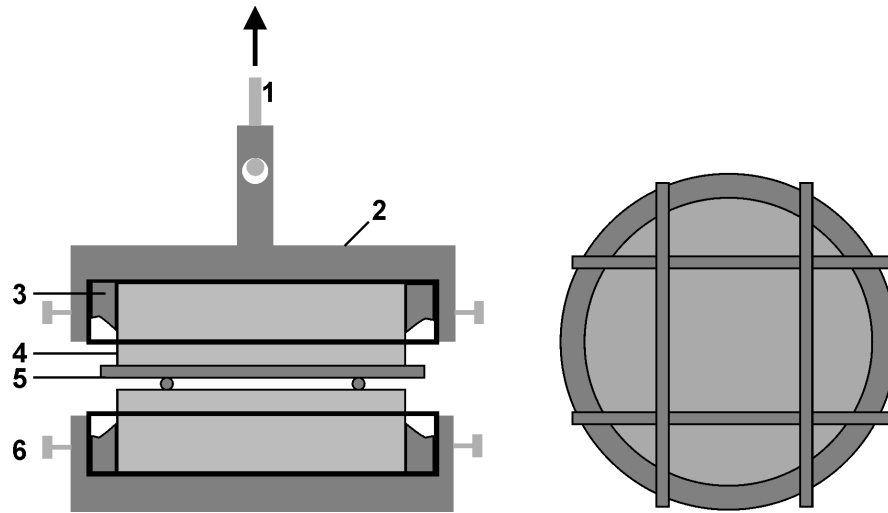
Figure 2. Experimental set-up for measurement of the tensile strength of the aerial hyphae that form a tight network between the two wheat dough disk surfaces, using a texture analyzer. Left: side view, right: top view on the wheat dough disk. (1) Hook of the texture analyzer, (2) holder of the petri-dish (3) agar (4) wheat dough disk (5) iron spacers (6) screw to pinch the petri-dish.
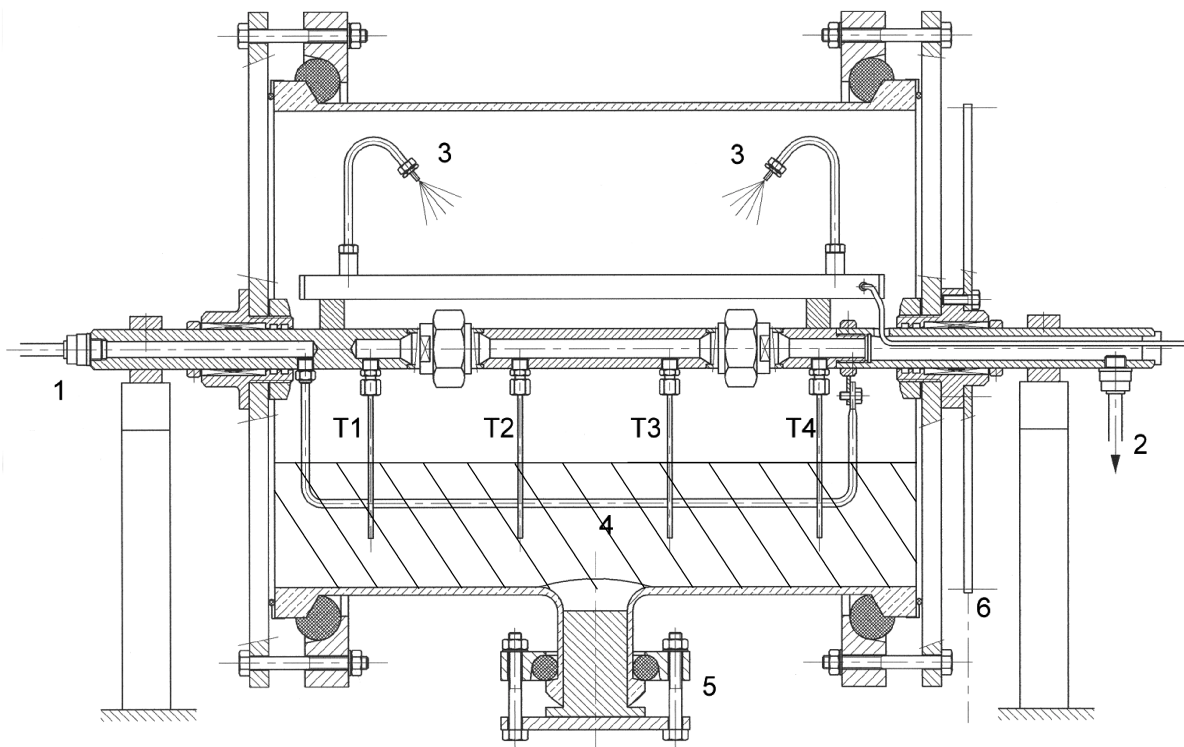
Figure 3. The 28-L rotating drum fermentor: (1) air inlet, (2) air outlet, (3) spraying nozzle, (4) channel for air distribution in the bed, (5) closed opening (possibility for attachment of a sampling device), (6) cog-wheal, (T1..T4) four temperature sensors adjustable in height. The large shaded area shows the bed.

Fermentor design

The rotating drum fermentor (Fig. 3) had the following dimensions: internal diameter 30 cm, length 40 cm and internal volume 28.3 dm^3. The bioreactor consisted of a glass cylinder (Scott, GE) with two polycarbonate (Lexan) side plates. The fermentor was entirely sterilized in an autoclave.

The drum rotated around the (non-rotating) horizontal axis, driven by a Watson Marlow drive (505DU, Cornwall, UK) fitted with a factor 10 gearwheel transmission. On the horizontal axis four temperature sensors (Pt-100 Ω Tempcontrol, NL) were mounted that penetrated the grain bed (Fig. 3). The position of the temperature sensors was adjustable in the radial direction of the drum; the angle of two temperature sensors could be adjusted as well. This allowed us to monitor the temperature of the bed at four different locations.

Air entered the reactor via a narrow tube with several holes positioned in the center of the bed; this tube was attached to the hollow horizontal axis (Fig. 3). The outlet air was collected at the opposite side of the air inlet via three holes in the horizontal axis. We decided to force the air through the bed rather than over the top of the bed, in order to improve the heat transfer from the bed to the air. We observed that the mixing behavior of the substrate bed (in absence of aerial hyphae) was not severely influenced by the presence of the small pipe and the temperature sensors. The air that entered the fermentor was humidified in a stainless steel column (diameter 30 cm, height 80 cm) filled with Raschig rings and demineralized water at 25ºC; we used humidified air to prevent fast local desiccation of the bed. The drum fermentor was placed in a temperature-controlled cabinet (34ºC). The humidified air was passed through a narrow pipe (diameter = 4 mm and length = 4 m) in the cabinet and therefore the temperature of the inlet air rose to 30ºC. The inlet and the outlet air were both filter-sterilized (Whatman Polyvent 1000 0.2 μm, UK). The outlet air was passed through a water-jacketed pipe (45 ºC) to prevent possible condensation of water vapor. The humidity of the off-gas was continuously measured with a cooled-mirror dew point analyzer (Dewmet SD, Michell Instr., UK). Before oxygen analysis (Xentra 4100, Servomex, NL) a small portion of the off-gas (400 mL/min) was passed through a glass condenser (at 4ºC) in order to remove most water vapor from the air.

The fermentation was monitored with a PC using Fieldpoint hardware and Labview software (both from National Instruments, NL). The fermentor was inoculated with two spraying nozzles (Bète PJ8*5-1/8, Spraybest, NL) placed in a position that allowed optimal coverage of the higher half of the surface of the bed (Fig. 3). Pressurized air (2 bars) pushed the spore suspension (60 mL) through a small pipe in the hollow axis and through the nozzles. Because some spore suspension remained in the piping system, 300 mL of sterilized demi-water was sprayed after spraying the inoculum to flush the system. During and some minutes after the inoculation procedure the bed was continuously mixed at 10 rpm to guarantee homogeneous

distribution of the spore solution throughout the bed. During fermentation the bed was not mixed. The flow rate of the inlet air during fermentation was initially set to 6 L/min with a mass flow controller (Brooks Instruments BV, NL), which is the minimum airflow required for off-gas analysis in the current fermentation set-up. At the end of each fermentation experiment we mixed the bed by rotating the drum at 1 rpm for five rotations. The fermentation time (after which the mixing was started) was chosen in such a way that it was difficult but still feasible to break up the aggregated substrate bed. The decision for mixing was based on the oxygen consumption measured at the end of the fermentation time.

After the mixing procedure we opened the drum carefully and separated the bed in three fractions: single grains, small aggregates (2 to 20 grains) and large aggregates (>20 grains). Each fraction was weighed and the weight fraction of aggregates was determined by dividing the weight of the fraction by the total weight of all three fractions. Samples of the bed were taken to determine the water content and the water activity in the fermenter contents.

Results and Discussion

Fermentation experiments

Several fermentation experiments were conducted to find the range of oxygen consumption rates indicating that a network of aerial mycelium had formed that was difficult to break up by mixing. Fig. 4a shows the oxygen consumption rate (mol m^{-2} h^{-1}) profiles of four fermentations; the oxygen consumption rate is expressed per total available surface area of the wheat grains (5.05 m^2) in the fermentor. The rectangular area in Fig. 4a shows the range of oxygen consumption rates that corresponded to a dense network of aerial mycelium between the substrate particles in the bed. We performed several fermentation experiments with final oxygen consumption rates in this region; after the mixing period at the end of the fermentation, we determined the number of remaining aggregates in the bed. Fig. 4b shows that the fraction of aggregates increased significantly over a small range of oxygen consumption rates (0.025-0.04 mol m^{-2} h^{-1}), which corresponded to a small range of fermentation times (40-48 h). It was necessary to mix before the oxygen consumption rate reached a value of 0.025 mol m^{-2} h^{-1}, to avoid the formation of a strong network of aerial mycelia between the grains and the presence of large aggregates after the mixing period.

In these fermentation experiments, we also observed that the mixing action pressed the aerial mycelia onto the surface of the grains. Simultaneously, we observed a decrease of the oxygen consumption rate by approximately 10% immediately after mixing (results not shown). These two observations are in agreement with the findings of Rahardjo et al. (2002) that aerial hyphae contribute significantly to the oxygen consumption of the fungus.
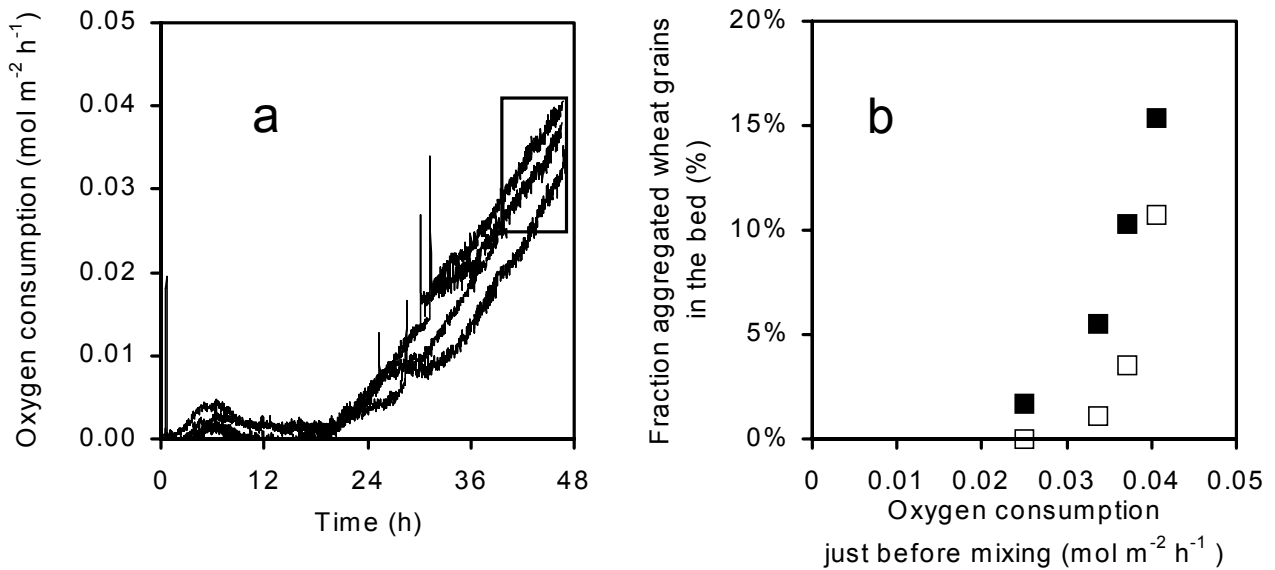
Figure 4a. Oxygen consumption versus time during four static fermentations of *A. oryzae* in the rotating drum fermentor. The fermentations are stopped after they reached a certain oxygen consumption value at which it is expected that the aerial mycelium of *A. oryzae* forms a fairly tight network between the grains. **b** At the end of the fermentation the drum is rotated for five minutes at 1 rpm, then it is opened and the fraction aggregates determined. The open symbols are large aggregates (>20 grains) and the small symbols are the small aggregates (between 2 and 20 grains).

During these experiments, the airflow rate was manually adjusted from 6 to 20 dm^3/min, to control the temperature in the bed. We monitored the temperature during the fermentation with four temperature sensors located at different positions in the bed. The temperature sensor located next to the aeration tube always measured a temperature of 30°C, which is lower than the optimum growth temperature (34°C), but still gives 92 % of the maximum growth rate of *A. oryzae* (M.J. Hoogschagen, unpublished data). The other temperature sensors measured bed temperatures between 33 and 36°C (>95% of the maximum growth rate), except during the last six hours of two fermentations, when temperatures up to 40°C were measured. However, even at 40°C the growth rate of *A. oryzae* is still 71% of the maximum growth rate. Therefore, we concluded that temperature differences in the bed did not significantly influence the growth conditions.

The average moisture content and the water activity were analyzed at the end of the fermentation runs and were found to be above the critical levels for growth, *i.e.* $x_w > 0.5$ kg H_2O kg^{-1} IDM and $a_w > 0.96$ (Nagel et al., 2001a). These measurements show that the moisture content of the bed did not yet hamper fungal growth at the time of mixing. Therefore, the first mixing event during our fermentation experiments with *A. oryzae* on wheat was necessary to disrupt the mycelium network, rather than to add water. Also, we hpothesixed that, for large-scale fermentors, water levels would not become critically low before the first mixing event is

necessary to prevent aggregate formation (Appendix 1). Disruption of the mycelium network by mixing has therefore higher priority than water addition. This implies that the morphological properties (formation of aerial mycelium) of the cultivated fungus must be taken into account for the design and scale-up of SSF.

The results of these mixing experiments allowed us decide when mixing is desired during cultivation of *A. oryzae* in the rotating drum fermentor. Because it is desirable to extrapolate these results to other process conditions or even fermentor designs, we implemented the presence of hyphal bonds in the discrete particle model. To model the hyphal bonds between the grain particles, information regarding their tensile strength was needed. We developed a novel experimental approach to obtain such information; the results of these measurements are described in the next section.

Strength measurements of aerial mycelium grown between two wheat dough disks

We used an experimental set-up with two wheat dough disks to measure the tensile strength of hyphal bonds formed by *A. oryzae* in SSF (Fig. 2). *A. oryzae* was cultivated between two wheat dough disks, and the force needed to separate the two disks after a certain incubation time was measured with a texture analyzer. Fig. 5 shows force-distance curves for three incubations times; the force was divided by the cross-section area of the sandwich, $\pi r^2 = 1.81 \cdot 10^{-3}$ m^2. Initially, the force required to lift the upper sandwich increased due to stretching of the aerial hyphae. At the maximum of the curves, most hyphal bonds broke and the force that was measured gradually decreased until all hyphae were broken and disentangled. The maximum force was assumed to be equal to the average tensile strength of the aerial mycelium between the two surfaces. Fig. 5 shows that the tensile strength of the aerial mycelium increased strongly with increasing incubation time.

The tensile strength of the aerial mycelium was measured after several incubation times. Below a certain incubation time, no force could be measured. Beyond a certain incubation time, the tensile strength of the aerial mycelium exceeded the strength of the agar used to glue the wheat dough disks to the petri-dish. However, reproducible experiments could be carried out between these extremes.

We believe that the wheat dough sandwiches can be used to acquire accurate data on the tensile strength of the hyphal bond between two wheat grains. For this purpose, three items were taken into account: First, we expressed all measurements per square meter of substrate surface area to allow for a comparison. Second, we had to account for differences in mycelium density with incubation time, because the development of respiration rate over time differed for the wheat dough disks and wheat grain, which could be due to the easier accessibility of the starch and the lack of a seed coat. Therefore, incubation time was not an appropriate independent variable to
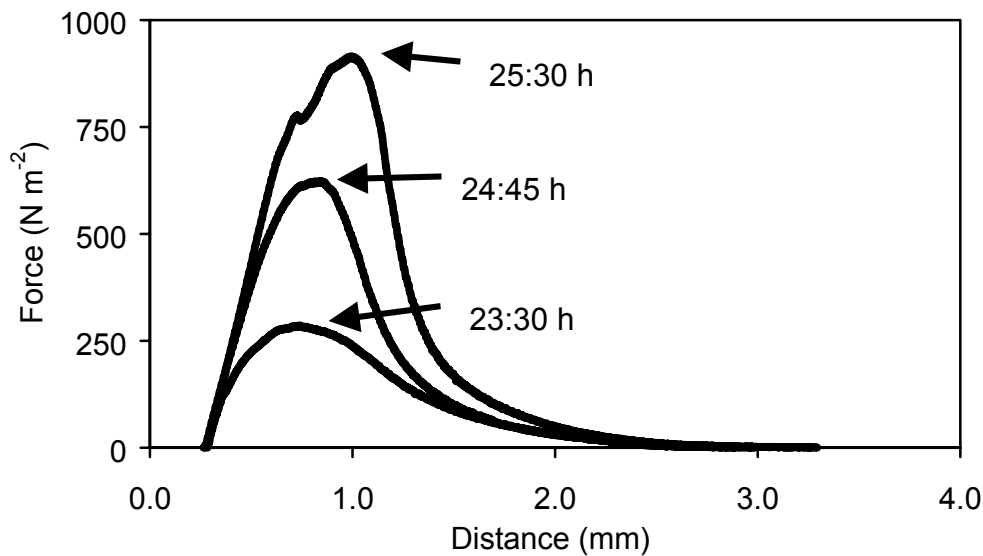
Figure 5. The measured force versus the distance for three different incubation times for *A. oryzae*, as measured with the texture analyzer. The maximum force equals the tensile strength of the aerial mycelium grown between the two wheat disks.
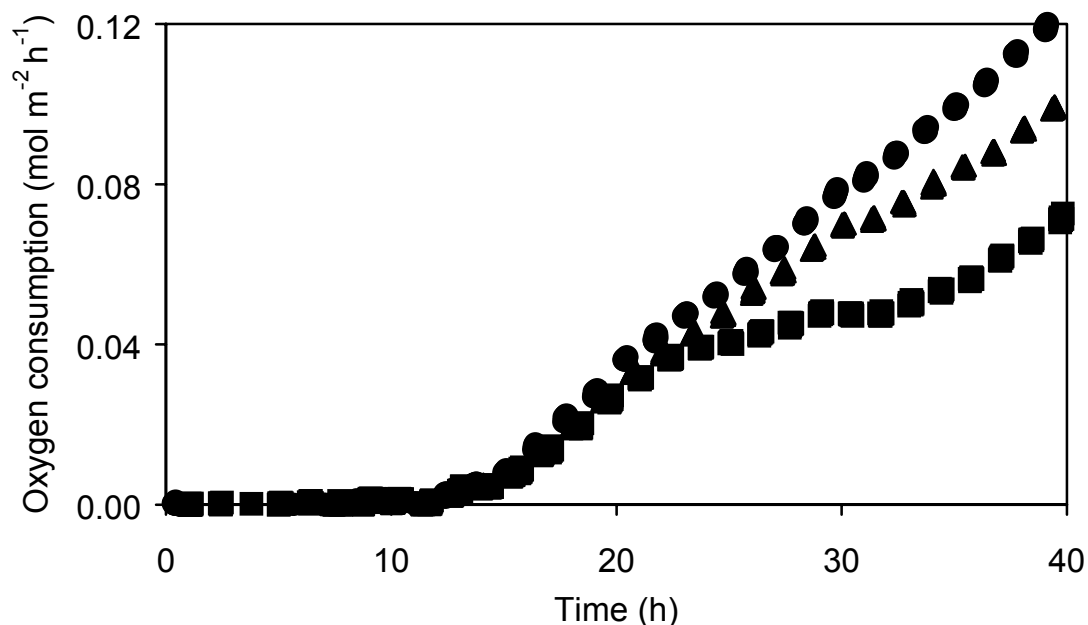

Figure 6. Oxygen measurement of *A. oryzae* as a function of the incubation time for three different distances between the wheat disks: ■ 1 mm, ▲ 1.5 mm and ● 2 mm.

translate the tensile strength measured in the model system to the tensile strength of the hyphal bonds during fermentation on wheat grain. We used the oxygen-uptake rate to provide an accurate translation. The oxygen-uptake rate is closely related to the growth of biomass, which in turn is closely related to the formation of (aerial) hyphae. Third, the distance between the two

wheat dough disks was considered an important parameter in the force measurements. We estimated the effective distance between two grains in the fermentor at 1.1 mm for two ellipsoidal particles piled on top of each other. The average distance between the grains is somewhat larger in practice because of the random irregularities in the packing structure. Therefore, the distance was assumed to be between 1.1 and 1.5 mm. To study the influence of the distance on the tensile strength of the hyphal bonds we performed experiments for three distances (1, 1.5 and 2 mm) between the two wheat dough surfaces.

Fig. 6 shows the oxygen consumption rate as a function of time for sandwiches with distances of 1, 1.5 and 2 mm between the disks. To obtain accurate oxygen consumption measurements, we placed three sandwiches in a glass jar for each distance. From Fig. 6 it is concluded that the oxygen consumption does not depend on the distance between disks up to an oxygen consumption rate of 0.035 mol m^{-2} h^{-1}. Beyond this level, the oxygen consumption rate for the distance of 1 mm levels off abruptly. This can probably be explained by the limited transport of oxygen between the wheat disks, due to the formation of a dense network of mycelia.

Fig. 7b shows the translation from wheat-dough disks to grains in the fermentor: The oxygen consumption rate is the independent variable and the strength of the bond between two grains is the dependent variable. We translated the tensile strength measured with wheat-dough disks (expressed in N m^{-2}) to the tensile strength of the bonds between two grains (expressed in N) by multiplying with the cross-section area ($\pi r^2 = 1.89 \cdot 10^{-5}$ m^2) of the spherical particles used in the model (d=4.9 mm). The diamond-shaped area in Fig. 7b indicates the boundary conditions derived previously; that is, oxygen consumption rate between 0.025 and 0.04 mol m^{-2} h^{-1} (Fig. 4) and distance between 1.1 and 1.5 mm. This resulted in a range of tensile strengths (10 to 65 mN) for the hyphal bonds between two grains, which would be expected to give rise to problems during mixing. This range was used in the discrete particle model as described in what follows.
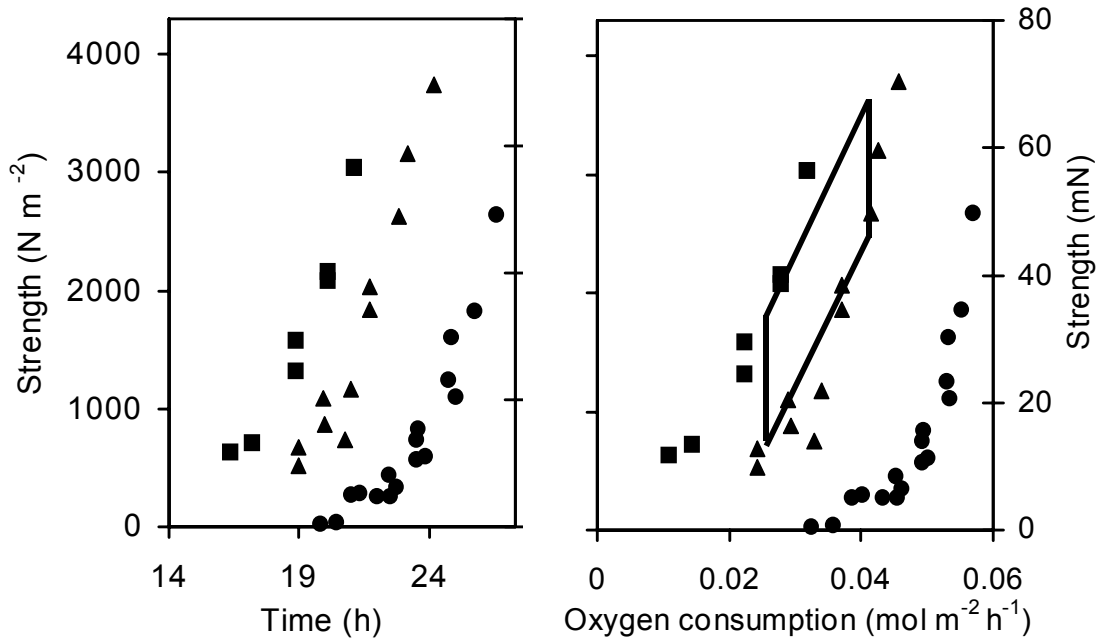
Figure 7. Tensile strength of the aerial mycelium of *A. oryzae* versus time and oxygen consumption for three different distances (■ 1 mm, ▲ 1.5 mm and ● 2 mm) between two wheat-dough disks **a** Tensile strength of aerial mycelium between two disk surfaces (N m^{-2}) **b** Tensile strength (mN) of the aerial mycelium grown between two grain particles (■ 1 mm, ▲ 1.5 mm and ● 2 mm). Note that both traces can be used to read tensile strength between two wheat-dough disks (N m^{-2}) as well as between two grains (mN).

Extended discrete particle simulation results

The effect on mixing behavior of different tensile strengths of the hyphal bond between wheat grains was simulated with the extended discrete particle model, using the range of tensile strengths derived earlier (10 to 65 mN for two grains). The initial configuration of the particles in the discrete particle simulation, which describes the breakdown of large aggregates into smaller ones, was obtained from a previous mixing simulation in which no bonds were present. Bonds were then defined between particles whose surfaces were separated by ≤ 1 mm. Subsequently, five rotations at 1 rpm were simulated. The mixing action resulted in the breakage of several bonds and thus in an increasing number of small aggregates (Fig. 8). From the simulation results it was clear that the number and size of aggregates present during and after the mixing period were larger when the tensile strength of the hyphal bond was increased (Fig. 9a). Fig. 9b shows the fraction of aggregates at the end of the simulation.

We found that the fraction of aggregates remaining after 5 rotations increased rapidly within a small range of hyphal bond tensile strengths. Within this small region the tensile strength of the

hyphal bonds exceeded a critical value that seriously hampered aggregate break-up. During the fermentation experiments we also found that the aggregation of the grain became much stronger within a small range of oxygen consumption rates (Fig. 4). The predicted and measured aggregate fractions after the mixing period agreed well, indicating that the tensile strength measurements with wheat dough (Fig. 7b) gave realistic values for the hyphal bonds between wheat grains. Therefore, we conclude that the extended discrete particle model can provide valuable information about the need for mixing, based on on-line respiration measurements in the drum fermentor and simple independent strength measurements. Because the extended discrete particle model can be easily adapted to different fermentor designs (e.g. implementation of baffles), different fermentor designs could be compared for their effectiveness in disrupting aggregates that are the result of the formation of aerial mycelia.

A question that remains to be answered is whether the model could estimate when a second mixing action would be required. With the help of the experimental set-up developed in this study, we may also be able to find an answer to this problem: After the force measurement experiment, we could return the upper wheat disk to its original position and study formation of new hyphal bonds by subsequent force measurement experiments.
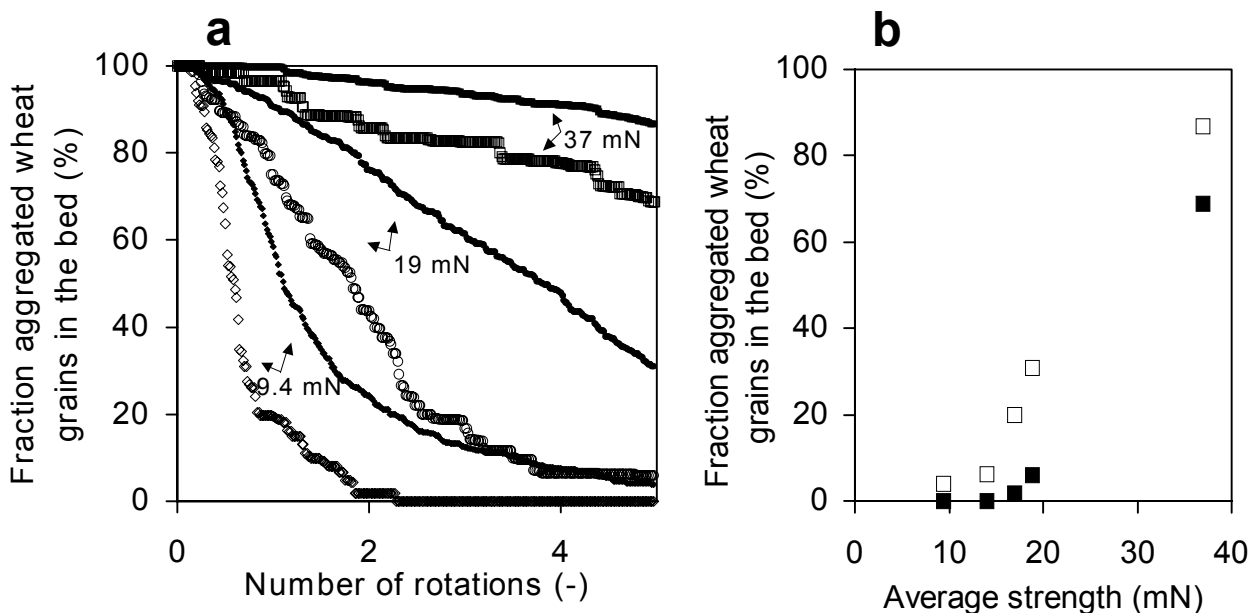
Figure 9a. Simulated breakdown of aggregates for three different implemented forces (9.4, 19 and 37 mN). The open symbols are the large aggregates (>20 grains) and the small symbols are the small aggregates (between 2 and 20 grains). **b** The fraction of aggregated wheat grains in the bed after 5 rotations of mixing as a function of the average force implemented between the particles in the model.
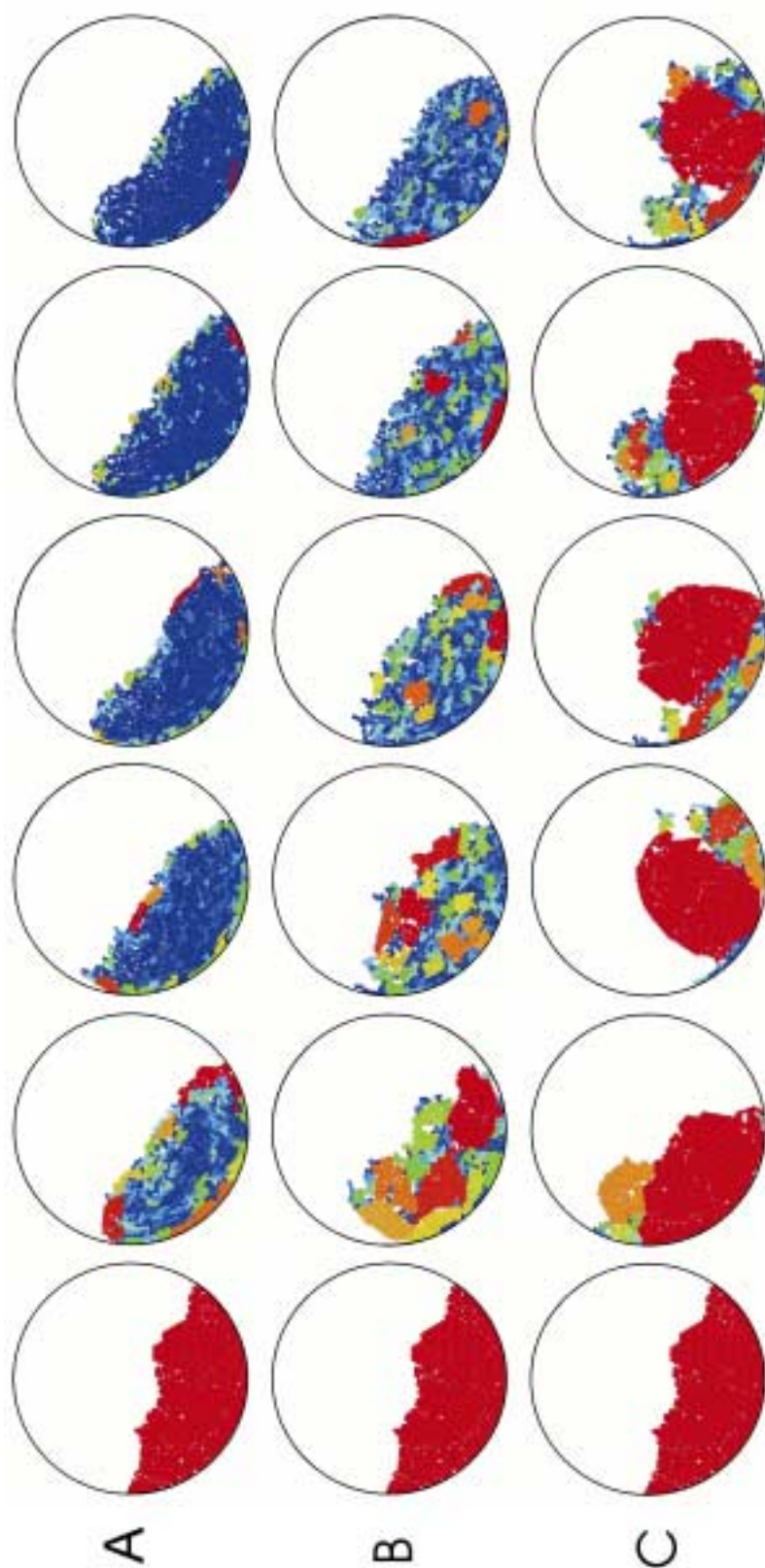
Figure 8. Visualization of the model predictions of the breakdown of aggregates during the mixing period for three different hyphal bond tensile strengths. For each hyphal bond five pictures are shown, after 0, 1, 2, 3, 4 and 5 rotations. Large aggregates are colored red and single particles blue. **a** 9.4 mN **b** 18.9 mN **c** 37.8 mN

Other fungi

The general applicability of the experimental set-up used to determine the tensile strength of the aerial mycelium was further explored by measuring different fungi. Because the development of aerial mycelium is dependent on the fungal species, fermentation behavior (i.e. substrate aggregation due to formation of a network of aerial mycelium) will vary for different fungi. We performed several tensile strength measurements with the fungi *R. oligosporus* and *A. niger* with a sandwich distance of 2 mm (Fig. 10). For *A. niger*, we obtained a similar curve for the tensile strength of the hyphal bond as for *A. oryzae*, whereas *R. oligosporus* was shown to outrun *Aspergilli*. This result indicates that, during discontinuously mixed SSF with *R. oligosporus* on wheat grain, a mixing action is required earlier during fermentation, whereas SSF with *A. niger* will behave similarly to SSF with *A. oryzae*.

An entirely different approach that may be followed to avoid aggregation problems is to select a fungus that produces very little or no aerial mycelium. We conducted tensile strength measurements with *A. sojae*, a species that forms no aerial mycelium at all. Only for the shortest distance of 1 mm we measured some irregular forces during separation of the two wheat disks (results not shown). During incubation of *A. sojae* we observed that the distance between the two disks decreased, because the surfaces of the wheat disks became wet and soft. Thus, the measured forces might have been due to growth from one surface to the other surface in absence of any aerial hyphae. First fermentation results with *A. sojae* showed oxygen consumption rates similar to those found for *A. oryzae*. We started mixing at an oxygen consumption rate of 0.045 mol m^{-2} h^{-1}, which resulted in large aggregates for *A.* oryzae. During fermentation with *A. sojae* no aggregates were formed. From these observations, it could be concluded that, with respect to aggregation there will be fewer problems during cultivation of *A. sojae* than during cultivation of the other species used in this study.
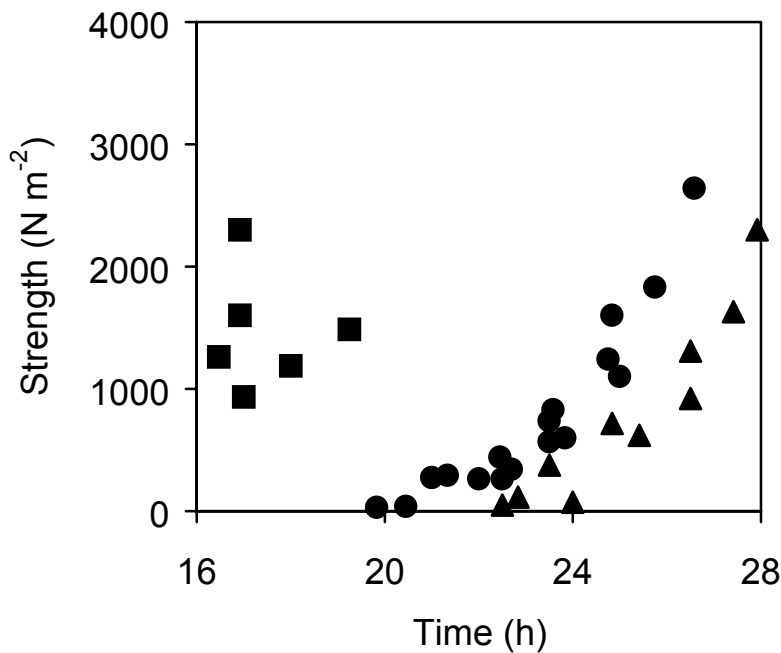
Figure 10. Tensile strength (N m^{-2}) of the aerial mycelium versus time for *A. oryzae* (●), *R. oligosporus* (■) and *A. niger* (▲) with a distance between the disks of 2 mm.

Conclusion

This study quantifies the effect of inter-particle mycelium networks in solid-state fermentation (SSF). We show that the tensile strength of mycelium-bonds between substrate particles can be measured using a wheat-dough model substrate. The tensile-strength measurement gave reproducible results with several fungi. A previously developed discrete particle simulation model was extended with inter-particle attraction forces to simulate the mycelium bonds in SSF with *A. oryzae* and wheat grain. This model successfully described the size and number of grain-aggregates remaining after the first mixing action in a discontinuously rotating 28-dm^3 drum fermentor. Fermentation experiments in this drum fermentor showed that mixing at 1 rpm during 5 minutes is needed when the oxygen consumption rate reaches 0.025 moles per m^2 substrate surface area per h. If mixing was postponed, aggregates remained after mixing, which are likely to develop internal oxygen concentration gradients. Disruption of mycelium-bonds is the most critical process in SSF with *A. oryzae* on wheat grain: Mixing is needed to disrupt mycelium-bonds before it is necessary to add water to compensate for evaporation losses. The new method to measure the tensile strength of inter-particle mycelium-bonds, combined with the extended discrete particle simulation model, provides a powerful tool to test the influence of fungal species, mixing regime and fermentor design on aggregate formation in discontinuously mixed SSF.

Acknowledgements

The authors thank the Mechanical Workshop ''de Dreijen'' for the construction of the rotating drum fermentor. We also gratefully acknowledge H. Baptist from the Food Physics Group (Wageningen University) for the technical support with the texture analyzer measurements.

Appendix I

Water loss due to evaporative cooling during cultivation of* A. oryzae*.

This calculation shows that the first mixing event during intermittently mixed SSF is needed to disrupt the mycelium network, and not to add water. We assumed that all the metabolic heat is removed by evaporation of water. This assumption is valid for large-scale SSF, in which the heat loss via wall cooling is negligible. We neglect heat removal by heating of dry air, but this is usually only a minor fraction and it makes our calculation conservative.

The measured cumulative oxygen consumption just before the mixing took place was $\Delta O_2 = 1.2 \cdot 10^{-3}$ mol·g_{IDM} (oxygen consumption of 0.04 mol m^{-2} h^{-1} in Fig. 4a). The amount of water that needs to be evaporated to remove the metabolic heat associated to this oxygen consumption, can be estimated from:

$$\Delta W_{ev} = -\frac{\Delta O_2 \cdot \Delta h_o}{\Delta h_w} \qquad (A1)$$

in which:

ΔW_{ev} = evaporated water [kg W kg^{-1} DM]

Δh_0 = $4.5 \cdot 10^5$ reaction enthalpy [J mol O$_2^{-1}$]

Δh_w = $2.5 \cdot 10^6$ evaporation enthalpy water [J kg W^{-1}]

Besides water evaporation, three other processes influence the water balance and these need to be included to calculate the final moisture content of the bed (Nagel et al., 2001a):

1 Water needed for starch hydrolysis ΔW_{hy}

2 Metabolic water production ΔW_{me}

3 Uptake of intracellular water during biomass production ΔW_x

The following equation is used to calculate the total net water loss (ΔW):

$$\Delta W = \Delta W_{ev} + \Delta W_x + \Delta W_{me} + \Delta W_{hy}$$

$$= \Delta W_{ev} - \Delta O_2 \cdot Y_{xo} \cdot Mw_x \cdot x_{wx} + \Delta O_2 \cdot Y_{wo} \cdot Mw_w - \Delta O_2 \cdot Y_{so} \cdot Y_{hyd} \qquad (A2)$$

in which (Nagel et al., 2001a):

Mw_x = $25 \cdot 10^{-3}$ Molecular weight biomass [kg Cmol^{-1}]

Y_{xo}	$= 1.16$	Yield coefficient	[Cmol X mol O_2^{-1}]
Mw_w	$= 18 \cdot 10^{-3}$	Molecular weight water	[kg mol^{-1}]
Y_{wo}	$= 1.22$	Yield coefficient	[mol W mol O_2^{-1}]
Y_{so}	$= 1.46$	Yield coefficient	[Cmol S mol O_2^{-1}]
Y_{hyd}	$= 3 \cdot 10^{-3}$	Water needed to hydrolyze starch	[kg mol^{-1}]

The dry-weight loss can be calculated from:

$$\Delta SDM = \Delta S + \Delta N$$
$$= -\Delta O_2 \cdot Y_{so} \cdot Mw_s - \Delta O_2 \cdot Y_{no} \cdot Mw_n \tag{A3}$$

in which:

Mw_s	$= 30 \cdot 10^{-3}$	Molecular weight starch	[kg mol^{-1}]
Y_{no}	$= 0.76$	Yield coefficient	[Cmol N mol O_2^{-1}]
Mw_n	$= 27.63 \cdot 10^{-3}$	Molecular weight protein	[kg mol^{-1}]

From the total water loss and the dry-weight loss we can calculate the moisture contents of the solid substrate bed at any point during the fermentation:

$$x_{ws} = \frac{x_{ws,i} + \Delta W}{1 + \Delta SDM} \tag{A4}$$

in which:

$x_{ws, i}$ = 0.8 initial water contents of the substrate [kg W kg^{-1} DM]

This calculation yields a moisture content of x_{ws} = 0.578 kg W kg^{-1} DM for the cumulative oxygen uptake of $1.2 \cdot 10^{-3}$ mol·g$_{IDM}$ that was reached when mixing was necessary to prevent aggregate formation.

The water activity (a_w) in the substrate bed can be calculated from the moisture content (Nagel et al., 2001a):

$$a_w = -2.917 + \frac{3.919}{1 + \left(\dfrac{x_{ws}}{0.0344}\right)^{-1.861}} \tag{A5}$$

The resulting water activity is 0.982, which is within the region of values (0.96-1) that do not restrict fungal growth. In conclusion, when the first mixing event is needed to disrupt inter-particle mycelium bonds, there is no need for addition of water to avoid limited growth due to low water activity, even when cooling is achieved entirely by evaporation.

References

Fernández M, Pérez-Correa R, Solar I, Agosin E. 1996 Automation of a solid substrate cultivation pilot reactor. Bioproc Eng. 16:1-4

Goldschmidt MJV. 2001. Hydrodynamic modelling of fluidised bed spray granulation. PhD Thesis, University of Twente, Enschede, The Netherlands.

Han B, Kiers JL, Nout RMJ. 1999. Solid-substrate fermentation of soybeans with *Rhizopus* spp.: Comparison of discontinuous rotation with stationary bed fermentation. J Biosc Bioeng. 88:205-209.

Mishra BK, Thornton C. 2001. Impact breakage of particle agglomerates. Int J Min Proc 61:225-239.

Mishra BK, Thornton C, Bhimji D. 2002. A preliminary numerical investigation of agglomeration in a rotary drum. Min Eng 15:27-33.

Mitchell DA, Krieger N, Stuart DM, Pandey A. 2000. New developments in solid-state fermentation II Rational approaches to the design, operation and scale-up of bioreactors. Proc Biochem 35:1211-1225.

Nagel FJI, Tramper J, Bakker MSN, Rinzema A. 2001a. Model for on-line moisture content control during solid-state fermentation. Biotechnol Bioeng 72:231-243.

Nagel FJI, Tramper J, Bakker MSN, Rinzema A. 2001b. Temperature control in a continuously mixed bioreactor for solid-state fermentation. Biotechnol Bioeng 72:219-230.

Ning Z, Boerefijn R, Ghadiri M, Thornton C. 1997. Distinct element simulation of impact breakage of lactose agglomerates. Adv Powder Technol. 8 :15-37.

Oostra J, Tramper J, Rinzema A. 2000. Model-based biorector selection for large-scale solid-state cultivation of Coniothyrium minitans spores on oats. Enzyme Microb Technol 27:652-663.

Pandey A. 1991. Aspects of fermentor design for solid-state fermentations. Proc Biochem 26:355-361.

Rahardjo YSP, Weber FJ, Comte le P, Tramper J, Rinzema A. 2002. Contribution of aerial hyphae of *Aspergillus oryzae* to respiration in a model solid-state fermentation system. Biotechnol Bioeng 78:539-544.

Schutyser MAI, Padding JT, Weber FJ, Briels WJ, Rinzema A, Boom R. 2001. Discrete particle simulations predicting mixing behavior of solid substrate particles in a rotating drum. Biotechnol Bioeng 75:666-675.

Schutyser MAI, Weber FJ, Briels WJ, Boom RM, Rinzema A. 2002. Three-dimensional simulation of grain mixing in three different rotating drum designs for solid-state fermentation. Biotechnol Bioeng 79:284-294.

Schutyser MAI, Weber FJ, Briels WJ, Rinzema A, Boom RM. 2003. Heat and water transfer in a rotating drum containing solid substrate particles. Biotechnol Bioeng 82:552-563

Thornton C, Ciomocos MT, Adams MJ. 1999. Numerical simulations of agglomerate impact breakage. Powder Technol 105:74-82.

Weber FJ, Oostra J, Tramper J, Rinzema A. 2002. Validation of a model for process development and scale-up of packed-bed solid-state reactors. Biotechnol Bioeng 77:381-393.

Chapter *7*

Combined discrete particle and continuum model predicting solid-state fermentation in a drum fermentor

Abstract

The development of mathematical models facilitates industrial (large-scale) application of solid-state fermentation (SSF). In this study, a two-phase model of a drum fermentor is developed that consists of a discrete particle model (solid phase) and a continuum model (gas phase). The continuum model describes the distribution of air in the bed injected via an aeration pipe. The discrete particle model describes the solid phase and allows prediction of the mixing behavior of the substrate bed. Although, in this study intermittent mixing events during SSF were not predicted, these could be implemented easily based on earlier work. Heat and mass transfer between the two phases and biomass growth were taken into account in the model. Validation experiments were conducted in a 28-dm^3 drum fermentor. In this fermentor, sufficient aeration was provided to control the temperatures (near) optimum growth temperature during the first 45-50 h. Found was also that during fermentation moisture levels did not drop below critical levels. It could however be concluded that mixing in this fermentor is needed in first instance to disrupt the network of mycelium after 40 h. Several simulations were conducted for different fermentor scales. Forced aeration via a single pipe in the drum fermentors did not provide homogeneous cooling in the substrate bed. Due to large temperature gradients, biomass yield decreased severely with increasing size of the fermentor. Improvement of air distribution would be required to avoid the need for frequent mixing events, during which growth is hampered. From these results, it was concluded that the two-phase model developed is a powerful tool to investigate design and scale-up of (mixed) SSF fermentors.

Introduction

An intermittent mixing strategy for solid-state fermentation (SSF) has been frequently used and proposed (Mitchell et al., 2000; Schutyser et al., 2003a). The main reason for this strategy is that minimal damage is inflicted on the substrate and the fungus. In previous work, we performed fermentations in a 28-dm³ drum fermentor (diameter = 0.3 m), with moistened wheat grains as a solid substrate and the fungus *Aspergillus oryzae* (Schutyser et al., 2003a). Surprisingly, it was found that mixing in this fermentor was needed in first instance to disrupt the mycelium network formed between the substrate particles, rather than to homogenize excessive temperature or moisture gradients.

The main heat removal mechanism during SSF with forced aeration is evaporative cooling (i.e. heat removal via evaporation of water). During experiments with the 28-dm³ fermentor, it was found that the aeration pipe positioned in the middle of the bed supplied adequate aeration and therefore efficient evaporative cooling to avoid large temperature gradients. Calculations also showed that the addition of moisture was not of concern.

However, it is likely that during scale up of this drum fermentor a single aeration pipe will not be able to supply adequate cooling for the whole bed. Large temperature gradients will quickly arise, because the distribution of air through the substrate bed is inefficient. Mathematical models can support efficient construction, scale up, and operation of SSF fermentors to minimize the occurrence of spatial heat and moisture gradients (Mitchell et al., 2000). Von Meien and Mitchell (2002) developed a two-phase model to predict temperature and moisture gradients in an intermittently stirred bioreactor with forced aeration. In contrast with earlier studies, the model included heat and mass transfer correlations. Intermittent 'mixing events' were simulated, after which it was assumed that: 1) all temperatures in the bed returned to the inlet temperature and 2) the water activity of the substrate returned to its initial value by adding an appropriate amount of water.

Unfortunately, the model approach of von Meien and Mitchell (2002) did not allow prediction of the mixing behavior of the substrate bed. Prediction of mixing behavior is needed to obtain information about the progress of the mixing process and its influence on the temperature and moisture gradients in the bed. As mentioned before, we also found that the break up of the mycelium network in the substrate bed by mixing is of large importance during intermittently operated SSF (Schutyser et al., 2003a). Therefore, we believe that there is a strong need for a two-phase model that is also able to predict mixing during SSF.

In this study, a two-phase model was developed consisting of a combined discrete particle and continuum model that allows prediction of the mixing behavior during intermittently mixed SSF. The discrete particle model can predict the flow behavior by calculation of individual

particle movements. In the work presented, mixing was not simulated, but it could be implemented easily, following our earlier work (Schutyser et al., 2001). For reasons of simplicity, we only considered the non-mixed period in the drum fermentor. The possibility to simulate mixing events makes this modeling approach very attractive.

The two-phase model can be subdivided into 1) a discrete particle model 2) a continuum model of the gas phase with heat and water exchange between the solid and the gas phase and 3) an empirical growth model for *A. oryzae*. The model parameters describing growth, water housekeeping, and heat and mass transfer were obtained from Hoogschagen et al. (in prep.) and Nagel et al. (2001a).

Theory

The two-phase model presented in this paper consists of two parallel models; the discrete particle and the continuum model of the gas phase. During earlier work the continuum model was not required, because we did not consider the gas flow and related phenomena, such as heat and moist exchange between the solid and the gas phase (Schutyser et al., 2003b). However, because the main mechanism for heat removal during SSF is evaporative cooling, we implemented an additional model for the gas flow through the substrate bed. Different modeling approaches can be applied to describe the gas flow through the substrate bed. In this study, we used Darcy's law. We injected air in the middle of the substrate bed via a pipe with sparger holes. In this way, a specific gas distribution pattern is obtained.

In our model, we assumed that porosity of the bed is constant, although during fermentation local porosities may decrease due to hyphal growth. The change in porosity may be taken into account in the future, however to do so, a relation ship between biomass growth and porosity is required.

During SSF the volume and therefore the mass of the substrate bed changes due to evaporation of water, biomass growth and substrate hydrolysis (Weber et al., 2002). In our approach, it was assumed that the volume of each particle remained the same, while the density of the particles changed during fermentation.

Convective gas flow

Darcy's law (1856) describes a linear relation between the flow velocity and the pressure drop through a packed bed, $\vec{v} = -K \vec{\nabla} \vec{P}$. Because the configuration of the porous bed in the drum was not rectangular and the air was injected in the middle of the bed, a cubic grid (number of cells: M x M) was used for calculation of the gas flow pattern in the bed (Fig 1). For each grid cell, it was determined whether it was a bed cell, a headspace cell, or a cell outside the drum. The air was treated as an incompressible fluid, which was legitimate because temperature differences in

the bed were relatively small (T = 298–313 K) and the pressure differences in the bed were expected to be small due to the low airflow rates ($1 \cdot 10^{-4}$ - $2.8 \cdot 10^{-3}$ m^{3}s^{-1}). Darcy's law can therefore be written as $\vec{\phi} = -K \vec{\nabla} P$. To calculate the gas flows in the bed we assumed for each cell conservation of mass. If we combine conservation of mass and Darcy's law, we can state that:

$$\phi_x + \phi_y = \Delta P_x + \Delta P_y = 0 \tag{1}$$

Subsequently, we can derive an equation for the relative pressure (P) in cell i (Fig. 1):

$$P_i = \frac{1}{4}\left(P_{i-1} + P_{i+1} + P_{i-M} + P_{i+M}\right) \tag{2}$$

Where M is the number of cells along the width of the grid. This equation is not valid for the cell in which air is injected. The pressure in this cell and the inlet flow are fixed. The pressures of the boundary cells (headspace cells) are set to zero. Subsequently, an iterative calculation is performed to find the pressures and the corresponding gas flows between the cells. Of course, the cells outside the drum are not considered during this calculation. Once the pressures in the cells are calculated, the corresponding flows follow directly because the inlet flow rate is defined and the flows are proportional to the pressure gradient:

$$\phi_{i \to j} \sim P_i - P_j \tag{3}$$

where j indicates one of the four neighbor cells.
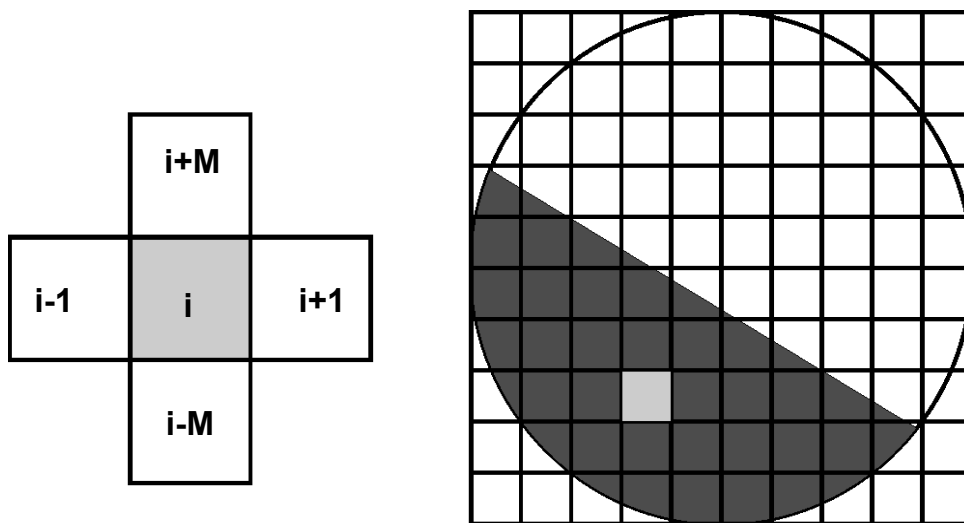
Figure 1. Rectangular grid applied for calculation of pressure distribution and gas flow pattern in the bed. Calculation of the pressure in cell i is based on the average of the pressures of its neighbors and the mass balance over the cell.

Balances for the gas phase

The balances were set up in analogy with the balances described by von Meien and Mitchell (2002). In the energy balance for the gas phase, we neglected the changes in specific heat and density, because they were small in comparison with the temperature changes. We also would like to emphasize that evaporation occurs at the surface of the solid phase and evaporation is therefore not considered in this energy balance. The energy balance over the gas phase is given for a single computational cell i, with neighbor cells q and k:

$$\varepsilon\, V_{cell}\, \rho_{air} cv_i\, \frac{dT_{gas,i}}{dt} = \sum_{q=1}^{N} \frac{1}{2} \rho_{air,q} cp_q \phi_{q \to i} \left(T_{gas,i} - T_{gas,q} \right)$$

$$+ \sum_{k=1}^{N} \frac{1}{2} \rho_{air,i} cp_i \phi_{i \to k} \left(T_{gas,k} - T_{gas,i} \right) - \sum_{particles} \left[ha_p \left(T_{gas,i} - T_p \right) \right] \tag{4}$$

where cp equal to:

$$cp = \left(1 - \frac{C_{vap}}{\rho_{air}} \right) cp_{air} + \frac{C_{vap}}{\rho_{air}} cp_{vap} \tag{4b}$$

Here we assumed that $1 - \dfrac{C_{vap}}{\rho_{air}} \approx 1$, because the moisture fractions were relatively small (≈ 0.033)

and cv (specific heat capacity at constant volume) was approximated by cp. The first two terms on the right-hand side represent the discretized description of the convective flow of dry air and water vapor. The third term describes the transfer of energy by convection between the gas phase and the solid phase. Please note that for each particle in the grid cell this transfer term is calculated. Because one cell contains 3 to 5 particles on average, multiple terms are summed in Eq. 4.

The volume of a single computational cell is equal to:

$$V_{cell} = \sigma \left(\frac{2\, R_d}{M} \right)^2 \tag{4c}$$

Subsequently, the mass balance over the gas phase in cell i is given by:

$$\varepsilon\, V_{cell}\, \frac{dC_{vap,i}}{dt} = \sum_{q=1}^{N} \phi_{q \to i} C_{vap,q} + \sum_{k=1}^{N} \phi_{i \to k} C_{vap,i} + \sum_{particles} \left[ka_p \frac{MW_w}{R} \left(\frac{a_w P_{sat}}{T_p} - \frac{mf\, P_t}{T_{gas}} \right) \right] \tag{5}$$

For calculation of the water transfer between the particle and the gas phase (third term, right-hand side), it is assumed that a small layer of water around the wheat kernel is present. The water gradient was calculated by comparing the actual vapor concentration in the gas phase with the vapor concentration that would be present if there is equilibrium between the water contents between the solid phase and the gas phase. The vapor saturation concentration in the

air depends on the temperature (273-333 K) according to the following Antoine equation (Kaye and Laby, 1995):

$$P_{wsat} = \exp\left(23.59 - \frac{4045}{T - 37.70}\right) \quad (5b)$$

The mole fraction of water present in the air is given by:

$$mf = \frac{C_{vap}MW_{air}}{C_{vap}MW_{air} + MW_w \rho_{air}} \quad (5c)$$

The water activity in the wheat grain is calculated according to an empirical relation (Hoogschagen et al. in prep, 2003):

$$a_w = 1 - \exp(-7.96\frac{X_w}{C_s}) \quad (5d)$$

Where X_w is the extracellular water content and C_s is the dry weight of the substrate of the wheat grain.

The mass transfer coefficient (k) in a packed bed is dependent on the superficial air velocity. Hoogschagen et al. (in prep) obtained the mass transfer coefficient, $k(v_1) = 0.00492$ ms^{-1}, from several experiments with a packed bed reactor at a superficial air velocity of $v_1 = 0.04$ ms^{-1}. The packed bed consisted of wheat grains pretreated according to the standard procedure for SSF. In the drum fermentor the average superficial air velocity was $v_2 = 0.0036$ ms^{-1}, for an aeration rate of 6 L/min. Subsequently, we could calculate the corresponding mass transfer coefficient, $k(v_2)$, under laminar flow conditions (Perry et al., 1997), according to:

$$\frac{Sh(v_2)}{Sh(v_1)} = \frac{k(v_2)}{k(v_1)} = \left(\frac{Re_2}{Re_1}\right)^{0.5} = \left(\frac{v_2}{v_1}\right)^{0.5} \quad (6)$$

Where Sh is the Sherwood number and Re is the Reynolds number.

Balances for the solid phase

The energy balance is given for a single substrate particle, taking into account the metabolic heat production, conductive heat transfer, convective heat transfer to the gas phase and evaporation of water. Since changes in substrate, biomass and water content were small in comparison with temperature changes we neglected this in the equation, of course they do change in time.

$$\left((C_s + X)cp_s + X_w cp_w + X_{wx}X cp_w\right)\frac{dT_p}{dt} = \frac{dQ^i_{cond}}{dt} + r_q + ha_p\left(T_{gas} - T_p\right) + \Delta H_v\, ka_p\, \frac{MW_w}{R}\left(\frac{a_w P_{sat}}{T_p} - \frac{mf\, P_t}{T_{gas}}\right)$$

$$(7)$$

The temperature of the solid substrate particle changes amongst others due to the conductive heat transfer through the contact points between the particle and its neighbors or the drum wall (Schutyser et al., 2003b). The change in heat, $\dfrac{dQ_{cond}^{i}}{dt}$, in particle i due to conduction depends on the number of contacts with its neighbors (n_c) and contact with the wall of the drum:

$$\frac{dQ_{cond}^{i}}{dt} = \left(\sum_{1}^{n_c} \alpha(T_p^j - T_p^i) + \alpha_{wall}(T_{wall} - T_p^i) \right)\left(C_{s0}cp_s + X_{w0}cp_w \right) \tag{8}$$

where

$$\alpha = 9 \cdot 10^{-5}\left(\frac{\left(T_p^i + T_p^j \right)}{2} - T_{ref} \right) + 0.0113$$

This relation includes the effect of temperature on the heat conductivity coefficient (α) between the particles. The coefficient (α_{wall}) between the wall and the particle was found to be independent of temperature. This equation was obtained only for substrate particles at the initial moisture contents. The heat conduction coefficients α and α_{wall} (s^{-1}) include therefore the heat capacity term. If we multiply the right side of the equation with the heat capacity term, we obtain again the change in energy due to heat conduction.

The mass balance over a single solid substrate particle is given by:

$$\frac{dX_w}{dt} = -ka_p \frac{MW_w}{R}\left(\frac{a_w P_{sat}}{T_p} - \frac{mf\, P_t}{T_{gas}} \right) + r_{w,prod} \tag{9}$$

Biomass Production

Maximum biomass growth rate is dependent on temperature. The following Ratkowsky equation is used to describe this (Ratkowsky et al., 1983):

$$\mu_{max} = \frac{1}{86400}\left\{ b_1\left(T_p - T_{min} \right)\left(1 - \exp\left(b_2\left(T_p - T_{max} \right) \right) \right) \right\}^2 \tag{10}$$

Subsequently, a logistic law describes the biomass growth (Okazaki et al., 1980):

$$r_x = \mu_{max} X\left(1 - \frac{X}{X_{max}} \right) \tag{11}$$

Growth is also dependent on the water activity in the solid substrate. Initially the water activity in the substrate is not the limiting factor for growth; however, during fermentation, the water activity may drop due to evaporation. In future work this dependency will be included. The amount of oxygen needed for maintenance of the biomass is also described by a Ratkowsky equation (Ratkowsky et al., 1983):

$$m_o = \frac{1}{86400}\left\{ a_1\left(T_p - T_{min} \right)\left(1 - \exp\left(a_2\left(T_p - T_{max} \right) \right) \right) \right\}^2 \tag{12}$$

Thus, the total amount of oxygen that is consumed is calculated according to the linear growth model (Pirt, 1965):

$$r_{O_2} = \frac{1}{Y_{xo}} \frac{MW_o}{MW_x} r_x + m_0 X \tag{13}$$

Please note that the oxygen concentration in the outlet air is directly coupled to the consumption of oxygen in the bed and is thus not delayed due to internal transport in the bed. This is allowed, because the growth process is very slow in comparison with the heat and mass transfer to and in the gas phase. The metabolic heat that is produced during growth is proportional to the oxygen consumption:

$$r_q = r_{O_2} \Delta H_o \tag{14}$$

During growth, metabolic water is produced, water is taken up intracellularly, and water is needed for hydrolysis of starch (Nagel et al., 2001a). Nagel et al., (2001a) described the effect of the different contributions on the extracellular water contents of the substrate.

$$r_{w,prod} = r_{O_2} \frac{1}{MW_o} \left(Y_{wo} MW_w - X_{wx} Y_{xo} MW_x - Y_{hyd} Y_{so} \right) \tag{15}$$

Due to the substrate conversion the amount of dry substrate will decrease during fermentation:

$$r_s = -Y_{so} \cdot \frac{MW_s}{MW_o} \cdot r_{O_2} \tag{16}$$

Integration method

A second order Runge Kutta (or midpoint method) was used for solving the set of differential equations in an explicit way (Press et al., 1992). Adaptive stepsize control was applied to exert some control over the accuracy of the solution. More information about these numerical methods can be found in literature (Press et al., 1992). The advantage of adaptive stepsize control is that during dynamic changes in the progress, numerical instability is avoided because the stepsize is automatically decreased. During our simulation studies, it was found that the changes in air temperature were determining numerical stability.

Simulation methods

The model was programmed in Fortran 90 and consisted of several subroutines that form the building blocks of the simulation program (Fig 2). This structure allows easy implementation or adaptation of sub models. A short overview of the actions of the different subroutines is given:

1/2.   The input parameters and the initial conditions are loaded.

3.   Particle positions that are obtained from a previous discrete particle mixing simulation are loaded.

4.   A single cell or a group of cells is appointed for injection of the inlet air and the subsequent pressure gradients are calculated across the bed.

5.   The airflow values between the bed cells result from the pressure gradients.

6.   The initial conditions of the simulation are written to a data file.

7.   A neighborlist is constructed in which for each particle its neighbors are stored.

8.   The main loop starts with calculation of the biomass production, oxygen consumption, water production/consumption, and the dry matter decrease.

9.   Conductive heat transfer is calculated with the help of the neighborlist.

10.   Heat and mass transfer are calculated between the particles and the gas phase.

11.   Convective heat and mass transfer in the gas phase is calculated with the cell and flow maps.

12/13. The main variables, T_p, X_w, C_s, X, T_{gas} and C_{vap} are updated and the time step is adjusted according to Eq. 24.

14.   Data is optionally written to a file and the calculation continuous with step 8.
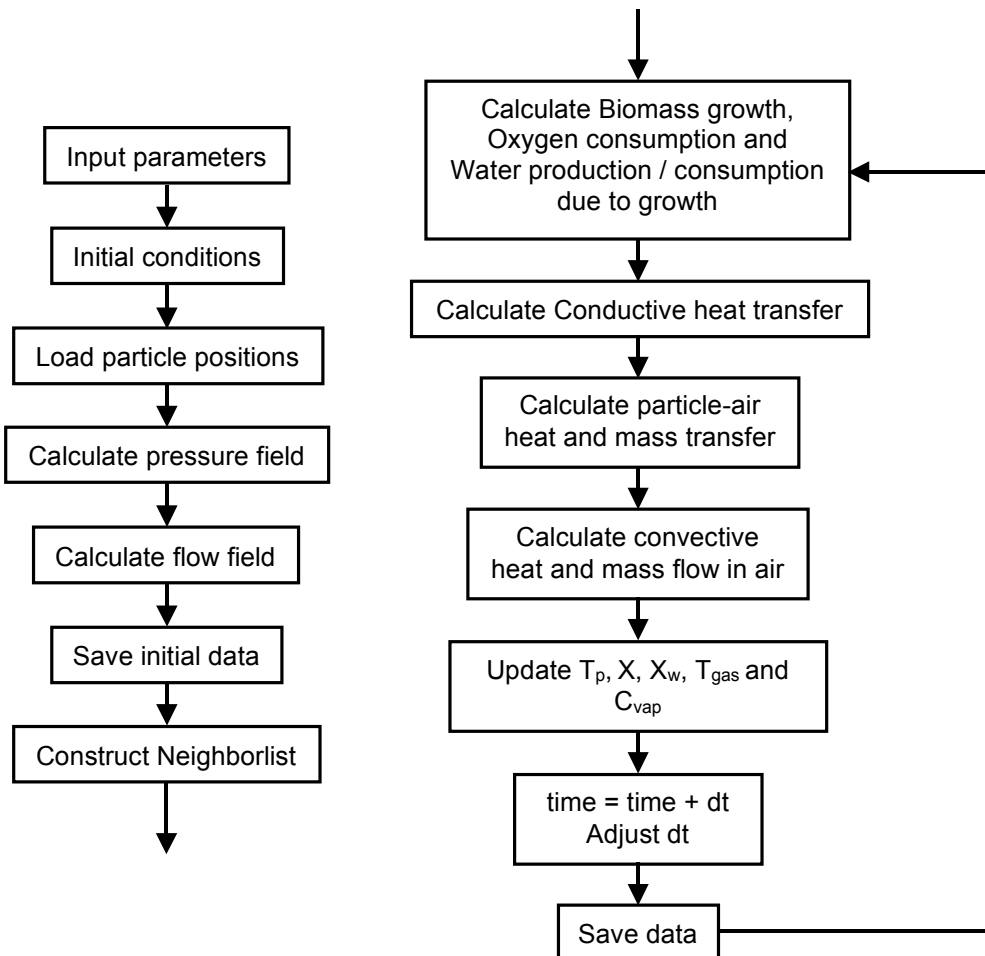
Figure 2. Scheme of the different building blocks in the model.

The conductive heat transfer is efficiently calculated with the help of a neighbor list in which for each particle its neighbors are stored (Allen and Tildesly, 1987). For efficient calculation of the pressure gradients, the flows and the convective heat and mass transfer in the bed, fast information supply about the identity of the neighboring cells and the airflows to or from neighboring cells appeared to be critical. By storing all these data in two maps, we could quickly retrieve information about neighboring cells and corresponding airflows to and from these neighboring cells. Each map existed of an array with a size of 4·Ncell, because there are four neighbors and four out- or ingoing flows per cell. The temperature and the moisture content of the outlet gas could also be quickly calculated, since all flows from the bed to the air cells were stored separately.

The simulations were run on two single-processor alpha workstations (XP1000). The data was visualized with the help of AVS/Express visualization edition, UK.

Experimental Methods

The experimental methods, such as for example the pretreatment of substrate and the inoculation procedure of *A. oryzae* CBS 570.64 have been extensively described in our previous publication (Schutyser et al., 2003a).

Fermentor design

The drum fermentor (Fig. 3) had an internal diameter of 30 cm, a length of 40 cm, and an internal volume of 28.3 dm^3. The bioreactor consisted of a glass cylinder (Scott, GE) with two polycarbonate (Lexan) side plates. The fermentor was entirely sterilized in an autoclave. On the horizontal axis four temperature sensors (Pt-100 Ω Tempcontrol, NL) were mounted that penetrated the grain bed (Fig. 3). The temperature sensors were adjustable in height in the radial direction of the drum; the angle of two temperature sensors could be adjusted as well. Air entered the reactor via the hollow horizontal axis at one side of the reactor and was further blown through a small channel with different holes into the center of the bed (Fig. 3). The outlet air was collected at the opposite side of the air inlet via three holes in the horizontal axis. The air that entered the fermentor was humidified by blowing the air through a stainless steel column (diameter 30 cm, height 80 cm) filled with Raschig rings and demi water of 25 ºC. The inlet and the outlet air were both filter-sterilized (Whatman Polyvent 1000 0.2 μm, UK). Before oxygen analysis (Xentra 4100, Servomex, NL) a small portion of the off-gas (400 ml/min) was passed through a glass condensor (at 4 ºC) in order to remove most water vapor from the air. Probably the remaining presence of moisture in the air caused a systematic error of the oxygen analyzer. Therefore, the oxygen consumption data presented in our previous study (Schutyser et al., 2003a) was corrected for this ($\Delta O_2 = -0.02$ mol/h). The oxygen consumption
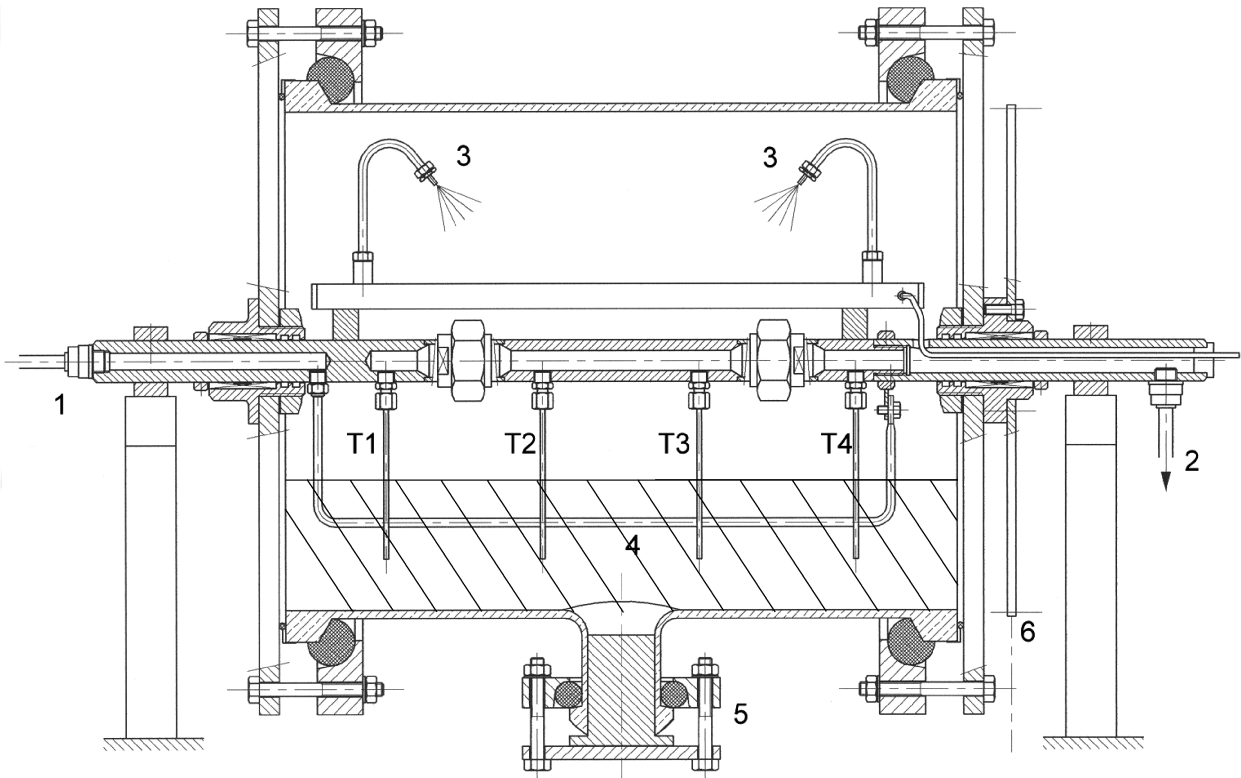
Figure 3. The 28-L rotating drum fermentor: (1) air inlet, (2) air outlet, (3) spraying nozzle, (4) channel for air distribution in the bed, (5) closed opening (possibility for attachment of a sampling device), (6) cog-wheal, and T1-T4 are four temperature sensors adjustable in height. The large shaded area represents the substrate bed.

that is presented in this study has not been corrected for this error, because the equations describing the growth kinetics (Eq. 13-16) were also fitted against data without correction for this error. The drum fermentor was placed in a temperature-controlled cabinet (34 ºC). The fermentation was monitored with a PC using Fieldpoint hardware and Labview software (both from National Instruments, NL). The fermentor was inoculated with two spraying nozzles (Bète PJ8*5-1/8, Spraybest, NL) that were placed in a position to obtain optimal coverage of the higher half of the surface of the bed (Fig. 3). Pressurized air (2 bars) pushed the spore suspension (60 mL) through a small pipe in the hollow axis and through the nozzles. The bed was mixed simultaneously. Because some spore suspension remained in the piping system, 300 mL of sterilized demi-water was sprayed to flush the system. The airflow of the inlet air during fermentation was initially set to 6 L/min with a mass flow controller (Brooks Instruments BV, NL), which is the minimum airflow required for offgas analysis in the current fermentation setup.

## Results

Validation of the model predictions

In previously published work, we reported about SSF of *A. oryzae* on whole wheat grains in a drum fermentor (Schutyser et al., 2003a). Fermentations were conducted to study the aggregation of substrate particles due to the formation of a network of aerial mycelium and the subsequent break up of the substrate bed due to mixing action. Experimental data obtained during these SSFs were used in the current work to validate the two-phase model. In Figure 4 the oxygen consumption rate is shown as a function of time for two SSF experiments and the model predictions under the same conditions. The aeration rate in the experiments and the model was manually adjusted after 30 h from 6 to 15 L/min to control the temperature in the bed. In this way, the temperature could be more or less controlled near the optimum growth temperature for *A. oryzae* (T = 34 ºC). It could be concluded that the measured oxygen consumption rate agreed well with the predicted oxygen consumption rate. After about 48 h the substrate bed was mixed for 5 minutes by rotation of the drum at 1 rpm to study the break up of the substrate bed aggregated due to aerial mycelium. Subsequently, the number of aggregates was determined and the fermentation was stopped.

In Figure 4 the predicted oxygen consumption is shown, in addition to the fermentation with manual airflow control from 6 to 15 L/min, assuming optimum growth conditions (T=34 ºC) and assuming a constant airflow rate of 6 L/min. From these predictions, we could conclude that during our SSF experiments with manual airflow control, the growth conditions were very close to optimal during the whole fermentation. After 48 h of fermentation, the oxygen consumption rate is 77% of the rate under optimum conditions. Better airflow control could reduce this growth difference even more. During our previous work, we found that a network of aerial mycelium in the bed was formed between oxygen consumption values of 0.14 and 0.25 mol h^{-1} (Schutyser et al., 2003a). Mixing was required at an oxygen consumption value of 0.14 mol h^{-1} (about 40 h) in order to avoid formation of aggregates after the mixing event. Growth is not severely restricted (97 % of optimal growth) under these conditions, because temperature differences in the bed are relatively small. Mixing in this drum fermentor would therefore be required to disrupt the network of mycelium. This is in agreement with the conclusions from our earlier work (Schutyser et al., 2003a). When the drum fermentor is scaled up, it will be likely that temperature gradients in the bed become larger and, therefore, mixing may be needed earlier to homogenize these gradients rather than to disrupt the aerial mycelium.

Three temperature sensors during the SSFs (at different locations in the bed) indicated that temperatures during the fermentation were near the optimum temperature for growth (>95% of the maximum growth rate), except for the last six hours (Fig 5). During the last six hours
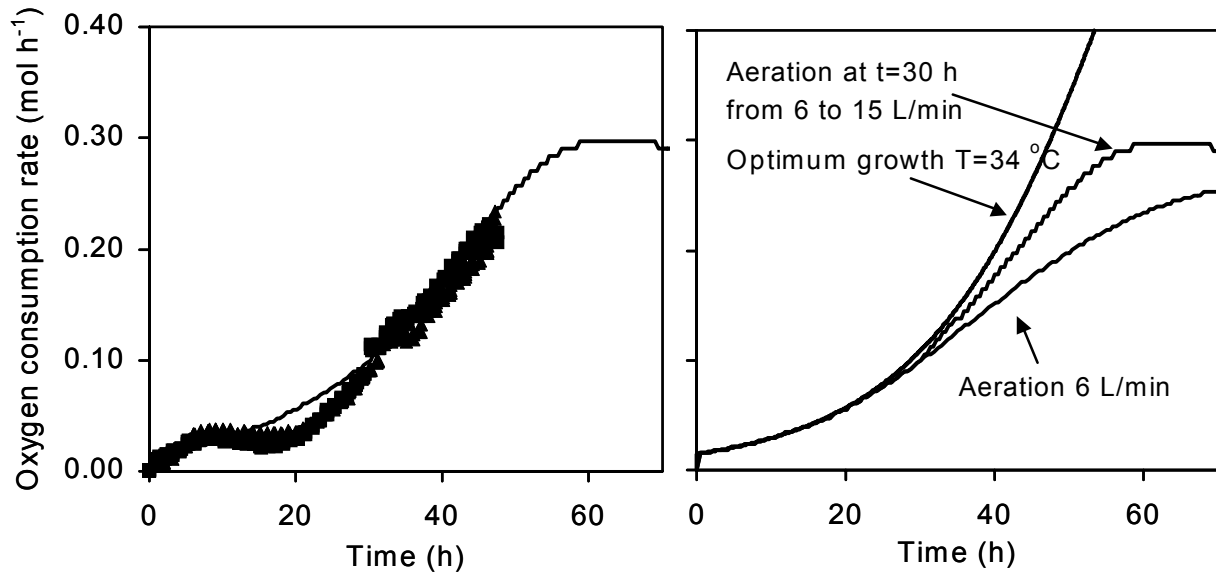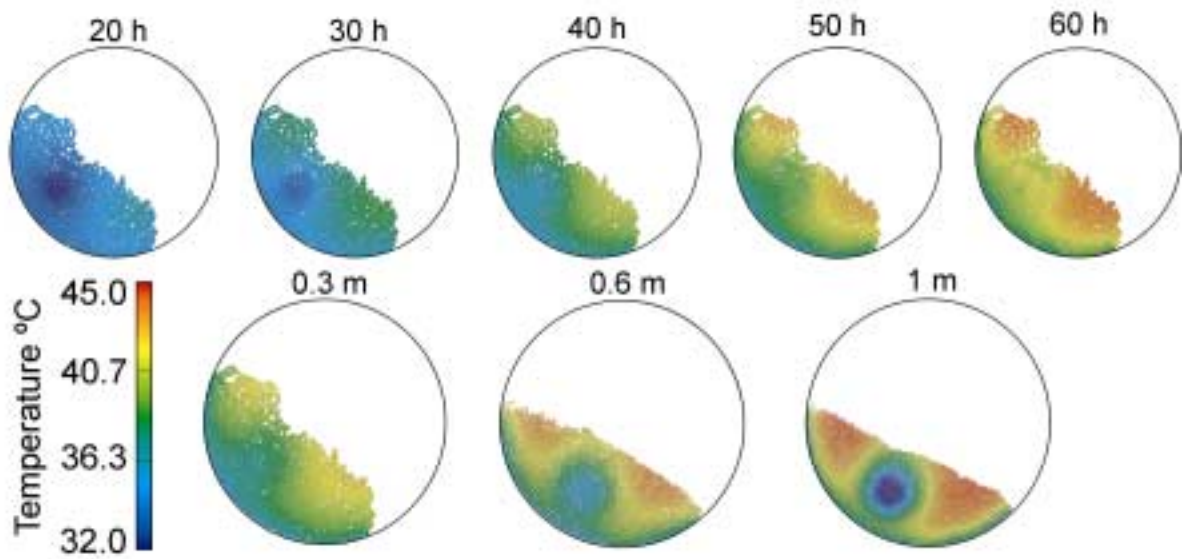
Figure 4. Left: The predicted oxygen consumption (line) and the measured oxygen consumption rate (duplicate, symbols) in a 28-L drum fermentor. After 30 h the airflow rate was adjusted in both model and experiment. Right: The predicted oxygen consumption versus time under a) optimum growth conditions (T=34 ºC), b) with a change in aeration rate after t=30 h from 6 to 15 L/min, and c) constant aeration rate of 6 L/min.
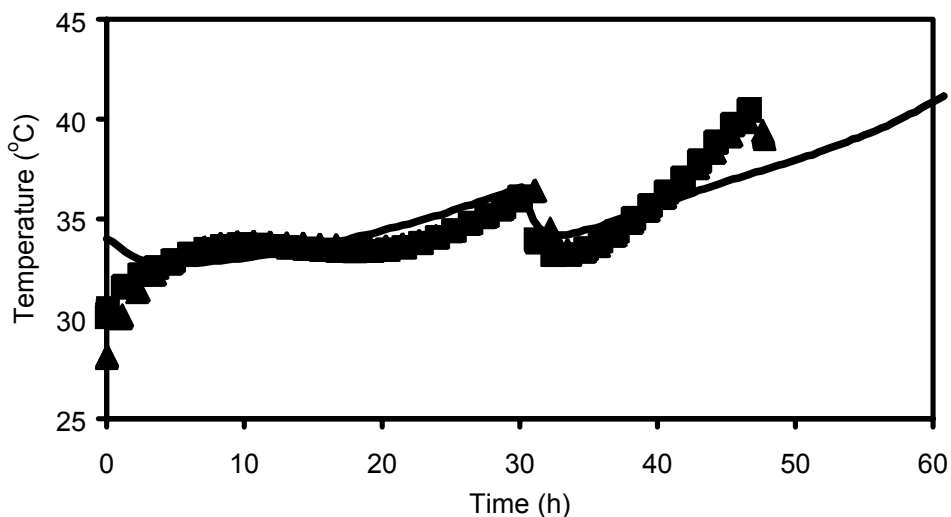

Figure 5. Predicted average bed temperature (line) and the average measured temperature of three sensors in the bed (symbols). After 30 h the airflow rate was adjusted in both model and experiment from 6 to 15 L/min.

temperatures rose above 40 ºC, resulting in a decrease of the growth rate (77% of the maximum growth rate). The predicted average temperature on corresponding positions in the bed are in agreement with the average measured bed temperature, although it appears that the measured

Figure 6. Visualizations of the temperatures in the bed for 1) the drum fermentor with a diameter of 0.3 m after 20, 30, 40, 50, and 60 h 2) the drum fermentors with diameters of 0.3, 0.6 and 1 m after 45 h.
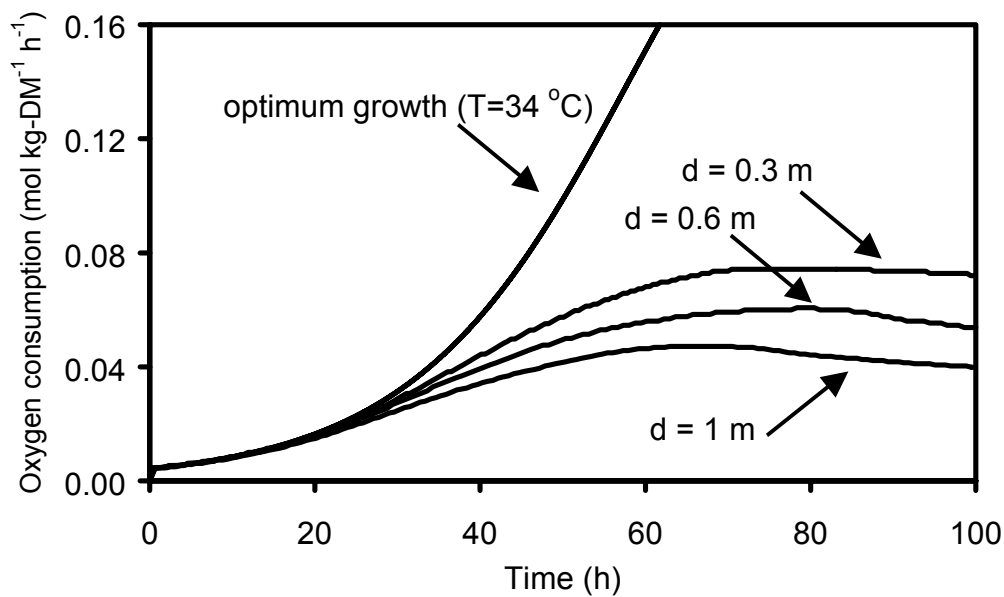
Figure 7. Predicted oxygen consumption for three different drum sizes (diameters = 0.3, 0.6 and 1 m) and under optimum growth conditions (T=34 ºC) during 100 h of incubation.

temperatures in the bed increase more rapidly during the last 10 h (Fig. 5). This could for example be explained by the fact that the model did not take into account the decrease of porosity and channeling due to hyphal growth and shrinkage of particles.

In Figure 6 the temperatures in the bed are visualized after different incubation times (constant aeration rate of 6 L/min). The temperature of the region in the middle of the bed is lower due to the presence of the aeration pipe. The wall temperature is set to the optimal growth temperature (34 ºC). Therefore, the temperature of the bed near the wall remains relatively close to 34 ºC. After 50 to 60 h, very high temperatures (>40ºC) occur. In addition to the visualization of the temperatures, we visualized local biomass production in a similar way. In agreement with the optimum growth temperature, we found highest biomass production (after 45 h) near the wall of the drum and near the air inlet. This information is valuable when studying the effect of different design parameters (e.g. construction of the aeration pipe) and operation conditions (e.g. aeration rates) on the performance of the fermentor.

### *Scale-up of SSF in a rotating drum*

Simulations were conducted for drum fermentors of three sizes (diameters: 0.3, 0.6 and 1.0 m). The airflow, needed to remove the amount of metabolic heat produced by the fungi, was adjusted proportionally to the volume ratio between the scales; 6, 24 and 66.7 L/min, respectively. In Figure 7 the oxygen, consumption versus time for the three drum sizes and under optimum growth conditions is shown. It can be concluded that the oxygen consumption and therefore biomass production decreases with increasing scale. This can be explained by the fact that the distribution of the air becomes worse. In the region near the gas inlet the temperature decreases considerably due to the high aeration rate, whereas in more remote regions temperatures rise quickly (Fig 6).

In Figure 8 the biomass per kg initial dry matter after 45 hrs of fermentation is plotted for three different drum sizes and three different aeration rates. This figure clearly shows that the proportional increase of the airflow rate with the volume ratio is not sufficient. An additional increase in the airflow can overcome the decrease in biomass yield. However, going from a drum radius of 0.15 to 0.5 m, adjustment of the aeration rate alone will not give the same yields, because, due to the high air flows near the entrance, steep temperature and moisture gradients cannot be avoided. To really improve the biomass yield at the larger scale, the fermentor design should be adapted, for example by applying multiple air injection points. More intensive mixing could also be applied to reduce temperature gradients; however, frequent mixing may damage the substrate and fungi.

The model approach developed in this study is well suitable to investigate the effect of the air distribution on the fermentor performance and the relation between reactor design and optimal process operation. For future work, we recommend to investigate systems in which a more homogeneous air distribution can be achieved than in a drum fermentor. The conical helical ribbon fermentor may be such a system (Schutyser et al., submitted). Here, the air inlet can be

positioned at the top and the air outlet at the bottom of the fermentor for efficient air distribution. Due to the conical shape, the air velocity will be larger towards the bottom of the fermentor. This increased air velocity can partially compensate the less efficient evaporative cooling process in the lower regions of the fermentor.

Further reduction of gradients during SSF and thus improved performance can be achieved by applying an appropriate control strategy during fermentation. Different control variables may be varied during operation: airflow rate, temperature, and moisture contents of the inlet air, wall temperature, mixing interval, and water addition via spray nozzles. It is clear however, that optimal control is not straightforward. An additional problem may be that there are differences between the practical situation and the model predicted process behavior (e.g. due to variability in the quality of the substrate (Hoogschagen et al., 2001). Control methods that take into account this variable process behavior, for example model based predictive control, may be used for achieving optimal performance (Schutyser and van Boxtel, unpublished).
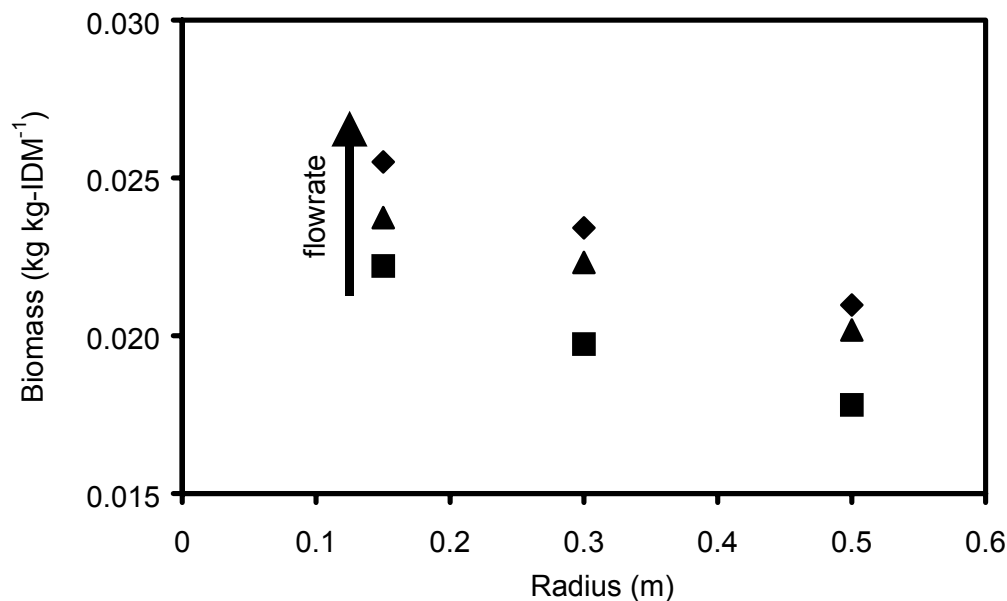
Figure 8. Predicted biomass yield after t = 45 h versus the drum radius for different flow rates. ■ 3 L/min ▲6 L/min ◆ 15 L/min (r = 0.15 m) The airflow rates for r = 0.3 and 0.5 m are obtained by multiplication with factors $\left(\dfrac{0.3}{0.15}\right)^2$ and $\left(\dfrac{0.5}{0.15}\right)^2$, respectively.

Future model extensions and improvements

It appeared that the process behavior (i.e. oxygen consumption and temperatures) was accurately predicted, even though several phenomena during SSF (e.g. air distribution) were modeled in a simplified manner. During further work, we may implement mixing and water

addition events, to study the effect of these events on the total process performance. The presence of aerial hyphae, holding particles together, may be estimated from the local biomass concentration. In this way, break up of small aggregates during mixing can be predicted. The only disadvantage is that computational time will increase significantly due to these additional mixing calculations.

Another phenomenon that can be studied in detail with this modeling approach is the occurrence of shrinkage and channeling during fermentation. It was found by Weber et al. (2002) that during cultivation of *A. oryzae* in a packed bed fermentor severe channeling occurred, which was due to the shrinkage of particles and the presence of a network of aerial mycelium. In the current model, the volume of the particles is assumed to remain constant and thus the density of the particles changes due to evaporation of water, biomass growth, and dry matter loss. Volume changes due to shrinking could be easily implemented in the model. Subsequent rearrangement of particles will depend on the volume and on the presence of aerial hyphae connecting neighboring particles.

The combined two-phase model can provide detailed information about spatial and temporal gradients in e.g. temperature, moisture content, and biomass concentration. Therefore, it will facilitate studies concerned with construction and scale-up of discontinuously mixed SSF fermentors.

Conclusions

In this study, a two-phase model for SSF in a drum fermentor without mixing was successfully developed. During further studies, mixing events can be implemented in the model based on our earlier work. The model predictions were validated with fermentation experiments in a 28-dm^3 drum fermentor. The model could predict spatial gradients in temperature, moisture contents, etc. in the substrate bed during fermentation. It appeared that temperatures were greatly affected by the airflow via the air pipe inserted in the middle of the bed. For the drum fermentor it was found that temperature gradients could be controlled (near) optimum growth temperature during the first 45-50 h of fermentation. Therefore, we could conclude that mixing in this fermentor is required in first instance to disrupt the mycelium network, aggregating the substrate particles after 40 h. Biomass yield decreased severely with increasing size of the drum fermentor, because temperature gradients increased with increasing scale. Aeration via a single pipe did not provide homogeneous cooling, which was clearly observed after visualization of the temperatures in the bed. Improvement of the air distribution is necessary to avoid the need for frequent mixing events. Finally, it is concluded that the two-phase model is well suitable to study the effect of construction and scale-up parameters on (mixed) SSF. The developed model

offers also opportunities to further study the effect of mixing events and the occurrence of channeling and shrinkage of substrate particles during SSF.

Acknowledgements

Nomenclature

Variables

ϕ	Volumetric flow rate ($m^3 s^{-1}$)
a_w	Water activity (-)
C_s	Dry matter per wheat grain (kg DM)
C_{vap}	Vapor concentration in the gas phase ($kg\ m^{-3}$)
dt	Time derivative (s)
h	Numerical stepsize (s)
P	Pressure (Pa)
Q	Energy (J)
r_{O2}	Oxygen production rate ($kg\ s^{-1}$)
r_q	Metabolic heat production rate ($J\ s^{-1}$)
r_s	Substrate production rate ($kg\ s^{-1}$)
r_x	Biomass growth ($kg\ s^{-1}$)
$r_{w,prod}$	Water production rate ($kg\ s^{-1}$)
t	Time (s)
T_{gas}	Gas temperature (K)
T_p	Particle temperature (K)
X	Biomass per wheat grain (kg DM)
X_w	Extracellular water contents per wheat grain (kg W)
v	velocity ($m\ s^{-1}$)

Parameters

ε	0.44	porosity of the void [m-void-space^3 m^{-3}]	
σ	$4.9 \cdot 10^{-3}$	particle diameter [m]	
ρ_{air}	1.14	density of dry air at T = 307 K [kg-dry-air m^{-3}]	(Meien von and Mitchell, 2002)
ΔH_o	$1.4375 \cdot 10^7$	oxidation enthalpy of oxygen [J/kg O2]	(Roels, 1983)
ΔH_v	$2.5 \cdot 10^6$	heat of evaporation of water at 273 K [J kg water^{-1}]	(Perry et al., 1997)
α_{wall}	0.003	heat conduction coefficient wall [s-1]	(Schutyser et al., 2003b)
a_1	0.0889	fit parameter in Eq. 12 [-]	(Hoogschagen et al. in prep., 2003)
a_2	0.0188	fit parameter in Eq. 12 [-]	(Hoogschagen et al. in prep., 2003)
a_p	$7.5 \cdot 10^{-5}$	outer surface area of a wheat grain [m^2]	
b_1	0.1355	fit parameter in Eq. 10 [-]	(Hoogschagen et al. in prep., 2003)

b_2	0.0386	fit parameter in Eq. 10 [-]	(Hoogschagen et al. in prep., 2003)
cp_{air}	1005	specific heat of dry air J kg-dry-air^{-1} K^{-1}	(Hamblin, 1971)
cp_s	2300	specific heat of the solids [J kg DM^{-1} K^{-1}]	(Hoogschagen et al. in prep., 2003)
cp_{vap}	1857	specific heat of water vapour [J kg-water-vapour^{-1} K^{-1}]	(Hamblin, 1971)
cp_w	4184	specific heat of water [J kg water^{-1} K^{-1}]	(Meien von and Mitchell, 2002)
C_{s0}	$4 \cdot 10^{-5}$	initial dry substrate per wheat grain [kg]	
dt	$1 \cdot 10^{-3}$	initial time step [s]	
h	40	heat transfer coefficient for oat [J s^{-1} m^{-2} K^{-1}]	(Hoogschagen et al. in prep., 2003)
k	0.00492	mass transfer coefficient for oat [m s^{-1}]	(Hoogschagen et al. in prep., 2003)
M		grid size (M x M)	
m_p	$7.2 \cdot 10^{-5}$	initial total mass of a wheat grain [kg]	
MW_{air}	$29 \cdot 10^{-3}$	molecular mass of air [kg mol^{-1}]	
MW_o	$32 \cdot 10^{-3}$	molecular mass of oxygen [kg mol^{-1}]	
MW_s	$30 \cdot 10^{-3}$	molecular mass of starch [kg mol^{-1}]	(Nagel et al., 2001a)
MW_w	$18 \cdot 10^{-3}$	molecular mass of water [kg mol^{-1}]	
MW_x	$24.42 \cdot 10^{-3}$	molecular mass of biomass [kg mol^{-1}]	(Nagel et al., 2001a)
N		number of particles	
P_{tot}	$1.01325 \cdot 10^5$	atmospheric pressure [Pa]	
R	8.314	ideal gas constant [J mol^{-1} K^{-1}]	
R_d	0.15	radius drum [m]	
T_{max}	321.94	fit parameter in Eq. 10 & 12 [K]	(Hoogschagen et al. in prep., 2003)
T_{min}	286.02	fit parameter in Eq. 10 & 12 [K]	(Hoogschagen et al. in prep., 2003)
T_{ref}	273.15	reference temperature [K]	
X_0	$1.32 \cdot 10^{-7}$	initial biomass per wheat grain [kg DM]	(Hoogschagen et al. in prep., 2003)
X_{max}	$1.845 \cdot 10^{-5}$	max. biomass per wheat grain [kg DM]	(Hoogschagen et al. in prep., 2003)
X_{w0}	$3.2 \cdot 10^{-5}$	initial water per wheat grain [kg]	
X_{wx}	2	water content biomass [kg kg^{-1} DM biomass]	(Nagel et al., 2001a)
Y_{hyd}	0.003	water needed to hydrolyze starch [kg Cmol^{-1}]	(Nagel et al., 2001a)
Y_{so}	1.46	yield for substrate on oxygen [mol mol^{-1}]	(Nagel et al., 2001a)
Y_{wo}	1.22	yield for water on oxygen [Cmol mol^{-1}]	(Nagel et al., 2001a)
Y_{xo}	1.16	yield of biomass on oxygen [Cmol X mol O2^{-1}]	(Nagel et al., 2001a)

References

Allen MP, Tildesly DJ. 1987. Computer simulation of liquids. Oxford, UK: Oxford University Press.

Hamblin FD. 1971. Abridged thermodynamic and thermochemical tables: SI units. Oxford, UK: Pergamon Press

Hoogschagen MJ, Yang Z, As van H, Tramper J, Rinzema A. 2001. Influence of wheat type and pretreatment on fungal growth in solid-state fermentation. Biotechnol Lett 23:1183-1187.

Kaye GWC, Laby TH. 1995. Tables of physical and chemical constants. Harlow Essex, UK: Longman.

Lian G, Thiru A, Parry A, Moore S. 2002. CFD simulation of heat transfer and phenol oxidation during tea fermentation. Comp Elect Agric 34:145-148.

Meien von OF, Mitchell DA. 2002. A two-phase model for water and heat transfer within an intermittently-mixed solid-state fermentation bioreactor with forced aeration. Biotechnol Bioeng 79:416-428.

Mitchell DA, Krieger N, Stuart DM, Pandey A. 2000. New developments in solid-state fermentation II Rational approaches to the design, operation and scale-up of bioreactors. Process Biochem 35:1211-1225.

Nagel FJI. 2002. Process control of Solid-State Fermentation. Ph.D. Thesis, WUR, The Netherlands.

Nagel FJI, Tramper J, Bakker MSN, Rinzema A. 2001a. Model for on-line moisture content control during solid-state fermentation. Biotechnol Bioeng 72:231-243.

Nagel FJI, Tramper J, Bakker MSN, Rinzema A. 2001b. Temperature control in a continuously mixed bioreactor for solid-state fermentation. Biotechnol Bioeng 72:219-230.

Okazaki H, Suguma S, Tanaka T. 1980. Mathematical model for surface culture of *Koji* mold. J Ferment Technol 58:471-476.

Perry RH, Green DW, Malony JO. 1997. Perry's chemical engineers' handbook. New York, US: McGraw-Hill

Pirt SJ. 1965. The maintenance energy of bacteria in growing cultures. Proc Soc London 163:224-231.

Press WA, Teukolsky SA, Vetterling WT. 1992. Numerical recipes in FORTRAN: the art of scientific computing . - 2nd ed. Cambridge, UK: Cambridge University Press.

Ratkowsky DA, Lowry RK, McMeekin TA, Stokes AN, Chandler RE. 1983. Model for bacterial culture growth rate throughout the entire biokinetic temperature range. J Bacteriol 154:1222-1226.

Roels JA. 1983. Energetics and kinetics in biotechnology. Amsterdam, NL: Elsevier.

Schutyser MAI, Padding JT, Weber FJ, Briels WJ, Rinzema A, Boom R. 2001. Discrete particle simulations predicting mixing behavior of solid substrate particles in a rotating drum. Biotechnol Bioeng 75:666-675.

Schutyser MAI, Pagter de P, Weber FJ, Briels WJ, Rinzema A, Boom RM. 2003a. Discrete particle modeling of substrate aggregation due to aerial hyphae growth of *A. oryzae* during discontinuously mixed solid-state fermentation. Biotechnol Bioeng, in press.

Schutyser MAI, Weber FJ, Briels WJ, Rinzema A, Boom RM. 2003b. Heat and water transfer in a rotating drum containing solid substrate particles. Biotechnol Bioeng 82:552-563

Weber FJ, Oostra J, Tramper J, Rinzema A. 2002. Validation of a model for process development and scale-up of packed-bed solid-state reactors. Biotechnol Bioeng 77:381-393.

Summary

This thesis reports on (intermittently) mixed solid-state fermentation (SSF). SSF involves the cultivation of microorganisms such as fungi on a moist solid substrate. It is applied in many traditional food fermentation processes and has perspectives for production of novel food products and ingredients. Unfortunately, application of large-scale SSF is limited due to a lack of knowledge about reactor design and operation. This study focused on the development of this knowledge. It is part of a substantial research project within Wageningen Centre for Food Sciences (WCFS) that aims at supporting the industrial application of SSF. The focus of the project is oriented towards developing more knowledge about fungal genetics and physiology and non-empirical engineering methods for SSF processes. SSF can be applied in both packed-bed and mixed fermentor systems.

Mixing during SSF facilitates the addition of water, reduces temperature gradients, and prevents formation of large aggregates of mycelium and substrate in the bed. An intermittent mixing strategy is often preferred, because the substrate and the fungus may be seriously damaged during intensive mixing. In this thesis the rotating drum fermenter was considered as a model fermentor system. The substrate consisted of wheat grains and the fungus *Aspergillus oryzae* was cultivated.

Hitherto, studies dealing with mixing during SSF have been mostly empirical. In this thesis we describe the use of a discrete particle modeling approach that allows prediction of individual movements of substrate particles during the mixing process. The individual particle trajectories were obtained via direct integration of Newton's equations of motion. The wheat grains were modeled as spherical particles and it appeared that, despite this simplification, accurate predictions of the mixing process could be obtained.

Firstly, successfully modeled was the radial mixing of wheat grains in a two-dimensional rotating drum. To quantitatively validate these model predictions, a rotating drum was filled with two layers of colored wheat grains. Image analysis techniques were used to process the pictures obtained from the experiments. It appeared that radial mixing is dependent on the fill level and the size of the drum. Straight baffles were successfully implemented in the model; only large baffles (67% of the drum radius) were found useful in improving the mixing rate. Subsequently, the model was extended to three dimensions to study the axial mixing process,

which is a slower process. Three different drum designs were studied: 1) without baffles; 2) with straight baffles; 3) with curved baffles. The predicted mixing behavior in the drum without baffles and with curved baffles matched the experimental mixing behavior, but this was not the case for the drum with straight baffles. The prediction could be improved by incorporation of particle rotation in the model. Apparently, axial mixing was dependent on particle rotation, which was not so in the other drum designs. In the drum with curved baffles, fast convective mixing was observed. The excellent axial mixing performance of this drum design may be beneficial during operation of SSF.

The discrete particle model was further adapted for prediction of mixing behavior in a helical blade mixer, a potential SSF fermentor. The predictions were validated with positron emission particle tracking (PEPT) experiments. With this technique the movements of a radioactive tracer particle could be followed without disturbing the flow behavior. The experiments were conducted in a transparent small-scale helical blade mixer. Agreement of the model predictions and the experimental flow behavior in the mixer was obtained. Deviations of the surface flow in the mixer were found to be due to the spherical shape of the particles in the discrete particle model. This was confirmed by experiments with spherical green peas. Further research is required to fully understand the effect of different parameters (e.g. rotation rate of the blade) on the mixing behavior of the helical blade mixer.

Heat and water transfer studies were conducted in a rotating drum filled with moist wheat grains. Conductive heat transfer was modeled via individual contacts between grains. The model was applied to predict the rate and homogeneity of the heating and the cooling of the substrate bed. Subsequently, the results were experimentally verified. Experiments and model predictions matched closely. The addition of water during fermentation is necessary to compensate for desiccation due to evaporative cooling. The discrete particle approach was again used to describe this process and distinguished the absorption of water and the transfer of water between individual grains. The water distribution in the bed during addition of water by spray nozzles was investigated with a fluorescent dye. Results were in agreement with the model predictions. Water gradients developed rapidly during continuous spraying. It was concluded that a short spraying period with mixing followed by a period of only intensive mixing minimizes the gradients in the bed.

Substrate aggregation due to the development of a network of aerial mycelium may seriously hamper mixing during intermittently mixed SSF. It was found that during SSF in a 28-L drum fermenter a first mixing event after a specific time interval was required to disrupt the network of mycelium rather than to reduce excessive temperature or moisture gradients. A novel experimental method was developed to investigate the tensile strength of aerial mycelium, holding wheat grains together. This method consisted of two wheat dough disks stacked on top

of each other. The fungus between the disks was cultivated and after a specific incubation time the strength of the mycelium was determined by monitoring the force needed to separate the disks. The measured strengths were applied in the discrete particle model to predict the effect of the presence of the aerial mycelium on the mixing. The predicted break down of the bed into smaller aggregates was similar to the results that were obtained from several fermentation experiments.

Finally, we studied the effect of evaporative cooling on the heat and mass transfer process during SSF in a drum fermenter and therefore we developed a two-phase model. A continuum model of the gas phase (based on Darcy's law) was implemented together wit a discrete particle model of the solids phase. Heat and mass transfer between the two phases and biomass growth were included. Comparison of the predictions of the model with fermentation experiments showed that the predictions matched the experiments accurately. We also found that (near) optimum growth conditions could be achieved by aeration in this fermenter, even after 40 h when mixing is necessary to avoid large aggregates being present after a mixing event. However, our model predicted during scale up of the drum fermenter large temperature gradients in the substrate bed. This could be explained by the inhomogeneous distribution of air via a single aeration pipe in the bed. Frequent mixing may lead to damage to the substrate and the fungus. It is therefore important that during design and scale-up of a solid-state fermenter sufficient distribution of air is achieved. If so, mixing will be only needed to avoid aggregation of substrate.

The discrete particle models developed in this study can be used for improvements in the design and scale up of solid-state fermenters. Furthermore, the operating window for mixed SSF may be based on model predictions. The major bottleneck will be the computational power needed to describe mixing in large-scale SSF fermenters, containing millions of particles. Model approaches that do not have to take into account each particle individually to resolve the mixing behavior may be developed. These models can be based on data provided by discrete particle models. In future, different processes involving discrete particle media, such as coating, dissolving and agglomeration can be subject of study.

Samenvatting

Dit proefschrift doet verslag van (discontinu) gemengde vaste-stoffermentatie (SSF). SSF betreft het kweken van micro-organismen, zoals schimmels, op vochtige vaste substraten. Dit proces wordt toegepast tijdens de traditionele bereiding van sommige levensmiddelen en biedt ook mogelijkheden voor de productie van nieuwe levensmiddelen en ingrediënten. De industriële toepassing van grootschalige SSF wordt belemmerd door een gebrek aan kennis van reactorontwerp en procesvoering. Deze studie richtte zich op het ontwikkelen van deze kennis. Het is onderdeel van een groot onderzoeksproject binnen het Wageningen Centre for Food Sciences (WCFS) dat gericht is op de bevordering van de industriële toepassing van SSF. Het project heeft als doel kennis te ontwikkelen over de genetica en fysiologie van schimmels en de parameters van belang bij het ontwerp van SSF op grote schaal. SSF kan zowel worden toegepast in gepakte bedden van substraatdeeltjes, als in reactoren waarin de deeltjes mechanisch worden gemengd.

Mengen tijdens SSF vergemakkelijkt de toevoeging van water, vermindert temperatuurgradiënten en voorkomt de vorming van grote aggregaten van mycelium en substraat in het bed. Een strategie waarbij alleen af en toe gemengd wordt, heeft echter vaak de voorkeur, omdat het substraat en de schimmel tijdens het intensieve mengproces ernstig beschadigd kunnen raken. In dit proefschrift is de roterende trommel bestudeerd als model fermentor systeem. Het substraat bestond uit tarwekorrels waarop de schimmel *Aspergillus oryzae* werd gekweekt.

Tot nu toe waren de meeste studies over gemengde SSF empirisch van karakter. In dit proefschrift beschrijven we een discreetdeeltjesmodel dat de bewegingen van ieder substraatdeeltje tijdens het mengproces berekende. De individuele bewegingen werden verkregen door directe integratie van de bewegingswetten van Newton. In het model werden de tarwekorrels als ronde bollen beschouwd. Ondanks deze versimpeling konden nauwkeurige voorspellingen van het mengproces gemaakt worden.

Allereerst werd met succes de radiale menging gemodelleerd van tarwekorrels in een twee-dimensionale roterende trommel. Kwantitatieve validatie van de voorspellingen vond plaats met behulp van een roterende trommel met twee lagen gekleurde tarwekorrels, waarbij beeldanalyse technieken werden gebruikt om de beelden van de experimenten te verwerken. Het bleek dat radiale menging afhankelijk is van de vulgraad en de grootte van de trommel. Rechte schotten

157

konden goed met het model beschreven worden; alleen grote schotten (67 % van de straal van de trommel) bevorderden de mengsnelheid. Daarna is het model uitgebreid naar drie dimensies om het axiale mengproces dat veel langzamer verloopt te bestuderen. Drie ontwerpen van de trommel werden bestudeerd: 1) zonder schotten; 3) met rechte schotten; 3) met gedraaide schotten. Het voorspelde menggedrag in de trommels zonder schotten en met gedraaide schotten kwamen overeen met het menggedrag zoals bepaald tijdens de experimenten. Dit was echter niet het geval voor rechte schotten. De voorspelling kon verbeterd worden door deeltjesrotatie toe te voegen aan het model. Blijkbaar was axiale menging hier afhankelijk van deeltjesrotatie, wat kennelijk niet zo sterk het geval was bij de andere ontwerpen. Snelle menging door convectie werd waargenomen in de trommel met gedraaide schotten. De uitstekende axiale mengprestaties van dit trommelontwerp kunnen voordelig zijn tijdens de procesvoering van SSF.

Het discretedeeltjesmodel werd verder aangepast voor de voorspelling van het menggedrag in een lintmenger, een potentiële SSF fermentor. De voorspellingen werden gevalideerd met behulp van positron emission particle tracking (PEPT) experimenten. Met deze techniek konden we de bewegingen van een radioactief gelabeld deeltje volgen zonder het mengproces te verstoren. De experimenten werden uitgevoerd in een kleine transparante lintmenger. De modelvoorspellingen bleken goed overeen te komen met het experimenteel bepaalde stromingsgedrag. Afwijkingen van de stroming aan het oppervlak van het bed konden worden toegeschreven aan de bolvormigheid van de deeltjes in het discretedeeltjesmodel. Experimenten met ronde groene erwten bevestigden dit. Verder onderzoek is noodzakelijk om het effect van verschillende parameters (bijvoorbeeld de rotatiesnelheid van het lint) op het menggedrag van de lintmenger volledig te begrijpen.

Vervolgens werden warmte- en wateroverdracht in een roterende trommel gevuld met vochtige tarwekorrels bestudeerd. Conductieve warmtegeleiding werd gemodelleerd via de contactpunten tussen de korrels. Het model werd toegepast om de snelheid en homogeniteit van opwarmen en afkoelen te voorspellen. Vervolgens werd de uitkomst experimenteel geverifieerd. Experimenten en modelvoorspellingen kwamen goed overeen. De toevoeging van water gedurende fermentatie is nodig ter compensatie van uitdroging door verdampingskoeling. Discretedeeltjesmodellen werden weer gebruikt om dit proces te beschrijven. In de modellen onderscheidden we absorptie van water en wateroverdracht tussen de korrels. Een fluorescente kleurstof toonde de verdeling van water in het bed aan gedurende het toevoegen van water met behulp van sproeikoppen. De experimentele resultaten waren in overeenstemming met de modelvoorspellingen. Watergradiënten ontwikkelden zich snel tijdens continu sproeien. Bevonden werd dat een korte sproeiperiode met menging, gevolgd door een periode van alleen grondig mengen, de gradiënten in het bed minimaliseerde.

Substraataggregatie door de ontwikkeling van een netwerk van schimmeldraden kan desastreuze gevolgen hebben voor de menging tijdens discontinu gemengde SSF. Tijdens SSF in een 28-L trommel werd gevonden dat een eerste keer mengen na een zeker tijdsinterval nodig was om dit netwerk van schimmeldraden af te breken. Menging ter vermindering van excessieve temperatuur- of vochtgradiënten bleek niet eerder noodzakelijk. Een nieuwe experimentele methode werd ontwikkeld om de sterkte van het luchtmycelium, dat de korrels tijdens fermentatie aan elkaar bond, te onderzoeken. Deze methode bestaat uit twee op elkaar gestapelde tarwedeeg plakjes, waartussen de schimmel wordt gekweekt. Na een specifieke incubatietijd wordt de treksterkte van het mycelium bepaald door de benodigde kracht om de plakjes van elkaar te trekken te registreren. De gemeten sterktes werden toegepast in het discretedeeltjesmodel om het effect van het mycelium netwerk op de menging te voorspellen. De voorspelde afbraak van het bed in kleinere aggregaten was gelijk aan de resultaten die werden verkregen van verschillende fermentatie experimenten.

Als laatste bestudeerden we het effect van verdampingskoeling op de warmte- en massaoverdrachtsprocessen tijdens SSF in een roterende trommel en ontwikkelden daarom een twee-fase model. Een continuüm model van de gasfase (gebaseerd op de wet van Darcy) werd gecombineerd met een discreetdeeltjesmodel van de vaste fase. Warmte- en massaoverdracht tussen de twee fasen en biomassavorming werden meegenomen. Vergelijking van de modelvoorspellingen met fermentatie experimenten toonde aan dat de voorspellingen accuraat waren. In deze fermentor kon door beluchting (vrijwel) optimale groeicondities verkregen konden worden, zelfs na 40 uur. Na 40 uur is menging vereist om de aanwezigheid van grote aggregaten na menging te voorkomen. Echter, het model voorspelde grote temperatuurgradiënten tijdens opschaling van de trommelfermentor. Dit kan verklaard worden door de niet-homogene beluchting via de enkele beluchtingpijp in het bed. Regelmatige menging kan leiden tot beschadiging van het substraat en de schimmel. Het is daarom belangrijk dat gedurende het ontwerp en de opschaling van vaste-stoffermentoren voor voldoende verdeling van lucht wordt gezorgd. Is dit het geval, dan is menging alleen nodig om aggregatie van substraatdeeltjes te voorkomen.

De in deze studie ontwikkelde discretedeeltjesmodellen kunnen gebruikt worden ter verbetering van het ontwerp en de opschaling van vaste-stoffermentoren. Verder kan de keuze voor de procescondities van gemengde SSF gebaseerd worden op modelvoorspellingen. De grootste bottleneck zal de rekenkracht zijn die nodig is om de menging in grotere SSF fermentors met miljoenen deeltjes te beschrijven. Modellen die niet elk deeltje mee hoeven te nemen om het menggedrag te beschrijven zijn interessant. Deze modellen kunnen gebaseerd worden op de data die aangeleverd worden door de discretedeeltjesmodellen. In de toekomst kunnen ook

andere gelijksoortige processen onderwerp van studie zijn, bijvoorbeeld coaten, oplossen en agglomeratie.

Nawoord

Ook wil ik hier de inzet van een drietal studenten bij het uitvoeren van mijn onderzoek bedanken. René en Arjon, veel Fortran frustraties werden gelukkig gecompenseerd met het winnen van kaartjes voor dè voetbalwedstrijd in Milaan. Philip, enorme hoeveelheden gelatine heb je verbruikt, veel dank voor je toewijding bij het uitvoeren van de trekexperimenten.

De werkplaats heeft een belangrijke rol gespeeld in mijn onderzoek. Jan, Hans, André, Evert en Erik, bedankt voor al jullie toewijding en ondersteuning.

Graag wil ik ook nog mijn (virtuele) WCFS collega's bedanken. Tijdens onze project meetings hadden we altijd interessante discussies en hebben we toch maar even laten zien dat technologen en moleculairen goed kunnen samenwerken. Ik heb genoten van het lekker uit eten gaan en het samen skiën in Oostenrijk.

Tot slot, ouders en Pieter, bedankt voor jullie adviezen en de interesse die jullie toonden voor mijn onderzoek. Zeker aan jou, lieve Susan, heb ik veel te danken. Je steun en toeverlaat waardeer ik enorm. Na elke reis die we samen maakten voelde ik me als herboren en kreeg ik weer de nodige energie om verder te gaan.

Maarten

Curriculum vitae

Maarten A.I. Schutyser werd geboren op 12 juli 1976 in de gemeente Rheden. In 1994 behaalde hij het Gymnasium-B diploma aan het Thomas a Kempis College te Arnhem. In het najaar van 1999 begon hij aan de studie bioprocestechnologie aan de Wageningen Universiteit. Gedurende zijn studie participeerde hij in onderzoek naar chirale scheidingen bij de sectie Proceskunde en naar geavanceerde procesregeling bij de leerstoelgroep Meet-, Regel- en Systeemtechniek. Tijdens zijn stage bij het Rensselaer Polytechnic Institute in de Verenigde Staten verrichtte hij een half jaar onderzoek naar microfiltratie. In september 1999 rondde hij de studie bioprocestechnologie cum laude af.

Van april 1999 tot mei 2003 deed hij een promotie-onderzoek aan de sectie Proceskunde van de Wageningen Universiteit. Het onderzoek maakte deel uit van het onderzoeksproject 'Solid-State Fermentations' gesponsord door het Wageningen Centre for Food Sciences (WCFS). Dit promotie-onderzoek is uitgevoerd onder begeleiding van Prof. R.M. Boom, Prof. W.J Briels en Dr. A. Rinzema. De resultaten van dit onderzoek staan beschreven in dit proefschrift.

Vanaf 1 juni 2003 is hij werkzaam bij Akzo Nobel BU Salt te Deventer.

List of Publications

Schutyser MAI, Briels WJ, Boom RM, Rinzema A. 2003. Combined discrete particle and continuum model predicting solid-state fermentation in a drum fermentor. Submitted.

Schutyser MAI, Briels WJ, Rinzema A, Boom RM. 2003. Numerical simulation and PEPT measurements of a 3D Conical Helical Blade Mixer: A high potential solids mixer for solid-state fermentation. In press, Biotechnol Bioeng

Schutyser MAI, Pagter de P, Weber FJ, Briels WJ, Rinzema A, Boom RM. 2003. Discrete particle modeling of substrate aggregation due to aerial hyphae growth of *A. oryzae* during discontinuously mixed solid-state fermentation. In press, Biotechnol Bioeng

Schutyser MAI, Weber FJ, Briels WJ, Rinzema A, Boom RM. 2003. Heat and water transfer in a rotating drum containing solid substrate particles. Biotechnol Bioeng 82:552-563

Biesebeke te R, Ruijter G, Rahardjo YSP, Hoogschagen MJ, Heerikshuisen M, Leven A, Driel van KGA, Schutyser MAI, Dijksterhuis J, Yang Z, Weber FJ, Vos de WM, Hondel KAMJJ, Rinzema A, Punt PJ. 2002. Aspergillus oryzae in solid-state and submerged fermentation. FEMS Yeast Research 2:245-248.

Schutyser MAI, Weber FJ, Briels WJ, Boom RM, Rinzema A. 2002. Three-dimensional simulation of grain mixing in three different rotating drum designs for solid-state fermentation. Biotechnol Bioeng 79:284-294.

Schutyser MAI, Rupp R, Wildeman J, Belfort G. 2002. Dean vortex membrane microfiltration and diafiltration of rBDNF *E. coli* inclusion bodies. Biotechnol Prog 18:322-329.

Schutyser MAI, Belfort G. 2002. Dean vortex membrane microfiltration non-newtonian viscosity effects. Ind Eng Chem Res 41:494-504.

Schutyser MAI, Padding JT, Weber FJ, Briels WJ, Rinzema A, Boom RM. 2001. Discrete particle simulations predicting mixing behavior of solid substrate particles in a rotating drum. Biotechnol Bioeng 75:666-675.

Schutyser MAI, Weber FJ, Briels WJ, Rinzema A, Boom RM. 2001. De ontwikkeling van een nieuw simulatiemodel bij onderzoek naar vaste-stoffermentatie. VMT 26

Overdevest PEM, Schutyser MAI, Bruin de TJM, Riet van 't K, Keurentjes JTF, Padt van der A. 2001. Separation of racemic mixture by ultrafiltration of enantioselective micelles. 2. (De)complexation kinetics. Ind Eng Chem Res 40:5998-6003.